Investigation on Photodarkening in Ytterbium-doped Fibers for High Performance Fiber Devices

Li Huizi

School of Electrical & Electronic Engineering

A thesis submitted to the Nanyang Technological University

in partial fulfillment of the requirements for the degree of

Doctor of Philosophy

2019

Statement of Originality

I hereby certify that the work embodied in this thesis is the result of original research, is free of plagiarised materials, and has not been submitted for a higher degree to any other University or Institution.

. . .19/03/2019 . . . . 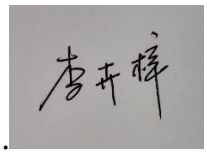 . . . . .

Date Li Huizi

Supervisor Declaration Statement

I have reviewed the content and presentation style of this thesis and declare it is free of plagiarism and of sufficient grammatical clarity to be examined. To the best of my knowledge, the research and writing are those of the candidate except as acknowledged in the Author Attribution Statement. I confirm that the investigations were conducted in accord with the ethics policies and integrity standards of Nanyang Technological University and that the research data are presented honestly and without prejudice.

. . . .19/03/2019. . . . .

Date Yoo Seongwoo

Authorship Attribution Statement

This thesis contains material from 2 published papers in the following peer-reviewed journal(s), and from 1 paper accepted at conferences in which I am listed as an author.

Chapter 3 is published as: H. Z. Li, L. Zhang, R. Sidharthan, Daryl Ho, X. Wu, N. Venkatram, H. D. Sun, T. Y. Huang, S. Yoo, "Pump Wavelength Dependence of Photodarkening in Yb-Doped Fibers," in Journal of Lightwave Technology, vol. 35, no. 13, pp. 2535-2540, 1 July1, 2017. doi: 10.1109/JLT.2017.2690383

The contributions of the co-authors are as follows:

- Prof. Yoo provided the initial project direction and edited the manuscript drafts.
- I prepared the manuscript drafts. The manuscript was revised by Dr. Zhang, Dr. Wu and Dr. Huang.
- Sample preparation was conducted by Dr. Sidahrthan and Mr. Ho.
- I designed the measurement setup and ran the experiments.
- Dr. Venkatram and Prof. Sun were helping for providing measurement equipment.

Chapter 5 is published as: Raghuraman Sidharthan, Junhua Ji, Kang Jie Lim, Serene Huiting Lim, Huizi Li, Jian Wei Lua, Yanyan Zhou, Chun Ho Tse, Daryl Ho, Yue Men Seng, Song Liang Chua, and Seongwoo Yoo, "Step-index high-absorption Yb-doped large-mode-area fiber with Ge-doped raised cladding," Opt. Lett. Vol. 43, No. 23,5897-5900 (2018). doi: 10.1364/OL.43.005897

The contributions of the co-authors are as follows:

- Prof. Yoo provided the initial project direction and edited the manuscript drafts.
- Dr. Sidharthan wrote the drafts of the manuscript. The manuscript was revised together with Dr. Ji and Dr. Tse
- I conducted the photodarkening measurement and cross sections measurement in the manuscript.
- Dr. Sidharthan, Dr. Kang Jie Lim, Dr. Serene Huiting Lim, Mr. Jian Wei Lua, Dr. Yanyan Zhou, Mr. Daryl Ho, Mr. Yue Men Seng, and Dr. Song Liang Chua conducted the fiber fabrication part mentioned in this manuscript.

Chapter 6 is published as: Huizi Li, Jie Ma, Mengying Zhang, Jun Wang, Dingyuan Tang, and Seongwoo Yoo "Carbon Nanoparticles as an Optical Modulator for Passively Q-switched Fiber Laser." in Conference on Lasers and Electro-Optics, OSA Technical Digest (Optical Society of America, 2018), paper JTu2A.174.

The contributions of the co-authors are as follows:

- Prof. Yoo provided the initial project direction and edited the manuscript drafts.
- I designed the experiment setup with Dr. Ma Jie and I ran the experiment.
- Dr. Zhang Mengying helped the sample preparation in the experiment.
- I drafted the manuscript and Dr. Ma jie, Dr. Wang Jun and Prof. Tang helped to revise it.

. . . . .19/03/2019 . . . . 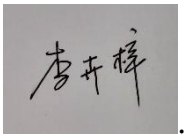 . . . . . .

Date Li Huizi

Acknowledgements

I would like to take this opportunity to express my heartiest and warmest gratitude to my supervisor --- Prof. Yoo Seongwoo. He is the one who lights up my journey of research. He did not just tell me what is research and how to do research, but inspired me how to enjoy research. I will never forget that at the first year of my PhD, I was very anxious for obtaining good experiment results and spent a lot time in lab to repeat the experiment without clear and rational thinking. At that time, Prof. Seongwoo recognized that I was not in a correct track. He told me: do not rush to do the experiment, think logically and comprehensively before starting, the last thing I want is you lose the motivation and interest in research. I will keep these words in my mind for my whole life. Prof. Seongwoo has a wide range of knowledge in our research field. Every time when I talk with him, I can broaden my horizons and fresh my mind. Thanks Prof. Seongwoo for making research not a dull thing but a great joy. When I meet problems in research, Prof. Seongwoo never hesitates to provide strong support. Although he is usually tied up, whenever I need discussion, he will reserve a timeslot from his busy schedule. I usually say to myself that how fortunate I am to have this great professor in my PhD period.

I also want to extend my heartfelt thanks to Dr. Ma Jie. At the most crucial moment of my PhD period, I met Dr. Ma Jie. We discussed a lot laser technology at the first beginning, he told me all he knows without any reservation. Later, we worked together to do experiment, we have a great cooperation experience. Although he has plenty of works to deal with, he never forgets to find time to work together with me. He is more than a good teacher, a good partner, he is a great friend.

I want to thank my friends and teammates: Yan Zhiyu, Yang Jiao, Zhang Mengying, Zang Jichao, Huang Xiaosheng, Xia Nan, Chen Shaoxiang, Zhou Yanyan, Ji Junhua, Daryl Ho, Liling Zhang, Sidharthan Raghuranman, Damien Chen, et al.

We shared happiness, hardships, and celebrated our achievements. They made my Ph.D. journey valuable, meaningful and unforgettable.

Last but not least, thanks to my husband, my parents, my lovely son and my parents in law. I cannot make it without their encouragement and strong support. Thanks for their endless love.

Table of Contents

Summary

Photodarkening (PD) is the phenomenon that induces optical power loss, related to material defects activated in a silica glass, when the glass is irradiated at wavelengths resonant to the defects. The PD can lead to serious performance degradations and lifetime limitations of optical devices such as fiber laser and fiber amplifier, and its suppression requires optimization of materials and device operation conditions. In particular, the PD can notably take place in an ytterbium (Yb)-doped fiber when the fiber is pumped at the wavelength corresponding to Yb absorption band or visible wavelength. PD in Yb-doped fiber induces a broad excess optical loss peaking at visible wavelengths, and extending to the Yb emission band in the near infrared (NIR) range. The induced loss is a detectable problem for high power operation. More seriously, the PD influences pump efficiency and impairs the Yb-doped fiber laser performances together with the excess loss. Therefore, PD should not be simply treated as an excess background loss, but ought to be explicated together with pumping efficiency for the power decay in both Yb-doped fiber laser and amplifier.

This thesis investigates on improving of performance of Yb-doped fiber laser through PD reduction spanning laser cavity design to material engineering. Firstly, I investigate device level PD suppression. It is found that the significance of PD is dependent of pump wavelength selection. It has been known that the Yb inversion is the only decisive factor considered for the PD. I show in this thesis that a pumping wavelength of Yb ions is another non-negligible factor to determine the PD effects. My experimental results indicate that under the same inversion level, a 976 nm pumping leads to more significant PD than 916 nm pumping. Therefore, provided that other conditions are invariant, selecting 916 nm as the pump wavelength is beneficial to supress the PD effect in laser or amplifier operations.

Besides the pump wavelength selections, the output coupling ratio of Yb-doped fiber laser has to be elaborately selected when the PD factor is considered. Output

power as function of cavity reflectivity has been investigated without considering PD effects. However, the extra cavity loss induced by PD is dependent on the selection of cavity reflectivity due to the variation of population inversion in cavity. Therefore, in this thesis I firstly point out that once the PD induced loss is considered, the optimal coupling out ratio has to be adjusted. This finding delivers non-trivial impact in fiber laser cavity improvement and guide more appropriate cavity parameter selection.

In a material level PD suppression, I report a method of suppressing PD while increasing Yb concentration. An equi-molar aluminium: phosphorus (Al:P) composition has been known to suppress the PD, but the realization of the equi-molar Al:P with very high Yb concentration has been hindered by complexity in fabrication process. A highly Yb doped Al:P fiber was fabricated at NTU, and I report its characteristics and PD suppression behavior.

Finally, this study led to investigation of new material for saturable absorber to build a 1 μm pulsed fiber laser. I adopted a novel carbon based material called carbon nanoparticles (CNPs), as a modulator in passive Q-switched Yb-doped fiber laser. Different from any other reported optical materials working as saturable absorber, CNPs can be efficiently obtained via a simple and low-cost flame synthesis process in-house without heavy equipment. I report this new finding in the context of demonstration of Q-switched fiber laser.

The works presented in this thesis provide a comprehensive analysis on impacts of the laser cavity structure and introduce a novel PD-free highly Yb-doped fiber with high lasing efficiency. Thus, this thesis contributes to technology progress on fiber lasers and devices adopting fiber lasers.

List of Figures

List of Tables

Chapter 1

Introduction

This thesis investigates the laser structure dependence of photodarkening (PD) on Ytterbium-doped (Yb-doped) fiber lasers and discusses the PD reduction from the perspectives of laser cavity design and material engineering. A comprehensive investigation of the PD effects on Yb-doped fiber laser and optimization the fiber laser cavity with appropriate pump wavelength and selected output coupling ratio for PD reduction are firstly demonstrated. This chapter presents the background of PD study on Yb-doped fiber, addresses motivation and objective of the research project, and lists originality and major contributions of the work accomplished.

1.1 Background

Silicon dioxide plays an essential role in most electronics and photonics technologies today. Currently, silica glass is widely applied in the cores and claddings of fiber optics for light transmission, amplification and generation. In many applications, even high purity silica glass cannot be free from structural defects which are introduced by manufacturing process, ionizing radiations or stressful operation condition [1]. In addition, pre-existed impurities can be served as a precursor for defect formation, and one defect can be transferred to other type of defect [2]. E'-center, oxygen deficiency center (ODC), non-bridging oxygen hole center (NBOHC) and peroxy radical are the well-known defects in silica glass fibers [3,4]. In Ge-doped silica, germanium-related E'-center exists as "Ge E'-center" which is analogous to silica E’-center. The optical absorption band of Ge E'-centers is located at 6.3 eV with full width at half maximum (FWHM) of 1.1 eV [5]. To date, Ge E’-center is likely to be most useful defect that enables Fiber Bragg Grating (FBG) inscription directly in the optical fiber [6].

Photosensitivity of the E'-center induces refractive index change for the FBG inscription. However, the same photosensitivity becomes problematic when it comes to transmission of ultra-violet and visible wavelengths. The refractive index change is accompanied with an excess absorption in the short wavelength region, hence reduces the transmission. By and large, such defects can deteriorate optical properties of silica and doped silica fiber [2].

The existence or creation of the optically responding defects in a rare earth doped fiber is considered as the main limitation of realizing efficient and reliability fiber lasers and amplifiers [7]. The main threats to the efficiency of the rare earth doped gain media is called PD effect. This phenomenon was not reported in the early time, until the year 1997, Paschotta observed the strong unsaturable absorption of Yb-doped fiber induced by pump wavelength [7]. Based on his experiment, he demonstrated that the unsaturable absorption is caused by excited state lifetime of a part of the Yb population is quenched by an unidentified, impurity or defect [8]. The knowledge on PD of Yb-doped fibers has increased significantly in the recent decades. The occurrence of the PD is identified as a permanent broad excess optical loss, peaking at visible wavelengths, and the loss extends to Yb emission band in the near infrared (NIR) range [9,10]. The excess loss is found to temporally develop to a saturation level. Thus, a fully developed loss or a saturated loss can be measured and used as a reference to state significance of the PD occurrence. J. J. Koponen et al. first standardized the way of measuring PD caused by photo induced structure change [9]. They proposed a method which is based on quantifying the observed difference of transmission changes at visible wavelengths as an indicator of PD at the signal wavelengths. Later on, a large number of studies have been conducted to identify influencing factors on PD and the generation mechanism of PD. It was revealed that Yb content, density of excited Yb ions, co-dopants and fiber fabrication conditions are the influencing factors [11–13].

The PD is somewhat reversible. A photobleaching effect has been investigated in order to reduce the damage caused by PD. It has been found that either partially or

completely reversible process is realizable through thermal bleaching or exposure to UV and/or visible light [14]. In the year 2005, Jasapara et al. demonstrated a complete recovery of the fiber to its fresh state by cooling the fiber to room temperature after heating at a temperature of 500 °C [15]. Recovering the excess loss by exposure under UV light at 355 nm was also reported at [16], they claimed that bleaching through this way can guarantee that lasing characteristics can be fully restored. Reduction of PD is also demonstrated by oxygen loading in [17], provided O_2 molecules reached the core zone and reacted with ODC, then a fraction of the ODC was removed. The O_2 loading technique is found to significantly suppress PD. Besides O_2 loading, inducing hydrogen is another alternative path to suppress PD [18]. H_2 molecules react with the hole defects generated on the oxygen atoms, form the hydroxyl groups and Yb^{2+} ions subsequently. The hole related color centers induce loss from visible wavelengths extending to near-infrared wavelengths. However, such post-processing is not applicable to field applications. Perhaps more practical approach is to modify the material compositions. Adding phosphorus in the Yb-doped silica glass is found to suppress PD in terms of an induced loss and a rate constant [19,20]. However, there are several non-negligible drawbacks of co-doping with phosphorus. It will lead to a damaging central dip at the refractive index profile as well as the Yb concentration distribution profile, a high background loss and reduction of emission cross section and absorption cross section. Alternatively, it was proposed that core compositions with equal molar content of aluminum and phosphorus is superior to achieve high performance Yb-doped fiber laser with largely suppressed PD effect. The PD loss is greatly suppressed in this composition albeit complicated in realization.

1.2 Motivation

Over the past five decades, fiber lasers have been drastically advanced in nearly all aspects of laser performances, leading to rapid deployment in wide applications. From the aspect of generated wavelength, the emission wavelengths range of fiber lasers is

not only including the mid-infrared area but also contain the ultraviolet and visible wavelength [21–24]. From the aspect of power scale, fiber laser stands out among its competitors due to ease of high optical gain building, effective cooling and superior wave guiding. Benefiting from these characteristics, industrial grade continuous-wave (cw) Yb-doped fiber laser with output power exceeding 100 kW has been realized [25]. The output power evolution of CW fiber lasers operating in the 1, 1.5, 2, and 3 μm regions is shown in Fig. 1.1. For pulsed fiber lasers, average power up to 265 W, pulse energy up to 10.6 mJ and pulse duration adjustable in the range 500 ps-500 ns has been achieved in 2013 [26]. Generation of 830 W average power was reported from a femtosecond fiber chirped pulse amplification system which compressed output pulses to 640 fs at 78 MHz repetition rate resulting in a peak power of 12 MW at the year of 2010 [27]. Ultrashort pulses as short than 10 fs [28,29] have been reported in 2009. The excellent performance of fiber lasers and their advantageous properties have facilitated widespread take-up for applications in industry, medicine, research, defence and security, and other areas.

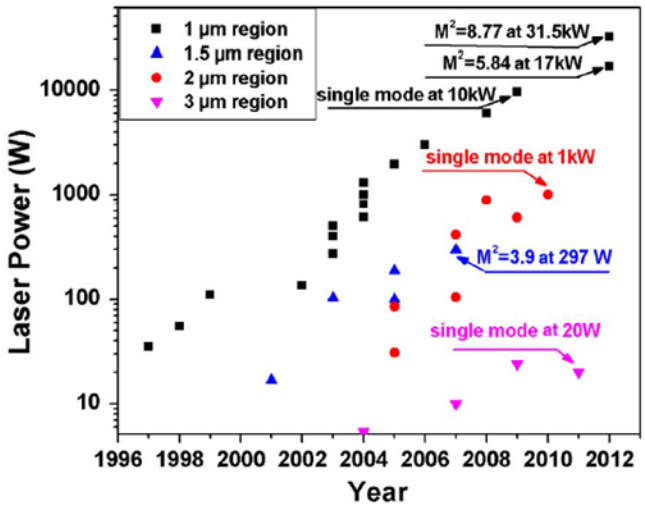

Fig. 1.1. Progress of output lasing power of CW fiber at 1, 1.5, 2, and 3 μm regions [30].

High-power CW Yb^{3+} doped fiber lasers operating around 1 μm have already occupied the largest market share of laser industrial material processing [30]. Compared with CO_2 laser, the 1 μm wavelength fiber laser has better performance on

cutting highly reflective materials and sheet thickness below 4 mm [31]. For instance, the better absorptivity of 1 μm laser radiation on highly reflective metal surfaces make Yb-doped lasers more suitable than CO_2 lasers for cutting Al and its alloys [32]. Furthermore, 1 μm fiber lasers have already been successfully employed for applications in cutting hydroformed automotive frames, welding the titanium of aircraft skins, and laser cladding for aerospace and oil industries [33].

Yb is the promising rare-earth material widely used as the dopant in active fiber. Compared with other rare-earth materials, Yb-doped laser crystals and glasses have a number of interesting properties. It is well known by its simple electronic structure guarantying no cross-relaxation and excited state absorption processes, while leading to low quantum defect (its absorption and emission wavelengths are close which results in the low quantum defect in the Yb-doped fiber laser), which potentially allows very high power and high efficiency of lasers via mitigating thermal effects in high-power operation. Additionally, the lifetimes of upper-state are relatively long, typically around of 1-2 ms, which is beneficial for Q switching [34].

Despite the advanced features of ytterbium medium, PD sets restriction in adopting the Yb-doped fiber in many fiber laser configurations. It was also recently found that the PD is coupled to the detrimental transverse mode instability that limits average power scaling [35,36]. Therefore, more alternative strategies to mitigate the PD are of great importance to free up the PD related restrictions in laser configurations.

1.3 Objective and Contributions

In this thesis, I investigate mitigating strategies in a device design level and in a material engineering level. It covers: (i) pump wavelength dependence of PD effect in Yb-doped fiber; (ii) PD influence on fiber laser cavity design; (iii) perfection of Large Mode Area (LMA) Yb-doped core composition for PD reduction.

The original contributions in this thesis are the following:

1）I demonstrated that the pump wavelength selection plays an essential role in PD dynamics. It is found that 976 nm pump source can bring more significant PD effects than 916 nm pumping at the same inversion levels.

2）I analyzed the analysis on the relationship of the PD loss of the output lasing power to the coupling out ratio of the laser ring cavity. I highlighted the significance of the PD loss changes with the different selection of output coupler. To achieve the maximum output lasing power, the selection of the output coupler must take into account when the PD factor.

3）I reported a highly Yb-doped step-index fiber with a PD free feature has an outstanding laser performance with 75% slope efficiency and generating more than 100 W laser output.

4）The PD study also led to investigation of a new material for pulsed laser operation. Carbon nanoparticles (CNPs), a promising new material in nano-tech field, are adopted to pulsed fiber laser demonstration. A passive Q-switched Yb-doped fiber laser has been successfully realized using the CNPs as the saturable absorber.

1.4 Thesis Organization

This thesis is divided into 7 chapters. Chapter 1 introduces the background, motivation, objective and contributions of this project. Chapter 2 reviews the reported studies on PD including the physical mechanism, characterization of PD, reduction of PD and impurity roles in PD. Chapter 3 demonstrates the research on pump wavelength dependence of PD in Yb-doped fiber, experimental results and mechanism analysis are presented. Chapter 4 centers on PD influence on fiber laser cavity design with different coupling out ratio selection. In chapter 5, a highly Yb-doped fiber with an outstanding PD free feature is reported and the corresponding fabrication and characterization are described. Chapter 6 presents the new nano material CNPs firstly applied in the Yb-doped fiber laser as a saturable absorber, this material could be used as a modulator in

a broad wavelength range. Chapter 7 concludes this thesis and proposes future works on further investigation on PD effects in rare earth doped fibers.

Chapter 2

Literature Review

This chapter reviews the reported studies on the physical mechanisms of PD including charge transfer state, oxygen deficiency center and Thulium co-dopants. Next, characterization of the PD is discussed, such as the measurement for benchmarking the PD behavior, the influence factors including population inversion level and temperature. In addition, prior studies on PD reduction are presented. Literature discussed here serve as a guidance to our research works which are demonstrated in details in the following chapters.

2.1 Physical Mechanism of PD Effect

The formation of color centers was acknowledged as the cause of PD. Color centers, attributed to the silica defects, contribute to the optical absorption spectrum of synthetic silica glass from UV to Near Infrared (NIR). An overview of different optical absorption bands of defects in synthetic silicas is given in Fig. 2.1 [37]. Although the formation of silica defects leading to color center formation is widely accepted, there are currently at least three different hypotheses to interpret the origin of PD. One assumption is that the photochemical reactions occurring under pumping involve not only trivalent ytterbium ions, but also divalent ytterbium. Namely, the charge transfer (CT) state would be the main cause of PD effect [38,39]. However, there is another, no less widespread perspective [17,38,40], that the main role in PD would be played by oxygen-deficient centres (ODCs). Co-doping of Tm in Yb-doped silica fibers is another possible mechanism for the formation of color centers.

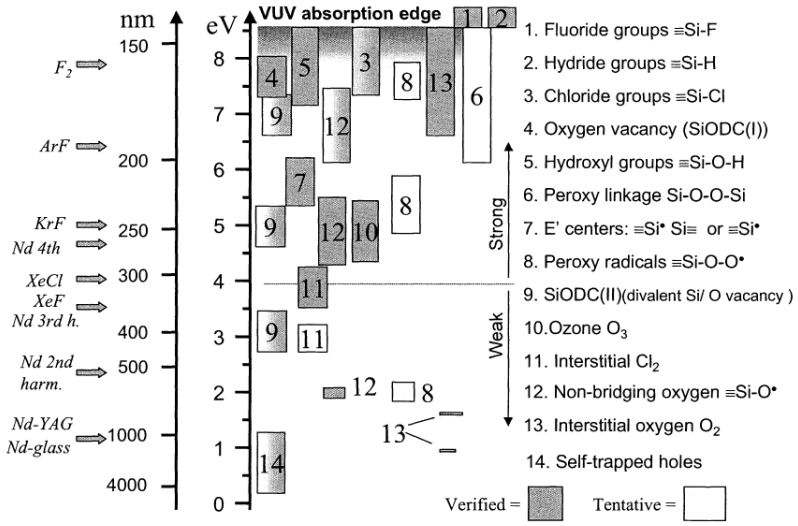

Fig. 2. 1. Main optical absorption bands in synthetic silica with their relation to the most popular lasers wavelengths. The bars height corresponds to FWHM of absorption bands. [37].

2.1.1 Charge Transfer State as the Main Mechanism in PD

Since the valence state of the Yb ions is known to be unstable [41], Yb^{2+} ions can be formed in the silicate glass matrix. A CT transition involves an electron transferring from the surrounding ligands to the central Yb^{3+} ion. Thus, an Yb^{2+} ion is formed with a hole left behind on nearby ligands. Namely, the original trivalent valence state of the Yb ion changes to divalent valence state accompanied by a released hole bound to the Yb ion, but left behind on the oxygen ligands. The generated free hole is the origin of color center. The model of Yb^{3+} excitation to a CT state and a possible transition of Yb^{3+} to Yb^{2+} is shown in Fig. 2.2.

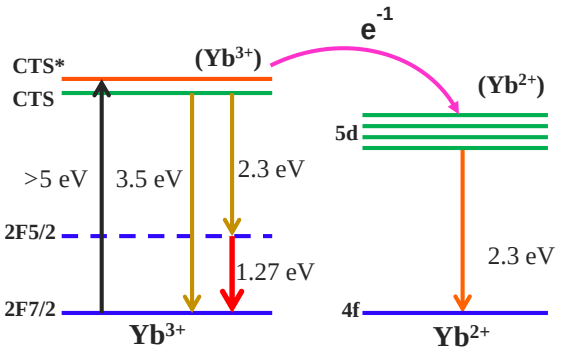

Fig. 2. 2. Model of Yb^{3+} excitation to a CT state and a possible transition of Yb^{3+} to Yb^{2+}.

The absorption spectra of Yb-doped aluminosilicate preform samples and non Yb-doped preform sample in the wavelengths ranging from 180 nm to 500 nm are shown in Fig. 2.3. The strong absorption band clearly seen at less than 250 nm wavelength is related to the presence of Yb. In the Yb-doped aluminosilicate glass prepared under reducing conditions, the absorption in the UV range is improved (see black line), due to the increment of Yb^{2+} fraction in the prepared aluminosilicate glass.

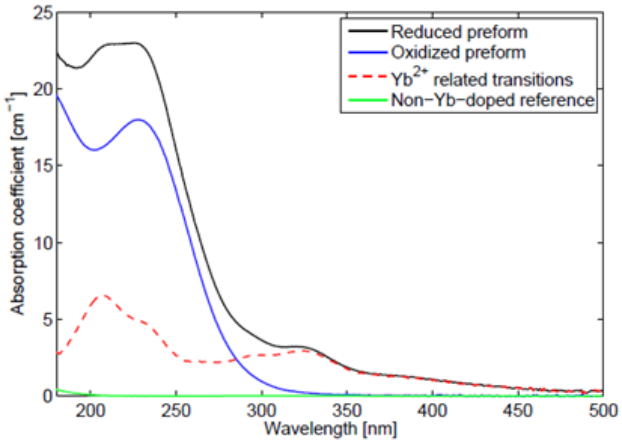

Fig. 2. 3. Absorption coefficient plots for the charge-transfer (CT)-band of the reduced preform (black), the oxidized preform (blue), the differential spectrum between the reduced and oxidized preforms(red dashed) and non-Yb-doped preform absorption spectrum (green) [18].

As shown in [18], in both the oxidized and reduced preform, the strong absorption band is centered around 230 nm which is related to CT transition between the oxygen ligands and the Yb ions. This is consistent with the optical electro-negativity formula proposed by Jørgensen [42]:

$$V_{CT} = 30{,}000[\chi_{opt}(O^{2-}) - \chi_{opt}(Yb^{3+})]cm^{-1} \qquad (2.1)$$

The location of the CT absorption band is estimated to be around 220 nm, which is approaching the absorption band present in both the oxidized and reduced Yb samples shown in Fig. 2.3. Thus, we conclude that this band is related to CT transitions. This is an important observation to explain the PD procedure occurring in Yb-doped silicate fiber lasers. CT transition results in the formation of hole related color center which induces optical losses at visible and NIR wavelengths [43].

Currently, the excitation route to reach the CT state under NIR laser diode pumping is still unclear. Some hypothesises on the excitation routes are reported. One perspective is that Yb-ion pairs which can reach the CT states may contribute to develop intermediate energy states under NIR laser diode pumping. With the increasing of Yb concentration, inter Yb atomic distances become smaller, generating a larger number of Yb ion pairs. In contrast to single Yb ion, the energy level structure of these Yb ion pairs slightly changes [44,45]. Besides the common 4f-4f transitions around 1000 nm, there are also transitions around 500 nm which can be considered as the Yb ions pair energy level. The energy required to reach the CT states is equal to the total energy of 3-4 pump photons [46].

Another possible excitation route which has been proposed is multi-photon absorption (MPA). It has been reported that MPA takes place in several kinds of rare-earth ions under the irradiation of near infrared wavelength. In this process, two (or more) photons are involved and simultaneous absorbed from ground level, or excited to intermediate level before reaching higher excited states of rare-earth ions [47,48]. Under high power pumping of near infrared wavelength, it is more likely that CT states originate from the excited ions on $2F_{5/2}$ level rather than the $2F_{7/2}$ level (ground level), this is in accord with the widely acknowledged conclusion that PD significance is dependent on the population inversion. Sufficient energy for reaching the first CT state of Yb aluminosilicate fiber can be obtained from two photons absorbed at the excited $2F_{5/2}$ level.

Both of these two hypothesises about the excitation routes to CT state are to be further verified. More studies will be necessary for thorough understanding about the CT state mechanisms behind color center formation that results in the PD phenomenon.

2.1.2 Oxygen Deficiency Centers (ODCs) as the Main Mechanism in PD

When Yb-doped fiber in heavy doping conditions, the number of Yb ions very likely exceeds the available voids in the silicate matrix. In this case, the amount of ill-valenced bonds from connection of two cations (eg. Yb-Al or Yb-Yb) has a large possibility to increase. In the germanosilicate glasses, generation of ill-valenced bonds resemble Ge-Ge or Ge-Si bonds originated from a deficiency of oxygen [17]. L. J. Poyntz-Wright observed the characteristic absorption peak of ODC in germanosilicate glass at 240 nm in the year of 1988 [49]. Under irradiation at a resonant wavelength, the heavy doped Yb fiber will release a free electron which will subsequently be trapped at nearby GeO_4 tetrahedra and form a color center called Ge(1). This Ge(1) color center possesses an absorption band peaks at 280 nm and extends to the near infrared. Appearance of this absorption band is similar to the PD loss distribution [50].

An experiment was carried out to verify that ODC is the precursor of color center in Yb-doped fiber in 2007 [17]. Two different fiber preforms were employed, an Yb-free fiber preform and an Yb-doped aluminosilicate fiber preform. The core sections of each preform were irradiated for 5 hours at wavelength of 488 nm with an intensity of 446 mW/mm^2. Absorption measurement results are shown in the following Fig. 2.4. For the Yb-free preform slice, no obvious absorption peak was detected before and after irradiation, and the irradiation induced loss was not significant as well (Fig. 2.4 (a)). Conversely, the Yb-doped preform slice has a distinct absorption peak at 220 nm (Fig. 2.4 (b)). Thus, the peak at 220 nm was attributed to the existence of Yb ions. Due to the broad 220 nm absorption peak in ODC, the employed Ar^+ ion laser which irradiates at 488 nm wavelength, may expectantly break the hypothesized ODCs in Yb-doped preforms. The breaking mechanism is considered to be two-photon absorption, free electrons are released upon two-photon absorption. One of the released electrons trapped at adjacent Aluminium or Yb sites could form a color center, resulting in PD effect. In [17], the CT state is not considered as the main mechanism of PD since the observed absorption curve shown in Fig. 2.4 (b) does not follow the typical divalent

Yb absorption [51]. The large excess loss induced after 488 nm irradiation can be the evidence for Yb-ODC model. In addition, reduction of PD by inducing high Al concentration as the co-dopant has been reported [52], this ODC model is consistent with the result, because high Al concentration can lead to more oxygen surrounding spaces generation. Thus, possibility of ODCs existence decrease, which means the hypothesized precursor to PD is suppressed.

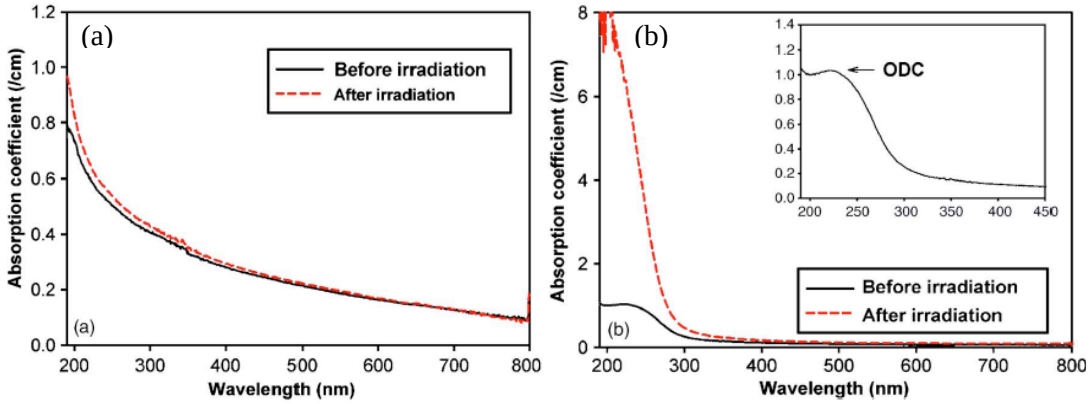

Fig. 2. 4. Optical absorption performance before and after 488 nm irradiation in (a) Yb-free fiber preform and (b) Yb-doped aluminosilicate fiber preform. The inset graph of (b) highlights the peak at around 220 nm with an enlarged scale [17].

Silica fiber defect non-bridging oxygen hole center (NBOHC) has been verified to appear in pair with the E' center [53,54]. It has been reported that Si ODC (II) defect in its lowest lying triplet manifold is the immediate precursor to the NBOHC [40]. A frequency-tripled, mode-locked Ti:sapphire laser system that can generate sub-200 femtosecond pulses in the deep UV, has been employed as the pump source to excite Yb-doped aluminosilicate fiber. Emission spectra from all optical active defects in silica fiber ranging from the UV and/or visible range were observed. As the fibers were prolonged exposed to 250 nm UV radiation, the triplet Si ODC population was significantly decreasing together with the dramatic increment of the NBOHC number density in the fiber, as shown in Fig. 2.5. This suggests that Si ODC(II) ->NBOHC excitation plays a dominant role in energy transferring in these doped glass fibers. With the generation of NBOHC, E' center appears simultaneously in the silica fiber.

Research results in [40] provide support for the speculation that the conversion of ODCs to E' centers is partly responsible to photodegradation of Yb doped fibers.

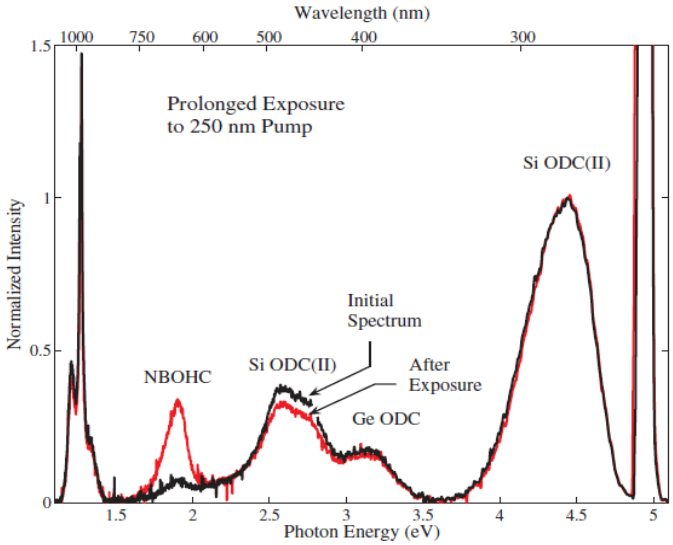

Fig. 2. 5. Spectra indicating the enhanced formation (or suppression) of optically active defects due to the Yb-doped fibers were long-term exposed to 250 nm pump [40].

2.1.3 Role of the Tm Impurity in Formation of Color Centers

Tm trace impurities effect on PD in Yb laser fibers was first addressed by Peretti et al. in the year of 2010 [55]. The fluorescence spectrum of the ytterbium-doped fiber is shown in Fig. 2.6 (black dotted) for a 500 mW pump wavelength centered at 976 nm, this fiber is phospho-aluminosilicate fiber doped with 1.7 wt% ytterbium, 3.3 wt% aluminum and 1 wt% phosphorus. There are four distinct emission bands observed across the spectral range. The four emission bands are shown separately and each band is normalized to its maximum. According to the spectroscopy database, all the emission peaks in the four bands is attributed to the presence of Tm^{3+} ions. The raw doping material for the fiber fabrication is in high purity, thus the purity of Tm contamination presents in very small quantities (lower than 340 ppbw).

To verify the relation of observed emission (black dots in Fig. 2.6) and Tm contamination, another fiber with the same ytterbium and co-doped with Tm is applied. In this second fiber, Tm^{3+} was induced intentionally and fixed to the level of 300 ppm-

wt which is 1,000 times higher than the Tm content in the first sample. The corresponding luminescence spectrum of this Yb: Tm fiber is reported in Fig. 2.6 (red line). It is obvious that the red line and the black dots can largely coincide mutually. This indicates that emissions at 300 nm, 360 nm, 475 nm and 650 nm are attributed to Tm^{3+} existence. According to the literature [56–59], the four emission bands originate from the $(^1I_6,^3P_0)\rightarrow{}^3H_6$; $^1D_2\rightarrow{}^3H_6$; $^1G_4\rightarrow{}^3H_6$ and $^1G_4\rightarrow{}^3F_4$ transitions. As illustrated in [56], the Tm luminescence is obvious in the Yb doped fiber as a result of energy transfer from the present Yb^{3+} ions pumped at 976 nm.

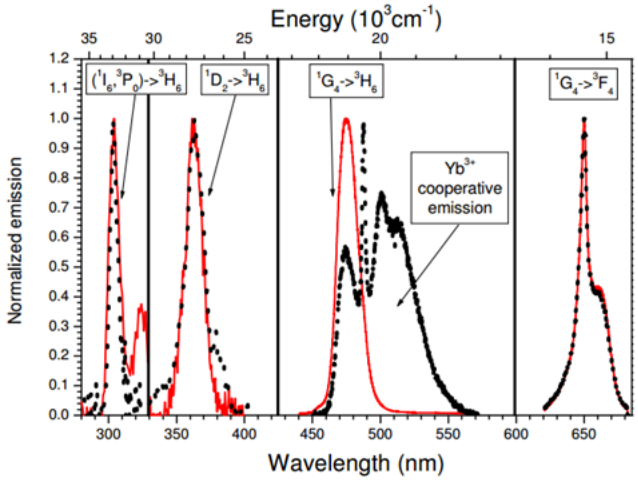

Fig. 2. 6. Normalized emissions the ytterbium doped sample of (black dotted) and Yb-Tm co-doped sample as red lines [55].

To clearly explain the multi-step process for these up-converted emissions from Tm^{3+}, the UV-visible-infrared energy level diagram of Tm^{3+} in silicate is depicted in the following Fig. 2.7 [55]. Green arrows on the diagram indicate the luminescence emissions. It is known that the 976 nm laser pump doesn't resonate at Tm^{3+} energy level difference for the step 1. Whereas, fortunately, Yb^{3+} ions serve as an intermediation, the Yb^{3+} ions can transfer 976 nm pumping energy to Tm, which is due to the Yb^{3+} (~10^4 cm^{-1}) is close to the $^3H_5$ level absorption (~8,500 cm^{-1}) of Tm^{3+} as shown in the step 1 of the Fig. 2.7. After excitation to $^3H_5$ level, non-radiative relaxation downward the $^3F_4$ level (~6 kcm^{-1}) is followed, excited state absorption (ESA) occurring in the $^3F_4$ level of via 976nm pump or energy transfer up-conversion is

attributed to the presence of other Yb^{3+} ion exciting to the ($^3F_2$-$^3F_3$) level and non-radiation to the $^3H_4$ level (~13 kcm^{-1}). Similarly, further up-conversion processes towards higher excited levels continue in consequence of the combined effect of the resonance with the pump wavelength or the Yb^{3+} emission wavelengths and the long decay lifespan of excited levels. As shown in the Fig. 2.7, up-conversion can cascade up to the highest $^3P_0$, and $^1I_6$ levels. Obviously, excitations to the highest energy level is responsible of emission in the UV window as shown in the Fig. 2.6.

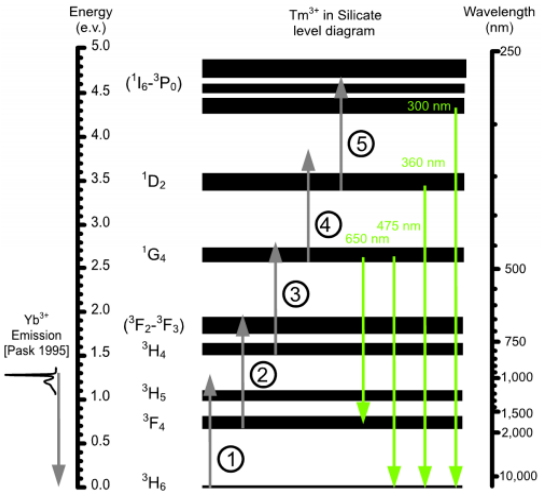

Fig.2. 7. Schematic of up-conversion processes in the Yb-Tm co-doped fibers [55].

Comparison of the host absorption spectrum and the up-conversion emission bands of Yb-doped fiber is reported in [55], as shown in the following Fig. 2.8. There is obvious overlap between the glass host absorption and the UV emissions measured from the Yb doped fiber sample. Thus, it can be deduced reasonably that the silicate matrix can absorb the energy corresponding to these emission bands. Since UV light is widely known to result in color centers in silica-glass [60], silicate matrix absorbed the UV might lead to the formation of colour centres which manifest as PD.

However, different perspective about the role of Tm in PD of Yb-doped fiber is demonstrated in [61], which concludes that the existence of Tm impurity is not the reason of PD effect occurring in Yb-doped fiber, PD in Yb: Al silica fibers is an intrinsic feature of this core material, Tm co-dopants reaching more than 10 mol-ppm

can cause a second path of PD by Tm-assisted path of color center formation. In the following Fig. 2.9 (a), VIS fluorescence intensities of two fibers with different Tm concentration are compared. Obvious fluorescence is observed in # 6 fiber with a Tm concentration of 7 mol-ppm. In contrast, fiber #3 with Tm concentration about 0.08 mol-ppm at the trace impurity level only shows a week blue fluorescence. As illustrated by the inset of the Fig. 2.9 (a), the intensity at 473 nm emission increases with growth of the Tm concentration. The 473 nm emission signal keeps increasing proportionally with Tm content at the beginning, but turns to be weakened at the higher amount of Tm, likely due to the decreasing molar ratio of Yb/Tm.

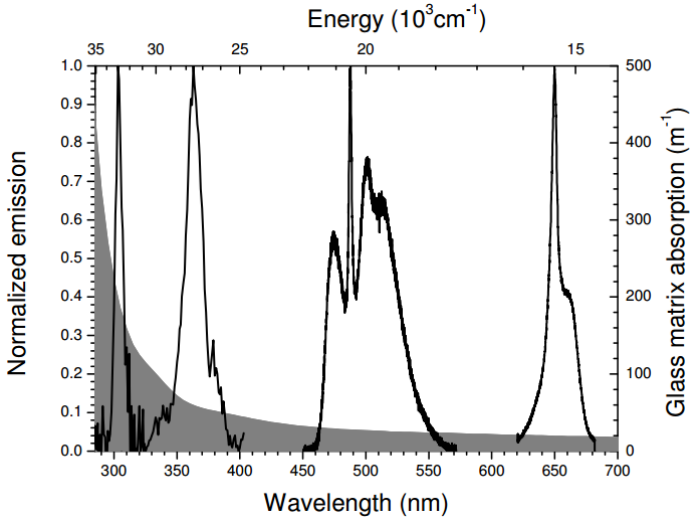

Fig. 2. 8. Spectrum comparison of the host absorption (grey-shaded area) and the up-conversion emission bands of Yb-doped fiber (black line) [55].

Fig. 2.9 (b) shows the PD kinetics of intentionally induced Tm codpants fibers (# 6-#11) compared to Yb-fibers with only trace impurities of Tm (#1-#3). All of the fibers under test have the same Yb concentration and are core pumped at 976 nm with a constant Yb inversion at 0.46. The measurement results lead to the conclusion that trace impurities of Tm (below 1 mol-ppm) do not have significant impact on the characteristics of PD in Yb-doped fiber. The concentration of Tm has to reach at least 10 mol-ppm to result in a strong acceleration of the PD process, and the PD induced loss at the final equilibrium state increases remarkably as well. However, in the fiber

#11 with the highest Tm content, after reaching the maximum point, the PD loss begins to decrease. It is speculated that this interesting behavior is on account of an intermediate state in PD bleaching path, and bleaching effect might happen due to the UV or VIS photons from Tm emission.

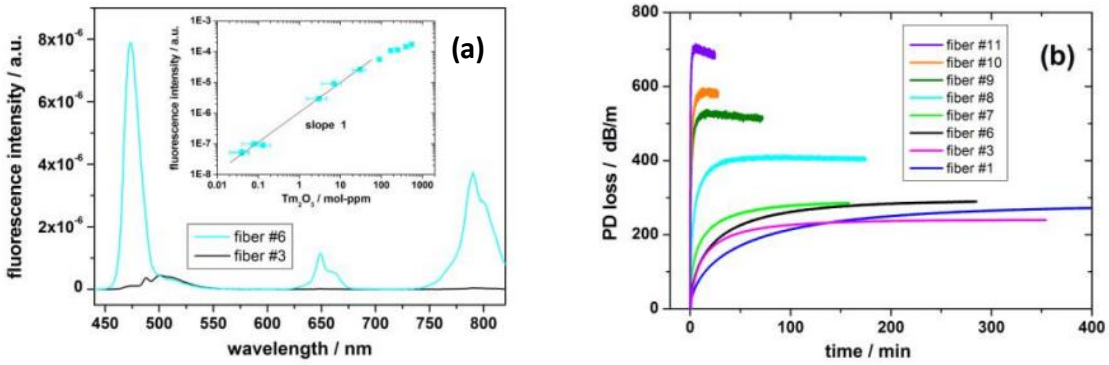

Fig. 2. 9. (a) NIR-induced fluorescence spectra of the low Tm co-doped fiber #3 in comparison to fiber #6; inset: Tm fluorescence intensity varying with Tm concentration, (b) PD kinetics of Tm co-doped fibers compared to Yb fibers with only trace impurities. Tm content increases along fiber #1 to fiber #11 [61].

2.2 Characterization of PD effect in Yb doped fiber

PD in Yb-doped fibers is a time-dependent effect which is commonly characterized by an exponential build-up function. Typical parameters of the function, the saturated PD loss α_{eq} (equilibrium for long-term measurements), a typical time constant τ and the stretching parameter β, provide the characteristics of PD effect. In this section, we will introduce the typical experimental setup for the measurement of PD and analyse the influential factors of PD characteristics.

2.2.1 Typical experimental setup for Yb-doped fiber PD measurement

J. J. Koponen firstly proposed a measurement techniques to quantify PD effect induced loss in the year of 2006 [9]. This measurement method is to quantify the observation of transmission changes at visible wavelengths range before and after PD. The typical measurement method for characterization of PD is shown in Fig. 2.10 [9]. This setup allows to measure the transmission spectra of white light propagating into the Yb-

doped fiber before and after pumping by laser diode, the PD induced excess loss spectrum is calculated by subtracting the spectrum before pumping and after pumping. As shown in the Fig. 2.10, HeNe laser wavelength of 633 nm was applied as the reference wavelength for the transmission spectrum measurements. Similarly, other sources of different reference wavelength can be utilized as well, as long as they are far from the Yb band and within the broad color center absorption band that induce the excess loss. This typical setup is limited to single mode, core pumping fibers, but can be used with different Yb-doped fibers.

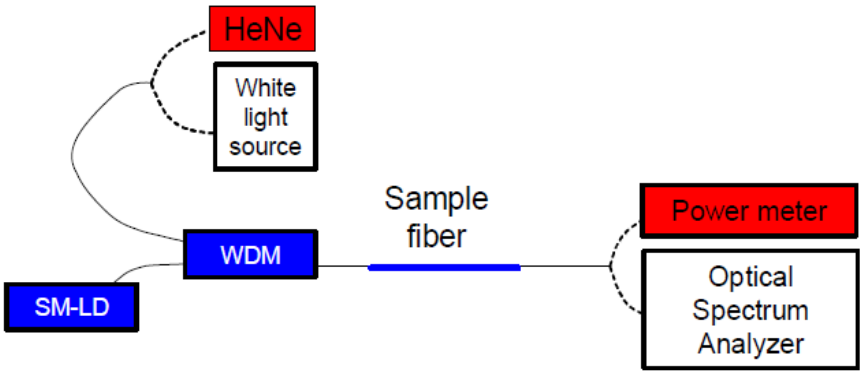

Fig. 2. 10. Setup for characterization of PD, where a white light source propagated the Yb-doped fiber before and after pumping by laser diode, the PD induced excess loss spectrum is calculated by subtraction the spectrum before and after the pumping. [9].

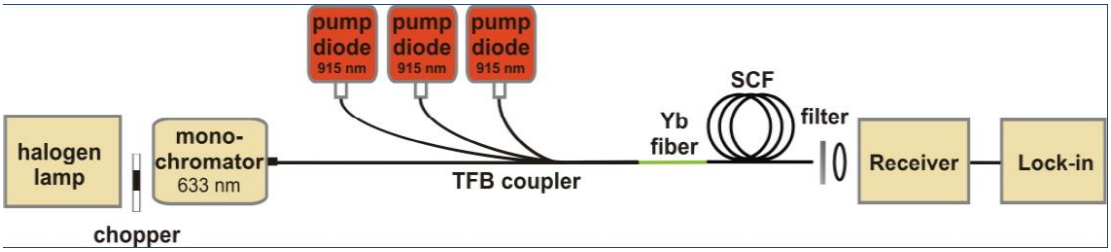

Fig. 2. 11. Setup for characterizing the fiber transmittance performance during PD by excited Yb ions [62].

To measure the temporal evolution of PD, an experimental setup has been proposed in [11,62], as shown in Fig. 2.11. The principle of the temporal evolution measurement is similar to the transmission loss measurement shown above.

The difference between the fiber transmittances needs to be recorded in a constant time interval. The fiber transmittance is calculated by

$$T(t) = P(t)/P_0 \tag{2.2}$$

where P_0 and P(t) depict the respective transmitted probe powers before and during PD. A stable, broadband light source (halogen lamp) and the chopper/lock-in technique are employed to facilitate the PD kinetics measurement with low-noise. The core excess loss was calculated through time-dependent PD curve by

$$\alpha(t) = -10\log(T(t))/L \tag{2.3}$$

the unit of $\alpha(t)$ is dB/m, $\alpha(0) = 0$, L is the length of fiber under test. The formula applied to fit the temporal evolution is

$$\alpha(t) = \alpha_{eq}[1 - \exp(-(t/\tau)^{\beta})] \tag{2.4}$$

In this fitting formula, α_{eq} is the saturated PD loss at equilibrium state, τ is the typical time constant τ and the β is the stretching parameter. A typical PD temporal evolution fitting curve is depicted in Fig. 2.12 with a set of parameter values used in this example.

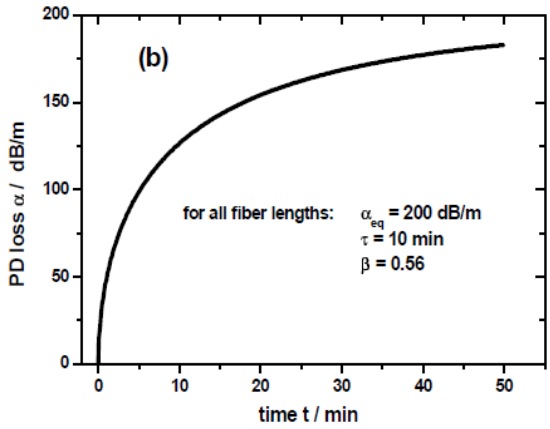

Fig. 2. 12. Exemplary PD loss curve corresponding to the stretched exponential function of Eq. (2.4) [62].

2.2.2 Yb inversion dependence of PD characteristics

Pump-induced PD was attributed to the number of excited Yb ions and can be characterized in accelerated PD procedure at high Yb inversions [11,63] . It has been found that the relaxation to well-defined equilibrium states of the core excess loss is dependent on the Yb inversion [11]. The measurement setup is shown in the Fig. 2.13, and the Yb-doped fiber under test is cladding pumped by a 915 nm laser diode. Modulated light from a halogen lamp with monochromator is used as a probe light source with 633 nm emission wavelength and spectral width of 25 nm. The length of the fiber under test is 5 cm. Lasing and strong amplified spontaneously emission (ASE) are unwanted in the PD measurement. For this purpose, in the setup, the feedback is suppressed by the multimode fiber at one side and by an angle connector at the output end of the single cladding fiber, as shown in the Fig. 2.13.

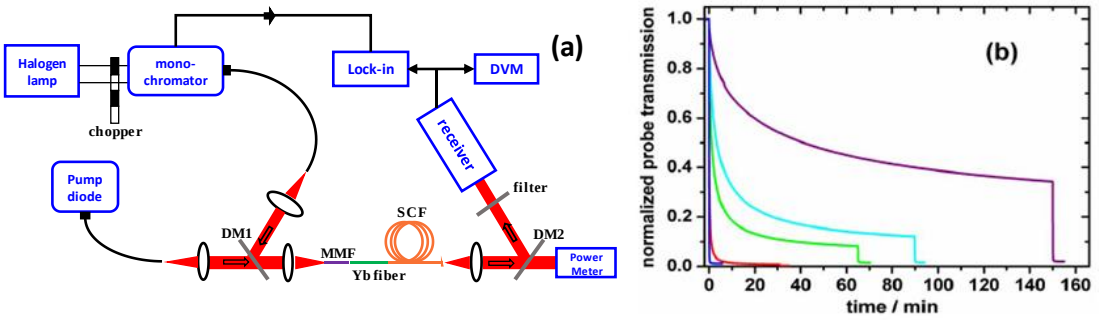

Fig. 2. 13. (a) Experimental setup for measuring PD, the modulation frequency of chopper is from 4 Hz to 10 kHz. Photodarkening dynamics is definitely slow than the chopping frequency; (b) Normalized probe transmission vs time measured in a Yb-doped fiber with a length of 5 cm using different initial cladding pumping powers: 1 W (lilac), 1.8 W (cyan), 2.1 W (green), 3.7 W (red) and 6.1 W (blue); after applying sufficient initial pump power, the Yb fiber core was "fully darkened" by applying a 13.2 W pump power (steep decrease section) [11].

The temporal transmission curves of the Yb-doped fiber under test are shown in the Fig. 2.13 (b). It is easily observed that with the larger input pump power, the loss of the probe light transmission is accelerated. Additionally, the final equilibrium state of probe light transmission is larger under higher pump power, which suggests more severe PD effect occurring under higher power pumping. After a nearly constant

transmission level had been reached with the selected pump power, the highest pump power (13.2 W) available in this setup was induced for strong darkening of the fiber core, a transmission of 0.003 to 0.02 was found for all fibers investigated under different selected cladding pump of 915 nm laser diode.

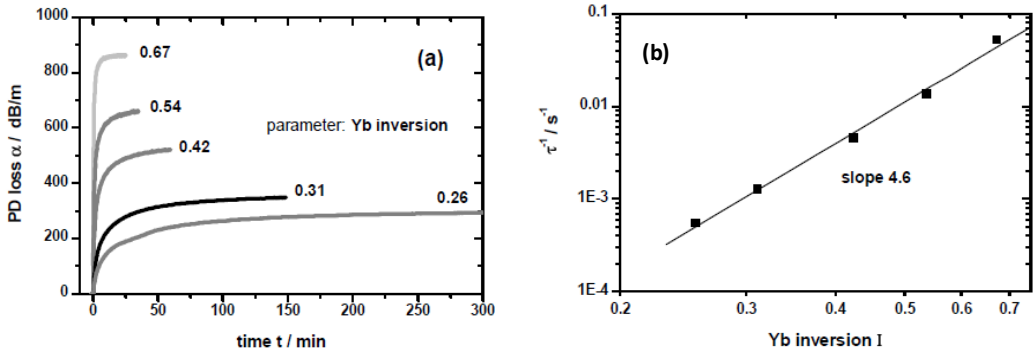

Fig. 2. 14. (a) PD induced temporal excess loss under test with different Yb inversions, (b) characteristic τ^{-1} (PD rate constant) of fiber under test with different Yb inverisons [62].

Higher pump power indicates a higher population inversion level of an identical fiber. For the case of short fiber piece, the inversion level of Yb can be calculated by Eq. (2.5) and Eq. (2.6)

$$I = \frac{\sigma_{abs}}{\sigma_{abs} + \sigma_{em}} \cdot \frac{1}{1 + P_{sat} / P_P} \tag{2.5}$$

$$P_{sat} = A \cdot h\nu_p / ((\sigma_{abs} + \sigma_{em})\tau_{Yb}) \tag{2.6}$$

where P_p is the launched pump power (photon energy is $h\nu_p$), σ_{abs} and σ_{em} are the absorption and emission cross sections at the pump wavelength, P_{sat} is the saturation pump power, A is the fiber cross section, and τ_{Yb} is the Yb^{3+} near-infrared fluorescence lifetime [13]. The two main parameters of the PD characteristics, time constant τ and saturated PD loss at equilibrium state α_{eq}, are investigated under different Yb inversion level respectively as shown in the Fig. 2.14 [62]. The inversion level is defined as n_2/n_0, the ratio of upper state population density to total ion density. In the condition of [62], Yb-doped fibers under examination are with core and cladding diameter of 10 μm and 125 μm, σ_{abs} is $5.6*10^{-25}$ m^2, τ_{Yb} is 830 us, the pump wavelength is 915 nm and its

maximum power is 20 W [62]. According to the equation and the corresponding parameters, when launched pump power is 12.6 W, the inversion level is 0.64, it is demonstrated by [62]. The highest inversion level 0.67 presented in Fig. 2.14 is at the launched pump power of 20 W. From the Fig. 2.14 (a), under the highest inversion demonstrated here (I = 0.67), the PD curve of temporal evolution saturates within 25 mins measurement. However, under the condition of lower Yb inversion, the PD procedure needs much longer time to reach the final equilibrium saturation state. It is obvious that α_{eq} is proportional to the inversion level. Furthermore, the relationship of the PD rate to the inversion level is shown in the Fig. 2.14 (b), fiber under test pumped to the higher inversion level has a faster PD rate.

2.2.3 Temperature dependence of PD characteristics

It has been reported that the characteristics of PD kinetics of Yb-doped fiber is strongly affected by the temperature [64,65]. It has been observed that enhanced temperature can result in PD rate accelerating. In [65], fiber samples in short piece (1 to 2 cm) with high Yb concentration were utilized to guarantee a homogeneous Yb inversion of 0.46 along the fiber. Temporal evolution measurement was investigated under wide temperature range from from 77 to 773K. The measurement results are shown in the Fig. 2.15.

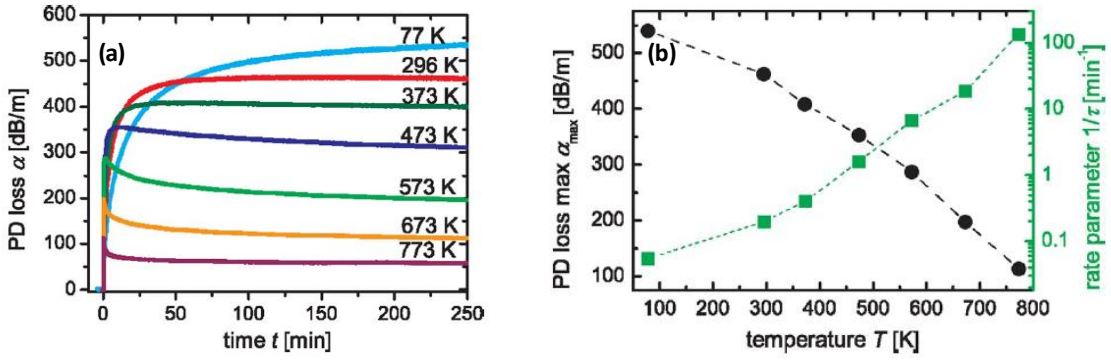

Fig. 2. 15. (a) Temporal evolution of PD loss at different temperatures during pumping, (b) Maximumm PD loss and rate constant vary with temperature growth [65].

From the Fig. 2.15 (a), the increasing tendency of the PD induced loss at the beginning seems to follow the typical fitting function Eq. (2.4); this tendency is most obvious for the measurement at 77 K and 296 K. The PD induced loss evolution at higher temperature ranging from 373 K to 773 K, reaches the loss maximum in the initial period, and then the PD loss starts to decrease. The maximum PD loss value, the rate constant, and the stretching parameter are determined according to the Eq. (2.4). Fitting results are shown in the Fig. 2.15 (b). It is clearly observed that, for highly doped Yb fiber, the maximum PD induced loss value decreases at higher temperatures, whereas the PD rate accelerates with temperature. However, for the Yb fiber with low concentration, things are different [64,65]. Measurement of temperature dependence of PD temporal loss evolution for a low concentration Yb-doped fiber is shown in the following Fig. 2.16 [65]. The PD speeds up noticeably with temperature increase. However, only at the temperature of 573K, PD loss maximum value could be calculated by fitting, whereas for lower temperature at 473 K and 296 K, there is no sure results by fitting with Eq. (2.4) for the temporal loss evolution plots.

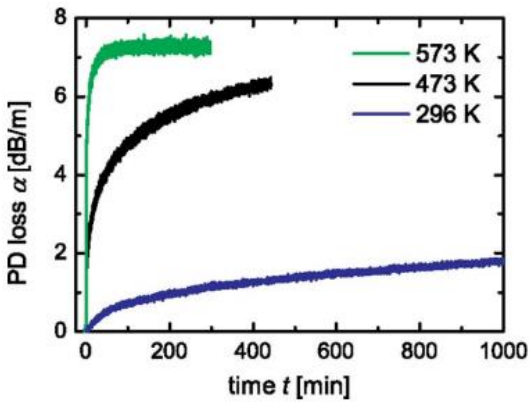

Fig. 2. 16. PD temporal loss evolution of a low Yb concentration fiber at different temperatures [65].

For the high concentration Yb-doped fiber, from beginning to the loss maximum, the rapid PD process is considered to be less affected by thermal annealing at high temperature. In contrast, Yb-doped fiber in the low concentration (Yb_2O_3 < 0.3 mol %), the PD loss temporal evolution is very low at the beginning and gradually slows down.

In these scenarios, the experimental PD rate is dominated by thermal processes. This investigation of temperature influence on PD is very important in practical PD measurement experiment. In Yb-doped fiber under pumping, the optical absorption will induce temperature increase and consequently lead to an acceleration of the PD rate. However, for a long measurement time, a lower PD loss value at finial equilibrium state may be achieved.

2.3 PD Reduction in Yb-doped fiber

Pump-induced PD is a widely acknowledged harmful process hindering the performance of Yb-doped fiber laser and amplifier in various applications. Several methods have been reported to reduce PD effect in Yb-doped fiber lasers. The techniques to reduce the PD effect can be divided into two categories, one is modifying the fabrication atmosphere of the preform of Yb-doped fiber and the other one is optimization of the core composition of the Yb-doped fiber.

2.3.1 Preparation in reducing atmosphere and hydrogen loading

For a preform of Yb-doped fiber fabricated under reducing conditions, a part of the Yb-ions will change to divalent valence state from the original trivalent valence state. The PD process in this sort of Yb-doped fibers is schematically depicted in the following Fig. 2.17 [18]. Once excitation to the upper CT-state, an electron shifts from the oxygen ligands to the nearby Yb^{3+} ion, and a free hole can be generated from an oxygen ligand between an Yb^{3+} ion and an Yb^{2+} ion. This generated hole very likely recombines with the electron originated from the pre-existing Yb^{2+} ion from the fiber prepared in reducing condition rather than recombine with the formed Yb^{2+} ion in the process of excitation to CT State. The net structure can be simply considered to result in a position shifting of the Yb^{2+} ion in the net structure of Yb clustering. Therefore, less PD induced loss at visible and NIR range can be observed. The PD measurement results for fibers under different preparation conditions is shown in the Fig. 2.18. No obvious PD loss can be observed for the preform sample prepared in reducing condition under UV-irra-

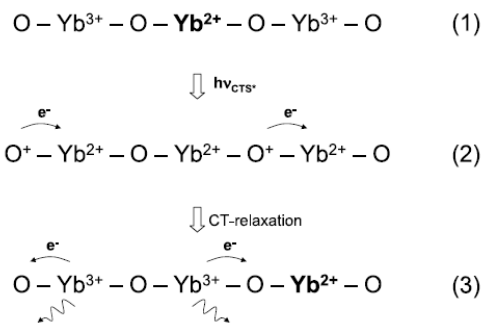

Fig. 2. 17. Excitation to the higher CT-state (CTS*) in a glass with pre-existing Yb^{2+} ions from the reduction condition results in a characteristic Yb^{3+} luminescence by CT-relaxation. The net result of the process 1-3 is merely a shifted position for the Yb^{2+} ion [66]**.**

-diation. The results from [18] are in accordance with previous results from [67]. [18] reported that no PD induced loss could be observed in transmission measurement for an Yb-doped fiber prepared in reducing condition under 976 nm radiation.

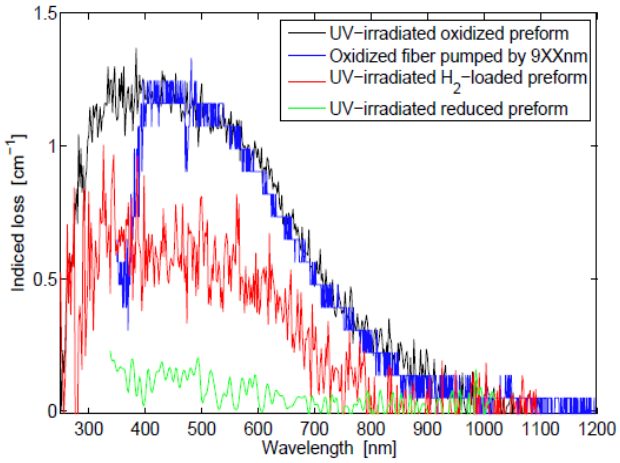

Fig. 2. 18. PD induced transmission loss measurement of prepared preforms under different conditions. [18].

An alternate method to reduce PD is by hydrogen loading of the Yb-doped fiber in a pressure chamber at room-temperature. In contrast with PD bleaching at high-temperature annealing in a H_2/N_2 atmosphere, the hydrogen loading of the glass material is different, since the hydrogen molecules do not undergo chemical reaction at room-temperature. Once the Yb-doped fiber is excited to the CT-band, the H_2 molecules will react with the generated holes on the oxygen ligands from CT process, thus forming hydroxyl groups and Yb^{2+} ions. The whole procedure is illustrated in Fig.

2.19 [18]. The H_2 molecules annihilate hole related color centers and PD induced loss decreases at visible and NIR wavelengths range, as shown in the red curve in the Fig. 2.18. However, as shown in the step 4 in the Fig. 2.19, the formed Yb^{2+} ions can be further photo-ionized, resulting in the formation of Yb^{3+} ions and free electrons. This will generated electron related color centers in hydrogen loaded Yb-doped fibers. This increasing number of electron related color center seems to be the reason why PD of the H_2 loaded Yb preform remains at a non-negligible levels at visible and near infrared wavelengths.

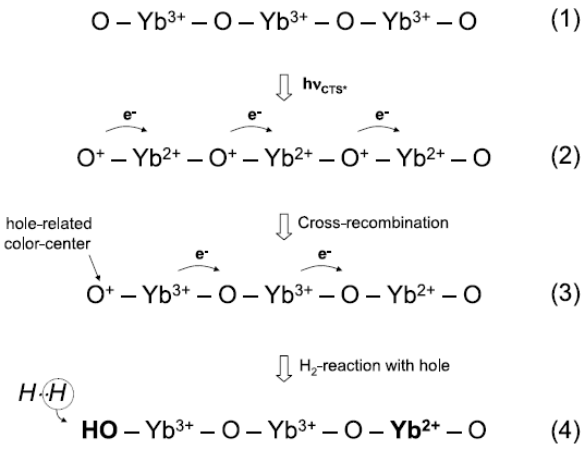

Fig. 2. 19. The hole related color center are generated form step 1-3, and eliminated by an electron under H_2 loaded case. [18].

2.3.2 Optimization of the core composition

The role of aluminium (Al) or phosphorus (P) as co-dopants in rare earth doped fiber was first proposed in the year of 1986 [68]. Influences of Co-doping on the fluorescence and structural properties of neodymium-doped silica glass were investigated in [68]. It was found that a slight doping level of Al or P was enough to disperse the clustering Nd ions in a glass matrix and facilitate lasing fluorescence of Nd doped fiber. Nd ions can be perfectly incorporated into a silica glass network by introducing Al or P as co-dopants. In the liquid state, Al oxide Al_2O_3 dissolves well in SiO_2, while Nd_2O_3 can dissolve in Al_2O_3 as well. As a consequence, $AlO_4/_2$ and/or $AlO_6/_2$ behave as solvation shells to facilitate Nd^{3+} ions distribution in the SiO_2 network. Similarly, it is well known

that P_2O_5 was good solubility in SiO_2 in the liquid state. $PO_{5/2}$ and/or $PO_{4/2}$ coupled with SiO_2 constitute the solvation shell for Nd^{3+} ions in the silica network.

For the Yb-doped fiber, the use of the Al and P co-dopants to suppress PD effect was proposed in [52,69]. It has been concluded that high Al concentration into Yb-doped fiber is effective to suppress PD [52] and P is more effective than Al to suppress PD in Yb-doped fiber, especially for operation at high upper level population [69]. In [20], by increasing Al content as a co-dopant, PD in Yb-doped fibers could be reduced, as shown in Fig. 2.20 (a). Fiber #1Al to #5Al share the same amount of excited Yb ions [Yb^*], the number of excited Yb ions [Yb*] was calculated as the product of the concentration of Yb ions and Yb ions inversion. Among the five fiber samples under test, #1Al has the lowest Al content and the Al content increases successively until reaching the maximum in #5Al. From the Fig. 2.20 (a), it is quite obvious that with the same amount of excited Yb ions, PD effect is suppressed with higher Al content.

While doping with Al or P can actually decrease the PD loss, however, both of these two methods have several serious disadvantages. High Al concentration will increase the reflective index of fiber core, and it leads to an enhanced core numerical aperture (NA) and reduced beam quality. On the other hand, heavy P concentration will cause a harmful central notch in the refractive index profile by P evaporation. In addition, similar to Al co-doping, P co-doping results in high core NA that makes the preparation of large-mode-area (LMA) fibers more complicated. Furthermore, the Yb absorption and emission cross sections decreases as well by co-doping with P [70].

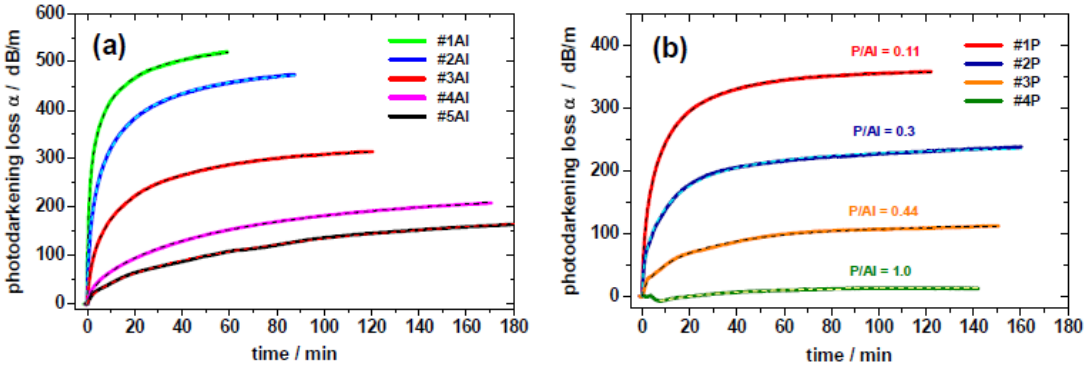

Fig. 2. 20. Photodarkening loss with time of the co-dopant fibers under different series (a) #Al and (b) #P. The respective fitting procedure with the stretched exponential function are shown as dashed lines [20].

The influence of the combination of Al and P was also investigated in [20]. As shown in Fig. 2.20 (b), when the number of excited Yb ions and the Al content are fixed as for a series of fiber samples, the P content keeps increasing from # 1P to # 4P. Apparently, additional co-doping with P can lead to further significant reduction of the PD loss. It has been concluded that co-doping P and Al at an equal concentration can lead to almost fully suppression of PD.

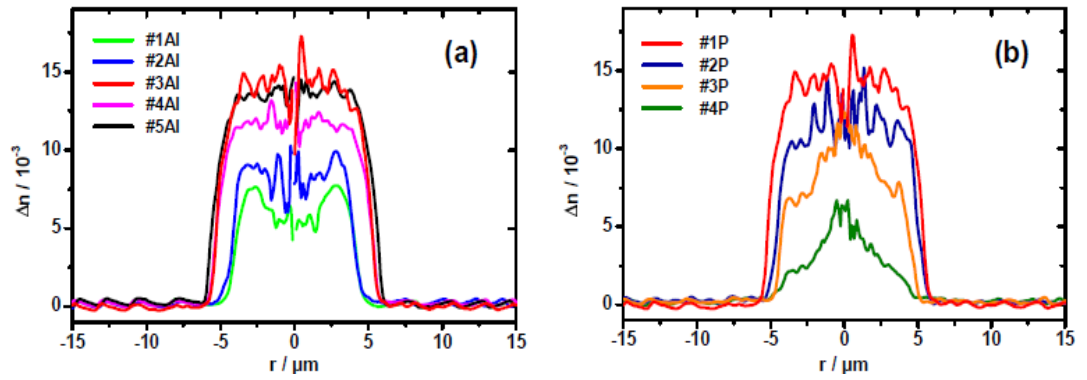

Fig. 2. 21. Refractive index profiles of the co-dopant fibers under differentseries (a) #Al and (b) #P [20].

Refractive index (RI) profiles which are measured on the preforms and then transferred to fiber radius r scale are shown in Fig. 2.21 [20]. In series of Al co-doped fiber samples, the refractive index increases with higher Al content, as shown in Fig. 2.21 (a). In the series of P co-doped fiber samples, the refractive index decreases

regardless of the P concentration, this anomaly results from the interaction of Al and P ions, which was explained in fibers without Yb [71]. As indicated by the Fig. 2.21 (a) and (b), all fiber samples under test are free from a central index notch by this combination of two co-dopants. Fortunately, reduction of the core refractive index (Fig. 2.21 (b)) in the series of P co-doped fiber is accompanied by a reduction of PD effect as shown in Fig.2.20 (b). This will not cause adverse effects on preparation of large-mode-area (LMA) fibers.

Chapter 3

Pump Wavelength Dependence of Photodarkening in Yb-doped Fiber

3.1 Background

It has been known that the pump-induced PD is tightly associated with the number of excited Yb ions, namely PD equilibrium depends on Yb ions population inversion level [12,63]. As discussed in Section 2.2.2, it has identified the relationship between PD saturation loss and inverted Yb ions [13]. Therefore, higher Yb concentration and more intensive pump power can lead to severe PD [12,72,73]. However, the previous studies assumed that the PD behavior follows Yb inversion regardless of pumping wavelengths.

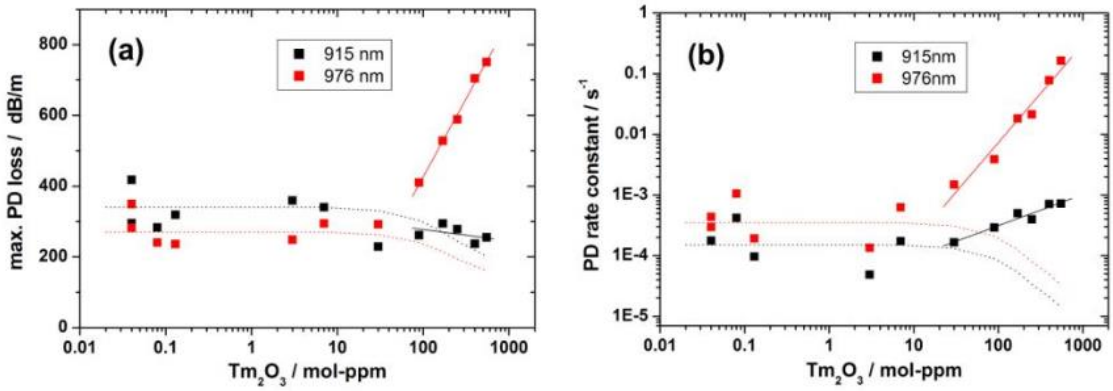

Fig. 3. 1. PD parameters (Yb inversion=0.46) varies with the Tm concentration for core pumping at 976 nm (red squares) and cladding pumping at 915 nm (black squares): (a) PD loss maximum, (b) PD rate constant [61]**.**

There is another route to induce PD in Yb-doped fiber as reported in [55,61,74]. A non-negligible level of Tm concentration can accelerate the PD effect in Yb: Al as well as Yb: P fibers through the so-called "Tm path to UV" process as discussed in Section 2.1.3 [55,61]. In such process, the energy transfer from Yb to Tm was proposed as a plausible route to induce the PD, and the process is pump wavelength dependent in that

the route becomes more efficient at 976 nm than 915 nm, thus causes more PD under 976 nm pumping [61]. As shown in Fig. 3.1, when the Tm concentration is less than 10 mol-ppm, no obvious influence of Tm on the measured PD loss and rate constant is only observed. On the contrary, 976 nm core pumping leads both PD loss and rate constant strongly increasing after the Tm concentration reaching 10 mol-ppm. This Tm induced PD path is strongly associated with multi-step Tm excitation including energy transfer from Yb ions to Tm ions and ESA of pump photons [55]. 976 nm affects the PD parameters of these fibers more significantly than pumping at 915 nm due to better overlap with the ESA spectrum of 976 nm pumping.

3.2 Theory

3.2.1 Yb^{3+} Energy Level and Basis for Inversion Level Calculation

An Yb^{3+} ion has a very simple electronic level structure, with only one excited state manifold ($^2F_{5/2}$) and the ground-state manifold ($^2F_{7/2}$), which consists of 3 and 4 sublevels, respectively. The Yb^{3+} energy levels based on the germanosilicate host are shown in Fig. 3.2 (a). The typical Yb^{3+} transition cross sections in a germanosilicate glass are shown in the Fig. 3.2 (b) [24].

As shown in the Fig. 3.2 (b), the two significant absorption peaks are located at 916 nm and 976 nm, becoming the prominent pumping wavelengths for laser and amplifier construction. Around 916 nm, there is a broad absorption bandwidth which can accommodate the pump light source with a broad linewidth. On the other hand, the absorption bandwidth at 976 nm is sharp, thus leading to a strict small linewidth requirement for the pump source. But the 976 nm pumping offers shorter absorption length and smaller quantum defect than the 916 nm counterpart, since 976 nm is more close to the lasing wavelength. Hence, the two wavelengths offer unique properties which can be selectively utilized for specific applications. For instance, the broad bandwidth at the 916 nm is more advantageous for high power cw lasers when laser wavelength drifting over a driving current is acceptable for the interest of cost. On the

other hand, the 976 nm pumping is more favourable when short absorption length is critical such as high power ultrafast laser construction. Hence, I investigate both the important wavelengths in my PD study.

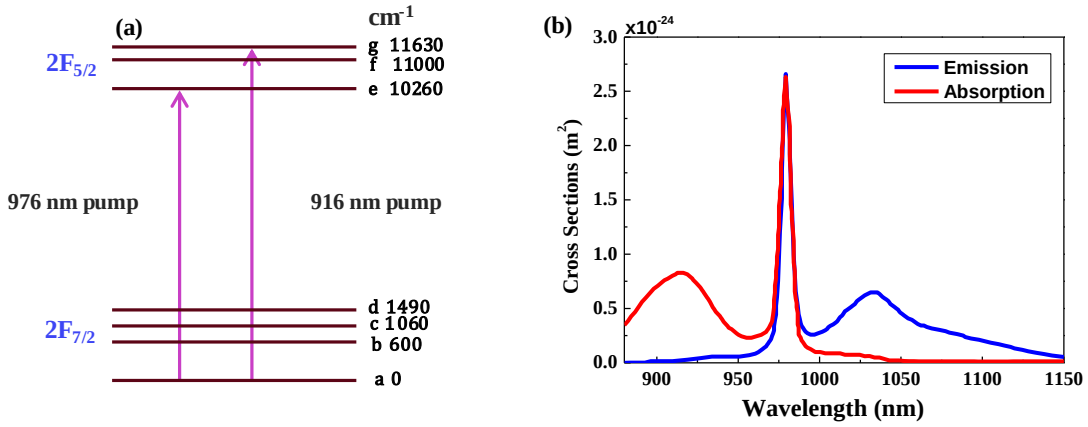

Fig. 3. 2. (a) Yb3+ energy level diagram, (b) Typical Yb transition cross sections of a germanosilicate glass [24] **.**

In my experiments, ensuring constant inversion level is the prerequisite of investigation when comparing both the wavelengths in the context of PD to study pump wavelength dependence of a PD effect. Therefore, accurate inversion level calculation is critical before experiment. ASE is efficiently suppressed in this experiment and purely homogenous broadening is assumed. Under this condition, a simplified numerical model of a Yb-doped fiber laser can be established similarly to the erbium doped fiber laser [34,75–77].

In Yb-doped fiber laser, population of upper and lower states are governed by the following rate equations [34]:

$$\frac{dn_2}{dt} = (R_{12} + W_{12})n_1 - (R_{21} + W_{21} + A_{21})n_2 \tag{3.1}$$

$$\frac{dn_1}{dt} = -(R_{12} + W_{12})n_1 + (R_{21} + W_{21} + A_{21})n_2 \tag{3.2}$$

From Eq. (3.1) and Eq. (3.2), the excited state population values at the steady-state are obtained:

$$n_2 = \frac{R_{12} + W_{12}}{R_{12} + R_{21} + W_{12} + W_{21} + A_{21}} \tag{3.3}$$

$$n_1 + n_2 = 1 \tag{3.4}$$

transition rate for pump light is given by:

$$R_{12} = \sigma_{12}^{(p)} I_P / h\upsilon_p \quad , \quad R_{21} = \sigma_{21}^{(p)} I_p / h\upsilon_p \tag{3.5}$$

transition rate for signal light is given by:

$$W_{12} = \sigma_{12}^{(s)} I_S / h\upsilon_S \quad , \quad W_{21} = \sigma_{21}^{(s)} I_S / h\upsilon_S \tag{3.6}$$

where $\sigma_{12}^{(p)}$ and $\sigma_{21}^{(p)}$ are the absorption and emission cross sections in m^2 at a pump wavelength, $\sigma_{12}^{(s)}$ and $\sigma_{21}^{(s)}$ are the corresponding values at a signal wavelength. I_p and I_s are the pump and signal intensities (W/m^2). A_{21} is the constant for spontaneous emission. $R_{12}, R_{21}, W_{12}, W_{21}$ and A_{21} are in the unit of s^{-1}. It is obvious that the n_1 and n_2 are determined by the I_P and I_s which are dependent on pump power and signal power along the fiber [34]:

$$\frac{dP_P}{dz} = \eta_P(\sigma_{21}^{(p)} n_2 - \sigma_{12}^{(p)} n_1) N_{tot} P_P \tag{3.7}$$

$$\frac{dP_S}{dz} = \eta_S(\sigma_{21}^{(s)} n_2 - \sigma_{12}^{(s)} n_1) N_{tot} P_S \tag{3.8}$$

where P_p and P_s are the pump and signal power, N_{tot} is the total density (m^{-3}) of Yb ions, and η_p and η_s are an overlap factor accounting for a transverse overlap of the optical beam with the dopant ions. In the experiment, the incident pump beam is single-moded through fibers under test. An overlap integral between the dopant and the optical mode in a core pumping configuration can be defined by the following formula [76].

$$\eta_{core\_pumping} = \int_0^{2\pi} \int_0^b i_1(r,\phi) r dr d\phi \tag{3.9}$$

where $i_1(r,\phi)$ is the normalized single mode optical intensity of pump light in radial and azimuthal coordinates and b is the Yb doping radius [76]. For cladding pumping

configuration, the Eq. (3.9) needs modification to factor in beam extension to the cladding area by adding a core to cladding area ratio as:

$$\eta_{claddig\_pumping} = \frac{Core\_Area}{Cladding\_Area}\int_0^{2\pi}\int_0^b i_1(r,\phi)rdrd\phi \tag{3.10}$$

In our experiment, fibers under test are all around 1 cm in length for the purpose of suppressing the unwanted ASE and achieving uniform inversion along the fiber length. Furthermore, fibers in such a short length hardly gather sufficient gain for stimulating signal power. Therefore, in the above rate equations, the values of I_S and P_s are so small that can be considered negligible.

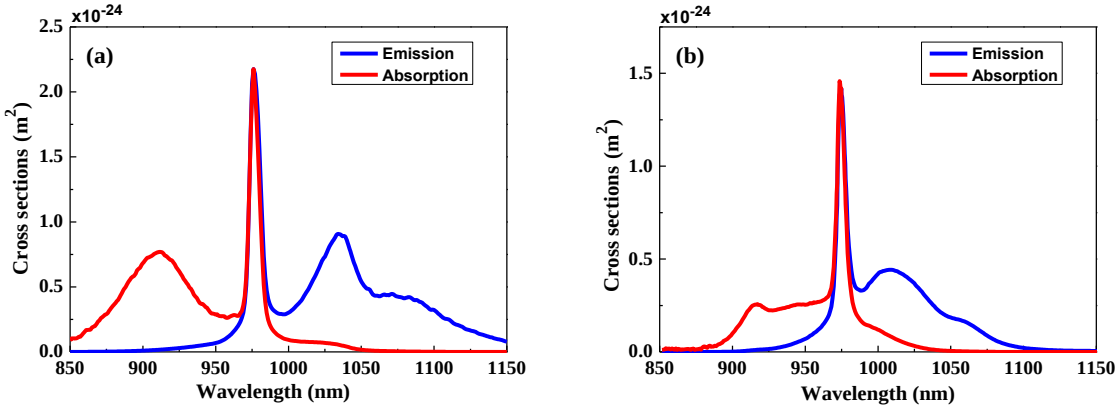

Fig. 3. 3. Typical cross sections of (a) Yb: Al fiber and (b) Yb: P fiber [78].

In the experiment, both of Yb: Al and Yb: P fibers are employed. The cross sections of Yb in the Yb: Al fiber and the Yb: P fiber are essential parameters to calculate the inversion level as described in the Eq. (3.3) and Eq. (3.4). The typical cross section spectroscopies of Yb: Al and Yb: P fiber from reference are shown in the Fig. 3.3 [78].

With the known cross sections and a calculated overlap factor, inversion level is increasing with the growth of the launched pump power, which apparently illustrates that specific inversion levels are obtained by adjusting the launched pump power.

3.2.2 Background Review: Core Composition Effects on Spectroscopic Cross Sections and Lifetime of Yb-doped Fiber.

For the purpose of inversion calculation, spectroscopic cross sections of tested fibers need to be obtained. In our experiment, two different Yb: Al fibers and one Yb: P are employed, which are different in fiber size, ytterbium concentration and core compositions. In [79], influences of Yb^{3+} ions concentration on the spectroscopic properties of silica glass fabricated by solution doping technique has been investigated. In that paper, six fiber samples with different concentrations of Yb^{3+} (0.15, 0.20, 0.25, 0.30, 0.60, and 0.85 wt%) and without codopants were prepared. The absorption spectrum of each fiber is recorded by a double-beam spectrophotometer in a range of 850 nm to 1100 nm at room temperature. The fluorescence decay curves of the $2F_{5/2}$ to $2F_{7/2}$ transitions have been recorded by exciting at 974 nm at room temperature and the excitation laser beam was modulated by a mechanical chopper. The upper-state lifetimes of the fiber samples were obtained from fluorescence decay curves using a digital oscilloscope.

There are usually two ways to obtain the emission cross-section of Yb^{3+}: $2F_{7/2}$ to $2F_{5/2}$ transitions. One is the reciprocity method based on McCumber relation shown as the Eq. (3.12) [80],

$$\sigma_{em}(\upsilon) = \sigma_{abs}(\upsilon)\exp(\frac{E_0 - h\upsilon}{k_B T}) \tag{3.12}$$

where k_B is the Boltzmann's constant, E_0 is the zero-line energy which is considered to be the energy separation between the lowest components of the upper and lower states. The zero-line energy is associated with the strong peak in the absorption spectrum of an Yb-doped glass.

If the absorption spectrum is unknown, there is another method to obtain the emission cross section that is the Fuchtbauer-Ladenburg (F-L) formula based on the analysis of fluorescence (shown as the Eq. (3.13)) [80].

$$\sigma_{em}(\lambda) = \frac{\bar{\lambda}^4}{8\pi c n^2 \tau_{rad}} \frac{I(\lambda)}{\int I(\lambda) d\lambda} \tag{3.13}$$

where n is the refractive index, c is the vacuum velocity of light, $\bar{\lambda}$ is the overlap peak wavelength of absorption spectrum and emission spectrum and $I(\lambda)$ is the fluorescence intensity at given wavelength.

In [79], the emission cross-section of Yb^{3+} ions was calculated by a reciprocity method. The absorption cross section spectrum from absorption measurement and its derived emission spectrum for two representative samples with 0.20 wt% and 0.85 wt% Yb^{3+} concentration are plotted respectively, at Fig. 3.4 (a) and 3.4 (b). It is observed that compared with 0.85 wt% Yb-doped fiber, Yb-doped fiber with 0.20 wt% Yb concentration has higher values in absorption and emission cross sections.

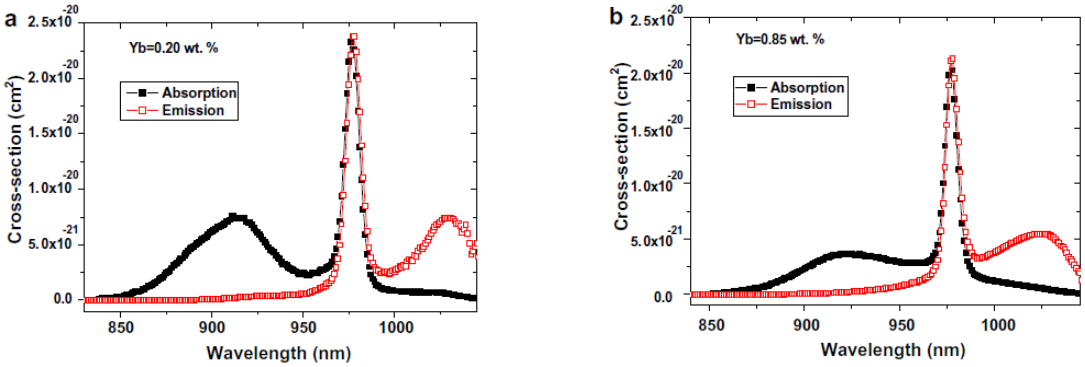

Fig. 3. 4. Absorption and stimulated emission cross-section of the silica glass samples doped with (a) 0.20 wt% and (b) 0.85 wt% of Yb^{3+} ions [79].

Table 3.1 summarizes the spectroscopic properties of these six Yb-doped fiber samples. As shown in Table 3.1, fiber sample with 0.15 wt% of Yb^{3+} concentration reveals the highest peak absorption cross-section with value of 2.40 pm^2 at 977 nm. With the growth of the Yb concentration, both absorption and emission cross sections keep decreasing, which results from the Yb^{3+} ions cluster effect into the silica glass matrix [81,82], leading to the spectroscopic properties being impaired.

Table 3.1 Various optical properties of Yb-doped silica glass preforms [79]

Yb concentration (wt %)	Ion density ($\times 10^{19}$ cm^{-3})	σ_{abs}(975 nm) (pm^2)	σ_{em}(1032 nm) (pm^2)
0.15	1.15	2.40	0.77
0.20	1.53	2.37	0.73
0.25	1.90	2.35	0.69
0.30	2.30	2.31	0.64
0.60	4.60	2.18	0.52
0.85	6.50	2.11	0.49

Normalized fluorescence decay curves of three representative samples doped with differentYb^{3+} irons concentration of 0.15, 0.30 and 0.85 wt% of Yb^{3+} are shown in Fig. 3.5. The Y axis is scaled in ln (I/I(0)). The upper-state population exponentially decays with a certain decay time, this certain decay time is the upper state lifetime. In measurement, the decay time is considered as the time after which the population has decayed to 1/e ($\approx$ 37%) of the initial value, namely the time duration for ln (I/I(0)) = -1. According to the plots in Fig. 3.5, it is can be figured out that Yb-doped fiber in 0.15 wt% has the longest time duration for ln (I/I(0)) = -1 and this time duration is decreased with the Yb concentration increasing. The lifetime reduction is explained by the radiative trapping and self-quenching by the clustering effect induced by heavy doping.

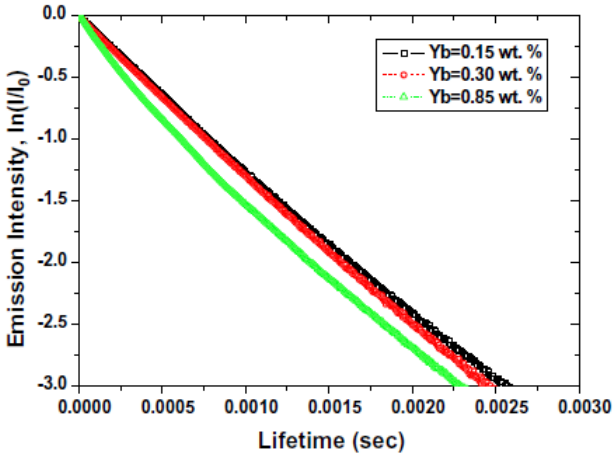

Fig. 3. 5. Normalized decay curves of $2F_{5/2}$ level for silica glass with three different Yb^{3+} ions concentration [79].

From [79], It is known that both transition cross sections and upper-state lifetime are effected by the Yb concentration. In addition, reliable measurement methods for transition cross sections and upper-state lifetime are obtained that could be the guide for our experiment in next section.

Besides the effect from the Yb^{3+} ions concentration, the compositional dependence of the spectroscopic properties of Yb^{3+} ions on various host glass oxides have been reported [83–86]. It has been shown that rare earth ions have much higher solubility in silica glass by codoped with phosphorus ions. Recently Yb_2O_3 of up to 11 wt% was doped in phosphosilicate fibers [87]. In [88], the difference in spectroscopic property and upper-state lifetime of ytterbium doped aluminosilicate fiber and ytterbium-doped phosphosilicate fibers are investigated. As shown in Fig. 3.6 (a), the line shape of transition cross sections of the two fibers is different. The emission peaks of Yb-doped phosphosilicate fibers are at shorter wavelengths compared to those of Yb-doped aluminosilicate fibers. Due to the Stark level split is distinctly smaller in the phosphosilicate fibers, emission wavelength has blue shift. From Fig. 3.6 (b), it can be observed that the upper-state lifetime in ytterbium-doped phosphosilicate fiber is longer than the ytterbium-doped aluminoslicate fiber.

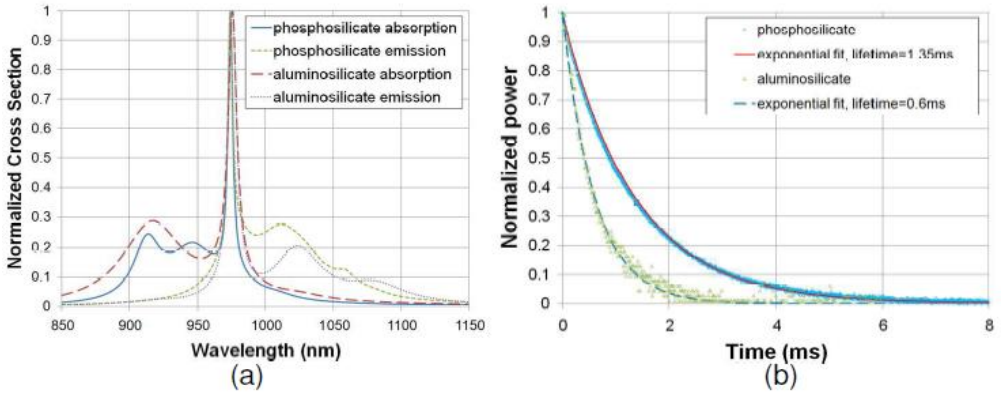

Fig. 3. 6. (a) Normalized absorption and emission cross sections of Yb-doped aluminosilicate and Yb-doped phosphosilicate fibers. (b) Lifetime measurement of the Yb-doped fibers [88]**.**

In summary, both ytterbium ions concentration and fiber composition with different co-dopants can make the difference in the line shape and value of transition cross sections. The upper-state lifetime is affected as well.

3.3 Experimental Results

PD has been widely understood to be closely associated with the number of excited Yb ions, namely PD induced loss at equilibrium state [11,12]. A linear relation between the PD saturation loss α_{eq} and the inversion of Yb ions is verified [13]. Core composition and launched pump power are determining factors of the Yb inversion in Yb-doped fiber and the influences of these two factors on PD were well investigated [89,90]. However, the previous studies assumed that the PD behavior follows only the inversion level regardless of pumping wavelengths.

In this section, I present the pumping wavelength dependence of PD of Yb-doped fibers. The PD dynamics is monitored by employing pump-probe technique [9]. Temporal evolution of optical power at a visible wavelength is traced when the Yb-doped fibers under test is pumped to reach the pre-determined inversion level. 916 nm and 976 nm pump sources are chosen to examine the pump wavelength effects on PD at the same Yb inversion level in Yb:Al as well as Yb:P fibers. Additionally, I interpret the pump wavelength dependence with a hypothesis of multi-photon absorption (MPA) [46]. Hence, this research contributes to insightful experimental results in pump wavelength dependence of PD, which has been overlooked in prior studies.

3.3.1 Experiment Setup

I examine the PD in the experimental setup with a core pumping configuration as shown in Fig. 3.7. A visible wavelength at 620 nm is selected as a probe since the PD induced loss can be easily detected and the wavelength is also located far from the Yb-band [9]. A tungsten white light source is coupled to the fiber under test (FUT) through a wavelength division multiplexing (WDM) coupler, and the transmitted power at the

probe wavelength is selected and monitored in a spectroscope. The WDM coupler combines the pump wavelength to the FUT. A short bandpass filter is inserted before the spectroscope to suppress unwanted pump wavelength, and avoid saturation of the detector in the spectroscope. The launched pump power is adjusted to control the level of Yb excitation. The temporal evolution of probe light intensity is monitored when the pump is on. A transmission spectrum through the FUT is recorded by an optical spectrum analyzer (OSA) before and after pumping. I keep the fiber length short at ~1 cm to suppress undesired amplified stimulated emission and maintain uniform inversion level through the fiber. In addition, the FUT is placed on a heat sink to avoid high temperature building during the measurement. The measurement was conducted at room temperature with controlled air convection. I did not notice a significant temperature rise which might affect the PD behavior [65,91].

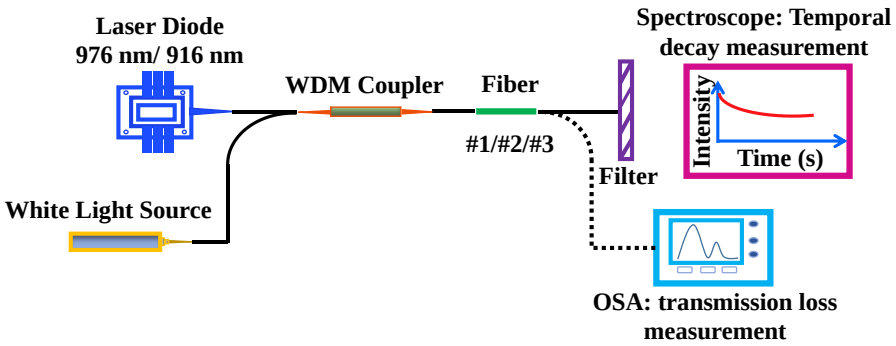

Fig. 3. 7. Experimental setup for PD temporal decay measurement. The pump light and white light source are combined via a WDM coupler, and coupled to YDFs. Transmitted power at the probe wavelength is monitored in the spectroscope. Transmission spectrum of YDF is measured by an optical spectrum analyzer (OSA).

3.3.2 Fabrication and characterization of Yb-doped fibers under test

In the experiments, two Yb:Al fibers and one Yb:P fiber are fabricated in-house using modified chemical vapor deposition process (MCVD) and solution doping technique. The key parameters of the fibers are listed in Table 3.2. To quantify the dopants in these three different fibers, we use electron probe micro-analyzer (EPMA) to scan the fiber preform slices. The EPMA results are shown in Fig. 3.8 and Fig. 3.9. Fiber 1 is highly

doped by 1.1 wt% of Yb dopant and 0.9 wt% Al dopant while Fiber 2 contains 0.5 wt% and 0.28 wt% of Yb dopant and Al dopant, respectively. In Fiber 3 (Yb:P) the concentration of the Yb dopant is 2.5 wt% and the concentration of P dopant is up to 9.0 wt%. Electron microscope images of each fiber are shown in the insets with a 20 um scale bar. The core size and numerical aperture (NA) of the fibers are listed in Table 3.2.

Table 3.2 Dopants concentration and parameters of FUT

No.	Yb (wt %)	Al (wt %)	P (wt %)	Core diameter (µm)	Cladding diameter (µm)	Core NA	Upper state lifetime (ms)
#1	1.1	0.9	0	10	125	0.11	0.76
#2	0.5	0.28	0	13.2	175	0.06	0.91
#3	2.5	0	9.0	8.2	125	0.23	0.83

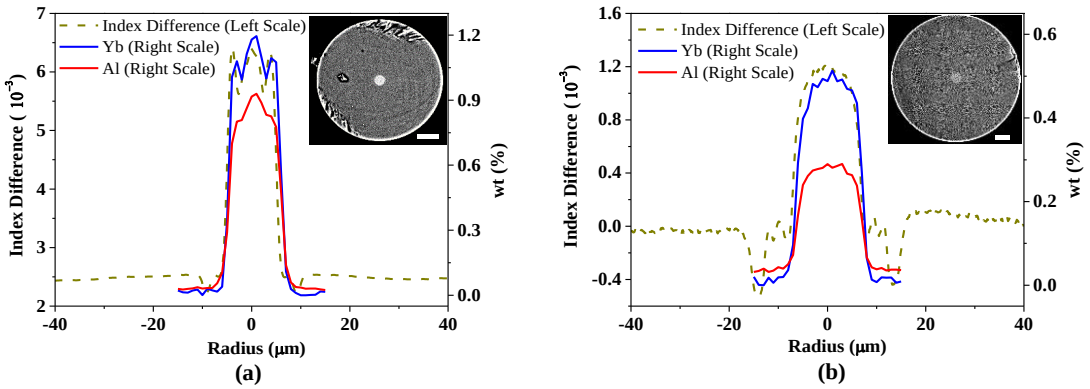

Fig. 3. 8. EPMA characterization with refractive index profile of Yb: Al fibers (a) Fiber 1 and. (b) Fiber 2 and (c) Fiber 3. The scale bars for the EPMA images are 20 µm.

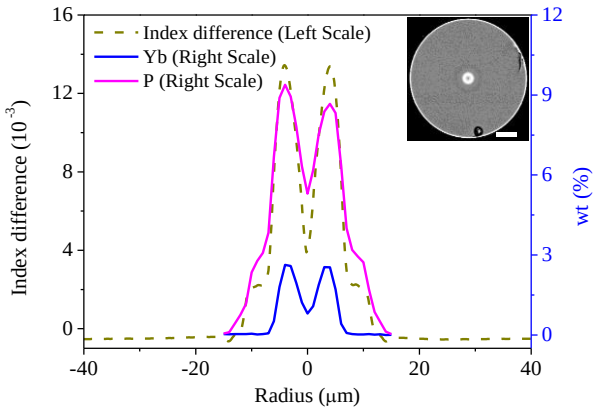

Fig. 3. 9. EPMA characterization with refractive index profile of Yb: P fiber (Fiber 3). The scale bars for the EPMA images are 20 μm.

The refractive index profiles (RIPs) of these three fibers are shown as the dash lines in Fig. 3.8 and Fig. 3.9. Apparently, the RIPs of two Yb:Al fibers follow the Yb and Al concentration in each fibers, while the RIP follows the Yb and P concentration in Fiber 3.

To control the Yb inversion level in the PD measurements, I first characterize absorption and emission cross-sections of the fibers. Transmission spectra from the fibers were collected using an OSA to determine the absorption cross-section. A tungsten white light source was used as a broadband source. The method to obtain the absorption spectra is similar to the method applied in [79] which is introduced in the last section 3.2.2. The emission cross sections were obtained by capturing transverse fluorescence from the Yb-doped fibers and its upper level lifetime measurements. The values of emission cross sections in this study were achieved through the Fuchtbauer-Ladenburg (F-L) formula (shown as Eq. (3.13)). The measured cross-sections scaled to unity at the maximum are presented in Fig. 3.10. The two Yb:Al fibers share the same spectral shapes but with different peak values. Fiber 1 has a higher Yb concentration and its peak value at 976 nm is 1.857 pm^2, while the Fiber 2 has peak value of 2.897 pm^2. This observation is consistent with the clustering effects on the cross sections demonstrated in [79]. The cross sections of Fiber 3 are shown in Fig 3.10(b), which vary from the Yb:Al fibers as expected [20]. In contrast to the Yb:Al fibers, the peak

value of the cross section of Yb:P fiber dramatically decreases to 1.298 pm^2. Cross sections of the Yb:Al fiber and Yb:P fiber from our measurement are in good agreement with the commonly applied cross-sections [20,34] respectively.

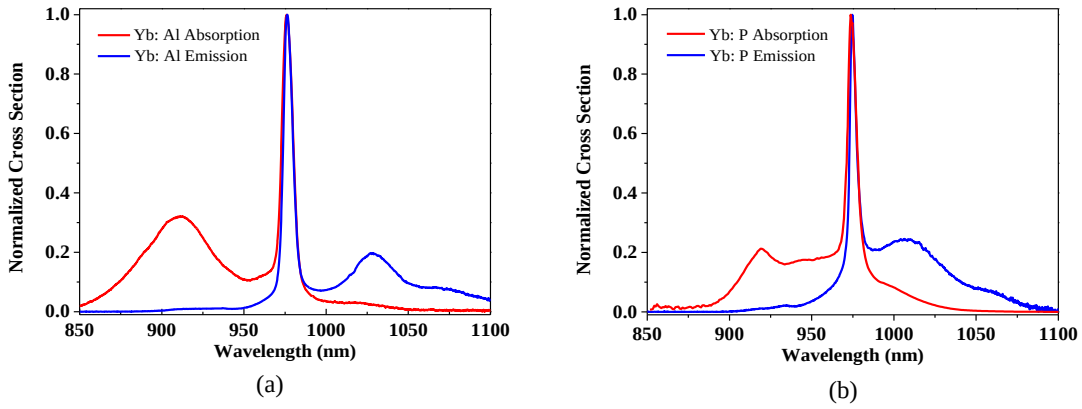

Fig. 3. 10. (a) Absorption and emission cross-sections of Fiber 1 and Fiber 2. The peaks at 976 nm are at 1.857 pm^2 and 2.897 pm^2 respectively. (b). Absorption and emission cross-sections of Fiber 3 with its peak value of 1.298 pm^2 at 976 nm.

3.3.3 Temporal Decay of Yb:Al Fibers and Yb:P fiber Induced by Photodarkening

To investigate the pump wavelength dependence, it is important to keep the same Yb inversion level under both pumping wavelengths at 916 and 976 nm. The inversion level is controllable by adjusting input pump power. The cross-sections in Fig. 3.10 are used to determine the pump power required for the same inverted Yb ions. In addition, we used the measured RIPs in Fig. 3.8 and Fig. 3.9 to find overlap between a pump beam in the fiber core and the dopant to accurately determine the required pump power. The calculation error for the overlap is anticipated within 3-4 % due to uncertainty of the pump beam profile in the tested fiber core. I consider a fundamental mode excitation and fully excited modes in the FUTs for the anticipated error. Variation of pump beam profile changes the pump-dopant overlap factor that generates discrepancy in inversion calculation. However, its influence on the inversion level is only 0.5-1.5%, thus insignificant.

The determined parameters are used in the inversion level calculation. A commercial software (Fiber Power) was used to calculate the inversion level, and consequently the required launched pump power [92]. A quasi-three level system is assumed for the calculation.

For Fiber 1, pump power at 976 nm is adjusted to 16 mW and 916 nm to 19 mW based on our calculation to achieve 37% inversion. According to the Eq. (2.5) and Eq. (2.6), because of the different cross sections at 916 nm from 976 nm, the inversion expressions under the two wavelengths pumping are different. Under 916 nm pump, its corresponding inversion level can be derived to be

$$I_{916\ nm\ pump} = \frac{56\ P_P}{68\ P_P + 2.973} \tag{3.14}$$

Similarly, under the 976 nm pump, its corresponding inversion level is derived to be

$$I_{976\ nm\ pump} = \frac{200\ P_P}{400\ P_P + 2.790} \tag{3.15}$$

From Eq. (3.14) and Eq. (3.15), it can be derived that when the inversion level below 43.8%, higher pump power is required at 916 nm pump. On the contrary, when the inversion level above 43.8%, higher pump power is required at 976 nm pump.

The measured temporal decay at 620 nm is represented in Fig. 3.11. Despite the same inversion level in both pump wavelengths, the PD appears more severe under 976 nm pumping. I fit the measurement with a stretched exponential function as shown in Eq. (2.4) in chapter 2.

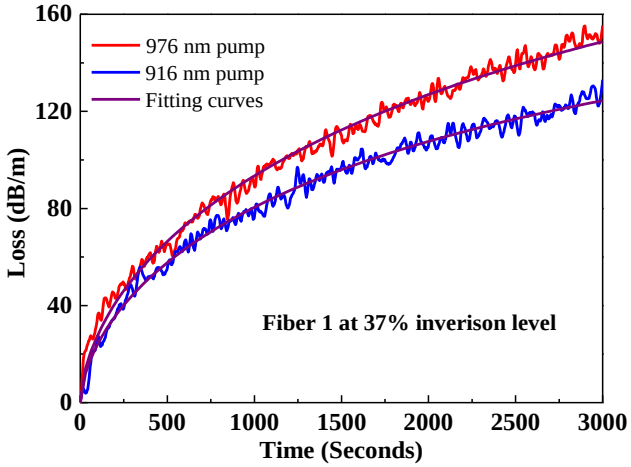

Fig . 3. 11. PD induced temporal decay loss of Fiber 1 at 620 nm under 976 nm (red) and 916 nm (blue) pumping. Fitting results are shown in the smooth curves.

Table 3.3 PD experimental conditions and fitting results of measured PD loss, α_{eq}, and rate constant τ^{-1}

No.	Inversion Level (%)	Pump Wavelength (nm)	Power (mW)	α_{eq} (dB/m)	τ^{-1} × 10^{-4} (s^{-1})
#1	37	976	16	210	4.5
		916	19	185	4.0
#2	37	976	30	57	5.9
		916	32.5	38	5.2
	46	976	86	62	6.6
		916	46	47	6.5
# 3	41	976	63	37	19
		916	66	17	18

The fitting curves are shown as violet lines in the figure. I summarize the temporal decay results in Table 3.3. It is revealed that there is a striking difference between the 976 and 916 nm pumping. The 976 nm pumping induces larger α_{eq} at a faster rate as compared to the 916 nm counterpart despite the same inversion level. The higher α_{eq} by 976 nm pumping was reported when the "Tm path to UV" is established with considerable Tm concentration [55]. However, the Tm contamination in our fibers is found as ~0.5 ppm-wt through fiber core absorption measurement. This is consistent with the manufacturer's note. Thus, our results evidence that the pump wavelength influences the PD. We note that, in the absence of Tm, variation of PD induced loss at

different pump wavelengths was reported in [61], but it was due to different pump configurations. By contrast, all my measurements were conducted under core-pumping configuration, hence our results truly indicate the pump wavelength dependence of PD at the same level of inversion.

The same pump wavelength dependence is observed in Fiber 2. Fig. 3.12 (a) and (b) represents the pump wavelength dependence in Fiber 2 for the 37% and 46% inversion level, respectively. It is clearly observed that, despite the same inversion level, the 976 nm pumping has greater PD effect as compared to the 916 nm pumping. The α_{eq} ratios between 976 and 916 nm remain within 1.3 to 1.5 at the given inversion levels as summarized in Table 3.3 above. It should be noted that the aforementioned error of 0.5 to 1.5% in the inversion does not affect our results. The error contributes to higher inversion at 916 nm, and reaffirms that the 976 nm pumping induces more significant PD.

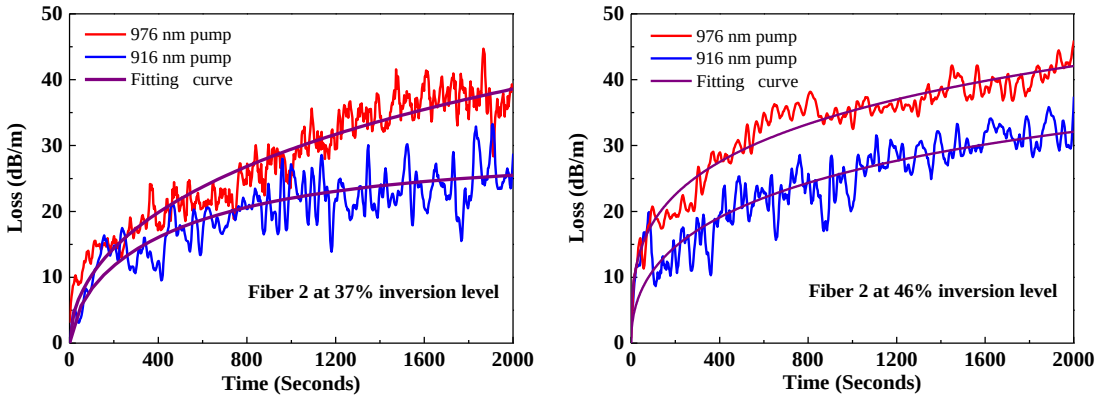

Fig. 3. 12. PD induced temporal excess loss for Fiber 2 at 620 nm under 976 nm (red) and 916 nm (blue) pumping. (a) The inversion level is 46%. (b) The inversion level is 37%. Fitting results are shown in the smooth curves.

It is also worth noting that the wavelength dependence doesn't necessarily follow the Al/Yb ratio. Fiber 1 has higher Yb and Al concentrations than Fiber 2. However, the Al/Yb ratio is much higher in Fiber 1 as well. A high Al/Yb ratio is expected to evenly disperse the Yb ions [93,94], hence suppressing the PD. However, I don't see

obvious benefit of the high ratio of Al/Yb when the Yb concentration is as high as in Fiber 1. The absolute Yb concentration seems to bring heavier impact in the PD than the Al/Yb ratio, which is consistent with the discussion in [72]. The measurement results in [72] reveal that even the PD effect is more severe in an Yb heavy doped fiber with lager Al/Yb ratio than another light Yb light doped fiber with lower Al/Yb ratio. This is similar to the experiment in this thesis. Fiber 1 has a higher Yb concentration and higher Al/Yb ratio, it has more severe PD effect than Fiber 2 which has a lower Yb concentration with lower Al/Yb ratio. It was concluded that absolute values of Yb and Al concentration rather than the Al/Yb ratio that play the decisive role. The reason is that no complete solvation shells for the incorporated Yb^{3+} ions are obtained with Al codoping in contrast to P codoping. Therefore, Yb concentration is more influential than Al/Yb ratio. If the absolute value of Al concentration is increasing greatly which enchances the Al/Yb ratio at the same time. Therefore, there is no doubt that the PD effect will be greatly suppressed compared to the demonstrated PD performance in the thesis, since more Al ions will be more helpful to homogeneously distribute the Yb ions and suppress the clustering effect.

I extend our experiments to Yb:P fiber, Fiber 3 in Table 3.2, to investigate the pump dependence in the PD suppressed fiber [20,95]. Key parameters of the fiber are tabulated in Table III. I place Fiber 3 in the setup in Fig. 3.7 to examine its PD. An inversion level of 41% is maintained at the both pump wavelengths. As shown in Fig. 3.13, the pump wavelength dependence is apparent even in the Yb:P fiber. The measured temporal power evolution at 620 nm exhibits 37 dB/m of α_{eq} under 976 nm pumping which is in contrast to 17 dB/m under 916 nm pumping. Thus, we conclude that the pump wavelength dependence is a general behavior in Yb-doped fibers. It would be of interest to test other types of PD suppressed fibers such as Ce:Yb co-dopoed fiber to gather more insightful results [96].

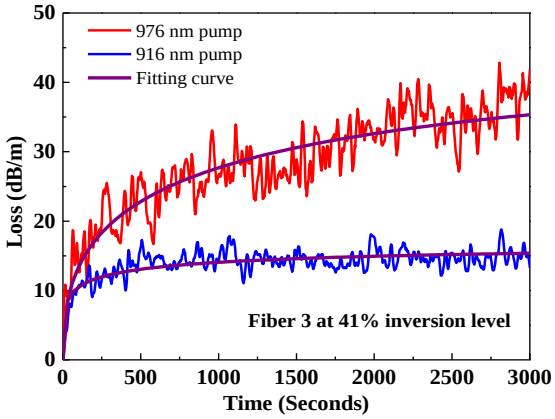

Fig. 3. 13. PD induced temporal excess loss for Yb: P fiber at 620 nm under 976 nm (red) and 916 nm (blue) pumping. The inversion level is 41%. Fitting results are shown in the violet smooth curves.

3.4 Mechanism for PD Dependence on Pump Wavelength

The physical mechanism of the PD in Yb-doped fibers has been intensively investigated in recent years. Formation of color centers is widely accepted as the cause of excess optical loss from PD [11,63]. However, the physical mechanism of the formation of defect centers is still a subject of discussion. For example, a valence state change of Yb ion occurring through a charge transfer (CT) process is believed to account for the generation of color center [97]. Also intrinsic defects such as Oxygen Deficiency Center (ODC) can serve as a precursor for the pumped induced hole-related color centers [98]. The charge transfer process and ODCs have been introduced in details in chapter 2. Validating the mechanism is out of the target of this research. Rather, it would be more interesting to understand the pump wavelength dependence under the context of both mechanisms. We assume both CT and ODC as a possible PD precursor generating the color centers. Reaching to the CT (~5.39 eV) [97] or ODC level (~5 eV) [99] under NIR pumping is plausible through MPA which involves absorption of two or more photons from the ground, or excited intermediary states to higher excited states [47,48]. Characteristics of the CT absorption band in Yb:Al silica fibers have been reported [46,100].

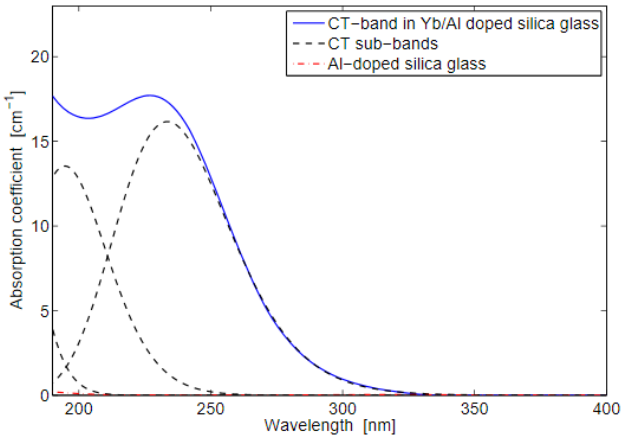

Fig. 3. 14. CT absorption band of the 0.2 at% Yb/Al doped silica glass preform (blue line). The black dashed lines show a Gaussian deconvolution of CT absorption band and the absorption spectrum of a non-Yb doped reference preform is shown as the red dashed-dotted line [100]**.**

As shown in the above Fig. 3.14, the CT band is characterized by a broad absorption band around 230 nm in a Yb:Al doped silica glass, and consists of several sub-bands, including a dominant one centered at 243 nm, spreading from 200 nm to 300 nm. Meanwhile, the absorption band of ODC has been thoroughly investigated in the Yb:Al fiber [101].

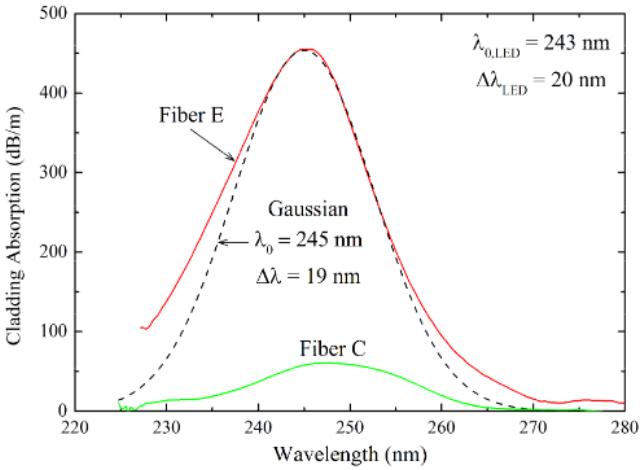

Fig.3. 15. Cladding absorption spectra measuremnt of two Yb-doped fibers: Green for Fiber C (green) and Red for Fiber. [101]**.**

As shown in the Fig. 3.15, two Yb-doped fibers with different Yb concentration and different fiber size share the similar absorption range and absorption peak. The absorption spectrum ranges from 220 nm to 270 nm and its peak centers around 245

nm. Both characteristics are consistent with the known parameters of the deep-UV absorption of the ODC (II) defect in silica [102,103].

In Fig. 3.16, the spectra of the dominated sub absorption band of CT and the ODC absorption band are manifested as demonstrated in [97,101]. The schematic diagram of excitation procedure to reach the precursors via MPA under 976 nm and 916 nm pumping is shown in Fig. 3.16. The MPA via 976 nm pumping could reach to the center of both the ODC absorption and the dominant CT sub absorption band. In contrast, the MPA under 916 nm pumping would be off-centered from the peak. Thus, it would suggest that reaching the absorption bands of the precursor (CT/ODC) is more efficient under 976 nm than 916 nm pumping through the MPA. This would result in more color centers generation accounting for the PD under 976 nm pumping in the Yb:Al silica fiber.

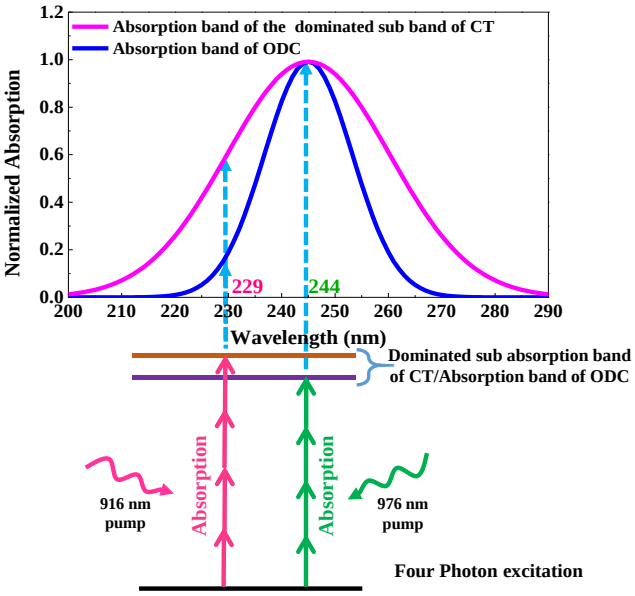

Fig. 3. 16. Multi photons absorption excitation mechanism in Yb:Al fiber under 976nm and 916nm wavelength pumping. Absorption band of the dominated sub band of CT and absorption band of ODC are based on [97] **and** [101] **respectively.**

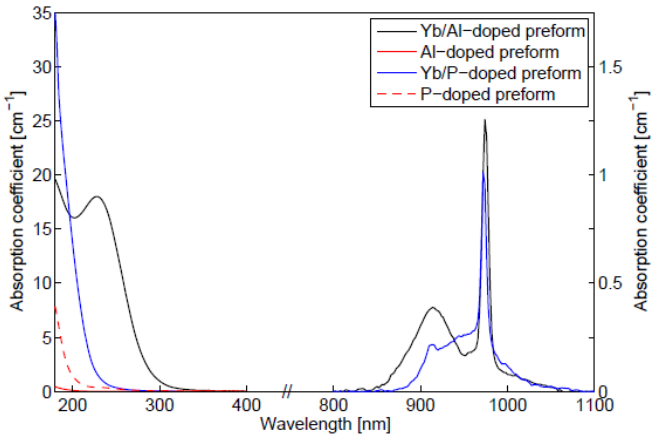

Fig. 3. 17. Absorption spectra for different dopant preforms[46]**.**

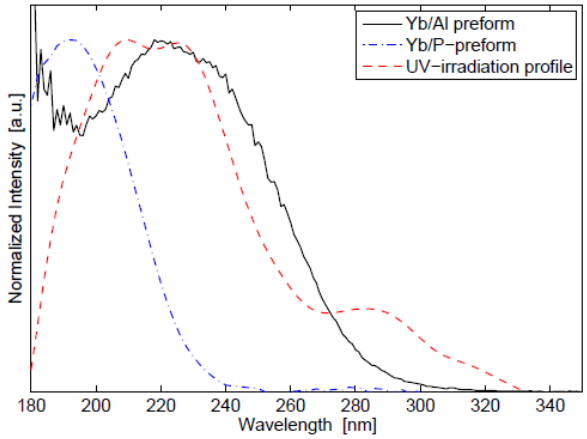

Fig. 3. 18. Excitation spectra characterization for the Yb/Al and Yb/P-doped preform. The UV-irradiation profile is also shown[46]**.**

In [46], the CT band of the Yb:P glass has been investigated. The absorption spectra and emission spectra are presented in the following Fig. 3.17 and Fig. 3.18, respectively. From the excitation spectrum in Fig. 3.18, it is found that the peak of the CT-band for the Yb: P preform appears to be centered on 192 nm. This is difficult to be observed in the absorption spectrum in Fig. 3.17 due to overlap with the host lattice absorption. Although the specific CT sub band absorption is not known, If we assume the 192 nm absorption band is the dominant CT band, at least five pump photons are required to reach the absorption band via MPA in the Yb:P fiber. This may suggest the low PD as compared to the Al:P counterpart. Moreover, the 976 nm pumping is more resonant with the 192 nm peak than the 916 nm pumping. Hence, this hypothesis seems evident

from the observed wavelength dependence, but it is necessary to locate all CT bands as well as ODC absorption in the Yb:P fiber to attain more comprehensive insights on PD routes.

In addition, from the above cross section measurement results, it has been observed that the absorption cross section at 976 nm is still much higher than the 916 nm. It reveals that even the four-photon absorption effect is considered, the 976 nm pump efficiency is still advantageous to 916 nm pump because of its larger absorption cross section.

3.5 Conclusion

This study presents the strong dependence of the PD on the pump wavelengths of Yb-doped fibers. The experimental results consistently indicate that the PD is severely influenced by the pumping wavelengths at the same Yb inversion level. It is found that the 976 nm pumping leads to more significant PD than 916 nm. Such dependence is persistent across various fibers with different compositions including the widely used Yb:Al and Yb:P. Thus this conclusion contributes to Yb-doped fiber lasers and amplifiers design. A plausible mechanism was discussed to portray the observed pump wavelength dependence, adopting the MPA model and absorption peaks of CT and ODC bands. In summary, my results provide an additional guide of pump wavelength selection in high power Yb-doped fiber lasers and help efforts in optimizing long term performance of high-power laser devices.

Chapter 4

Photodarkening Influence on Fiber Laser Cavity Design

4.1 Background

With the larger development of fiber lasers in these few decades, the performance of the fiber laser keeps breading records. The design of the cavity is of great importance for achieving high output lasing power. Generally speaking, the parameters influencing the laser performance include the active fiber length, the intracavity losses, and the output coupling ratio. Investigation of the laser cavity design is crucial for achieving high performance laser [104,105]. For instance, fiber length and output coupling ratio were theoretically and experimentally identified as critical parameters [105] to optimize a 980 nm pumped erbium-doped fiber ring laser. In [105], theoretical calculation of the output power utilized an analytical gain equation that was derived for erbium-doped fiber amplifiers [106], the experimental setup used for cavity design investigation is shown in Fig. 4.1.

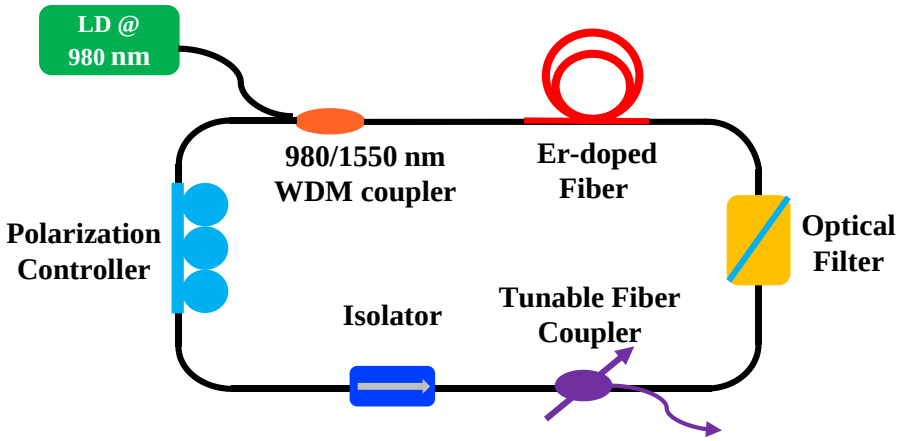

Fig. 4. 1. Experimental setup used for cavity design investigation of the erbium-doped fiber ring laser [105].

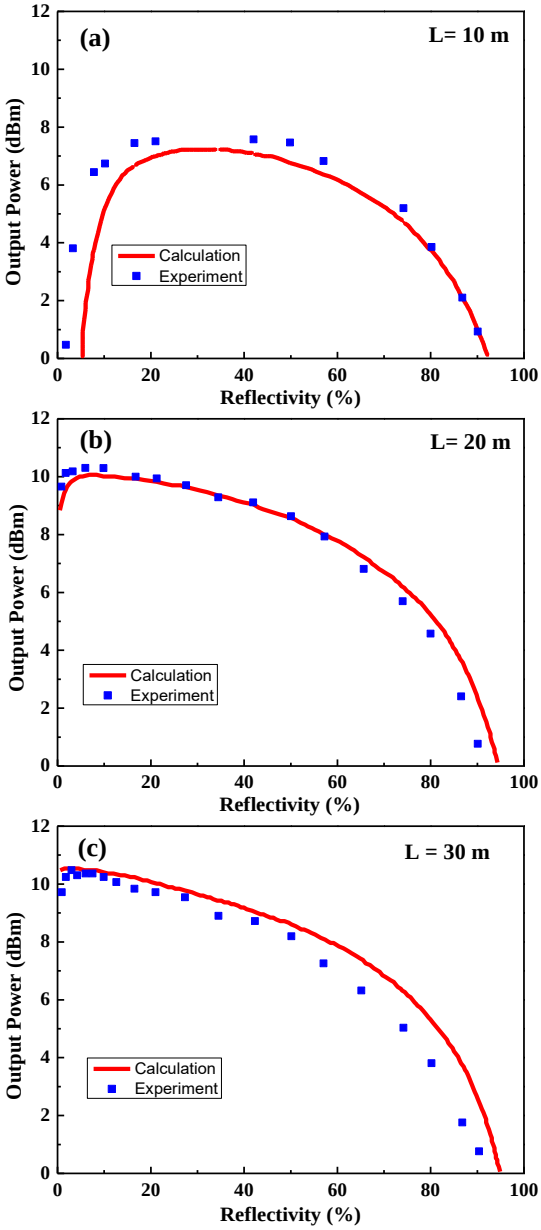

Fig .4. 2. Output power as a function of reflectivity R for λL= 1533 nm. Pump power 52 mW, active fiber length (a) L = 10 m, (b) L = 20 m and (c) L = 30 m [105].

In the Er-doped fiber laser experiments of [105], output lasing power variation with reflectivity R is shown in Fig. 4.2 for different fiber lengths (L = 10-30 m) at λ_L = 1533 nm. The reflectivity of a fiber ring laser means the percentage of the signal power stay in the cavity after propagating through the output coupler. From Fig. 4.2 (a), it can be observed that the maximum output lasing power is achieved when the reflectivity is selected around 35 %. Furthermore, this fiber laser with 10 m Er-doped fiber length

cannot lase for a reflectivity below 2%, since the fiber is short and cannot provide enough gain to compensate the high ring losses. For the cases at L=20 m and L=30 m, the laser can oscillate at all values of reflectivity and the maximum output lasing power can be realized when the reflectivity is around R=5-10%, as shown in Fig. 4.2 (b) and Fig. 4.2 (c). The agreement between experimental results (shown in dots) and theoretical calculation (shown in solid lines) is good. Some uncertainties occurred in experiments are responsible for the slight deviations between the theoretical curves and experimental points. This investigation shows a guideline for the impact of cavity reflectivity on the output lasing power.

4.2 Theoretical Analysis of Output Coupling Ratio Influences on PD Induced Loss in Cavity

4.2.1 Fiber Laser Cavity Setup

To theoretically analyze the influence of the laser output coupling ratio on PD induced loss, I utilize the model of Yb-doped fiber laser setup from RP fiber power software for modelling calculation [92]. The Yb-doped fiber laser cavity employed in this study is shown in Fig. 4.3.

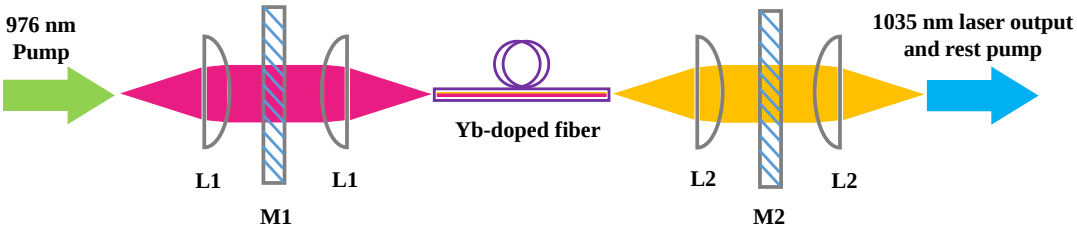

Fig.4. 3. Yb-doped linear cavity fiber laser setup. L1 and L2 are lenses, and M1 and M2 represent mirrors.

In this fiber laser setup, a 976 nm single mode laser diode with 600 mW power is used as the pump source for core pumping. I chose 976 nm as a pump source to highlight significance of the PD in laser cavity design. Nonetheless, the overall trend of cavity optimization won't be affected by pumping wavelength. I expect the similar

trend with 915 nm. The pair of lenses L1 is used for alignment and coupling for launching the pump light into the Yb-doped fiber. The pair of lenses L2 is utilized for alignment and collecting the output lasing signal. M1 and M2 construct the lasing resonant cavity. The 976 nm pump wavelength is considered to fully transmit through M1 and M2. The 1035 nm lasing wavelength is 100% reflected by M1 and partly reflected by M2 with adjustable output coupling ratio. The Yb-doped fiber employed in this setup is an Yb: Al fiber possessing 6 μm core diameter with 1 wt% Yb dopant concentration. Since the fiber is highly doped, the spectroscopic cross sections of Fiber 1 in Chapter 3, shown in Fig. 3.10 (a), is employed for the calculation here. To simplify the analysis, I assume that the pump power launching efficiency is 100%. The Yb-doped fiber with different fiber length and different cavity loss are discussed in this chapter. For the fiber length, conditions of 5 cm, 10 cm and 15 cm are selected for the analysis. For the cavity loss, conditions of 0.3 dB, 0.45 dB and 0.75 dB are considered.

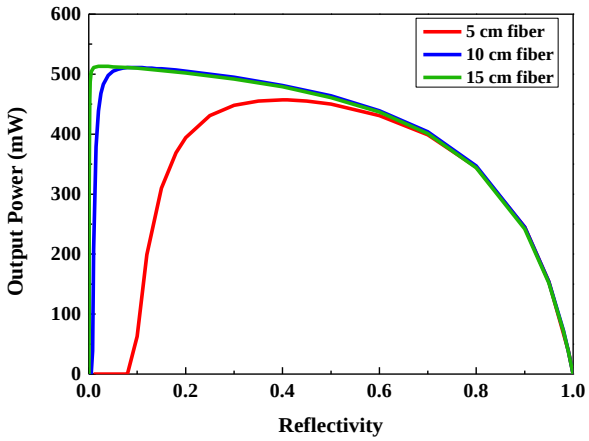

Fig. 4. 4. Output lasing power as function of reflectivity for Yb-doped fiber length L= 5 cm (red), 10 cm (blue), 15 cm (green).

Firstly, I use three Yb-doped fibers with three different fiber length to understand the relationship between cavity reflectivity and the output lasing power. These three fibers with different length have same background loss of 0.1 dB/m and same devices loss of 0.285 dB. As shown in Fig. 4.4, the calculation results for these three fibers present the same features as found in [105]. As illustrated in Fig. 4.2, the shorter the

active fiber is, the more reflectivity of the resonant cavity is required for achieving the maximum output lasing power.

4.2.2 Variation of Inversion Distribution with Reflectivity of Output Coupler

It is expected that the output coupler of a laser cavity determines the ratio of the generated lasing power between inside a cavity and outside the cavity. With an output coupler providing higher reflectivity, more lasing signal reflects back into the cavity and stays inside the cavity. Under this condition, the inversion level inside of the cavity will be affected as well. Here, the rate equations described in chapter 3 are employed for numerical analysis;

$$n_2 = \frac{R_{12} + W_{12}}{R_{12} + R_{21} + W_{12} + W_{21} + A_{21}} \tag{3.3}$$

where R_{12} and R_{21} are the transition rate for pump light, which are given by:

$$R_{12} = \sigma_{12}^{(p)} I_P / h\upsilon_p \quad , \quad R_{21} = \sigma_{21}^{(p)} I_P / h\upsilon_p \tag{3.5}$$

W_{12} and W_{21} are the transition rate for signal light, that are given by:

$$W_{12} = \sigma_{12}^{(s)} I_S / h\upsilon_S \quad , \quad W_{21} = \sigma_{21}^{(s)} I_S / h\upsilon_S \tag{3.6}$$

where $\sigma_{12}^{(p)}$ and $\sigma_{21}^{(p)}$ and are the absorption and emission cross sections for pump wavelength, $\sigma_{12}^{(s)}$ and $\sigma_{21}^{(s)}$ are the corresponding values for signal wavelength. I_P and I_s are the pump and signal intensities (W/m^2). A_{21} is the constant for spontaneous emission. In this setup, the pump wavelength is assumed to be 976 nm, according to the spectroscopic characteristics of Yb: Al fiber, $\sigma_{12}^{(p)} = \sigma_{21}^{(p)}$. Therefore, $R_{12} = R_{21}$. The signal wavelength selected here is 1035 nm, based on the spectroscopic characteristics of Yb: Al fiber,$\sigma_{12}^{(s)}$is a very small value when compared with $\sigma_{21}^{(s)}$. For this reason, W_{12} becomes negligible.

The condition analyzed here is that the value of the reflectivity of the output coupler becomes larger and it results in increasing of the I_S inside the cavity. Here, parameter a is introduced in this discussion for describing the increasing magnitude of signal intensity. I assume that the signal intensity inside the cavity change to I_S', and $I_S' = aI_S$,

a>1. Therefore the transition rates of signal light change to aW_{12} and aW_{21}. The corresponding upper state population changes to n_2' which is expressed as:

$$n_2' = \frac{R_{12} + aW_{12}}{R_{12} + R_{21} + aW_{12} + aW_{21} + A_{21}} \tag{4.1}$$

Then, the difference between n_2 and n_2' is found to be:

$$n_2 - n_2' = \frac{R_{12} + W_{12}}{R_{12} + R_{21} + W_{12} + W_{21} + A_{21}} - \frac{R_{12} + aW_{12}}{R_{12} + R_{21} + aW_{12} + aW_{21} + A_{21}} \tag{4.2}$$

Following my earlier assumptions, $R_{12} = R_{21}$ and $W_{12} = 0$, Eq. (4.2) is reduced to:

$$\begin{aligned} n_2 - n_2' &= \frac{R_{12}}{2R_{12} + W_{21} + A_{21}} - \frac{R_{12}}{2R_{12} + aW_{21} + A_{21}} \\ &= \frac{(a-1)R_{12}W_{21}}{(2R_{12} + W_{21} + A_{21})(2R_{12} + aW_{21} + A_{21})} \end{aligned} \tag{4.3}$$

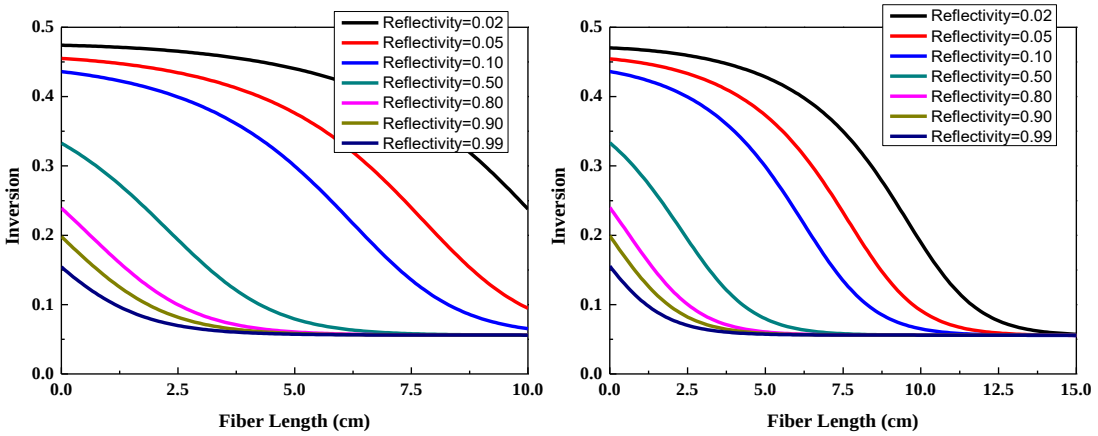

Fig. 4. 5. Inversion distribution along the fiber length with different reflectivity of output coupler (a): 10 cm Yb-doped fiber, (b): 15 cm Yb-doped fiber.

Since a>1, therefore $n_2 - n_2' > 0$, namely, inversion level becomes smaller when the reflectivity of output coupler increases. Intuitively, with higher reflectivity, more energy of the lasing signal will stay inside the cavity. The strong signal causes quick depopulation, thus large W_{21}, that makes the population in the upper level becomes smaller as indicated in Eq. (3.3). Hence, high reflectivity induces lower n_2 as deduced from Eq. (4.3). To confirm this, I numerically calculate the inversion distribution along a fiber by changing reflectivity. Two different fiber lengths, 10 cm and 15 cm, are

selected for the calculation. As shown in the Fig. 4.5(a) and (b), the inversion level is high at the pump input end and decreases along the fiber length. More importantly, for both 10 cm and 15 cm fibers, it is clearly observed that the inversion level keeps decreasing with the growth of reflectivity of the output couple. Thus, the conclusion is consistent with the prediction from Eq. (4.3).

4.2.3 Variation of PD induced loss with reflectivity of output coupler

It is widely known that the PD induced loss is dependent on the population density in the upper state level which has been introduced in the chapter 2, section 2.2.2. In [73], it has been reported that the PD losses at 633nm is linearly dependent on the density of the excited ions on the upper state of the active fiber. On the other hand, in [11], it was shown that the maximum PD loss at 633 nm is nearly quadratic dependent on the total Yb^{3+} ion concentration in the Yb-doped fiber. In [107], they combined the two factors to generate a single formula as shown in the following Eq. (4.4):

$$PD^{633nm}(dB/m) = \left(175 \cdot (\frac{N}{8.74 \cdot 10^{25}})^{2.09}\right) \cdot \frac{N_2 / N}{0.46} \tag{4.4}$$

where $PD^{633\,nm}$ represents the PD induced losses at 633nm in the unit of dB/m, N is the total concentration of Yb^{3+} ion in the fiber in the unit of ion/m^3 and N_2 is the population density of the excited ions on the upper state level in the unit of ion/m^3. Therefore, the factor N_2/N represents a fraction of population density in the upper laser level, namely the inversion level that I use in this thesis. An inversion level of 0.46 is assumed in Eq. (4.4), and a conversion factor of 8.74×10^{25} is employed to change the ion concentration from ion/m^3 to wt%.[73],

According to [9,108], the PD loss at ~1μm is directly proportional to the loss measured at 633 nm with a fixed ratio. Therefore, it can be written in the Eq. (4.5):

$$PD^{1\mu m}(dB/m) = \frac{PD^{633nm}(dB/m)}{\gamma} \tag{4.5}$$

Where the value γ is within the range of 10-70 [8, 9]. In my simulation, a single mode Yb-doped fiber is assumed to be core pumped by a single mode 976 nm laser diode. This follows experiment condition in [9]. Thus, the value γ is set to be 70 for the calculation here.

Based on the above Eq. (4.4) and Eq. (4.5), the PD induced loss distribution at the 1035 nm lasing wavelength along the Yb-doped fiber can be calculated based on the earlier calculated inversion distribution. Here I choose 15 cm Yb-doped fiber of 0.1 dB/m fiber background loss with three different reflectivity of the output coupler. The PD distributions along the fibers are shown in Fig. 4.6

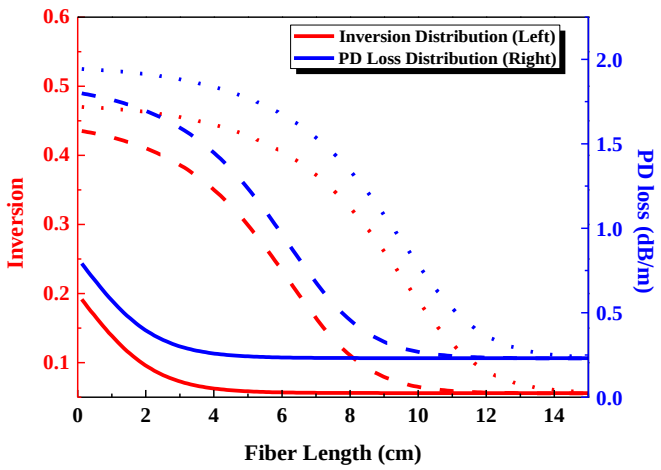

Fig. 4. 6. PD loss distributions at 1035 nm lasing wavelength along the fiber length with corresponding inversion distribution at three different reflectivities of the output coupler. Solid line: reflectivity = 0.9, Dash line: reflectivity = 0.11, Dots: reflectivity = 0.002.

It can be observed that the PD loss distribution follows the inversion level distribution in all the reflectivity selected. The average PD loss in the fibers can be given by:

$$PD_{average}^{1035nm}(dB) = \int_{0}^{fiberlength} PD^{1035nm}(dB/m) * dz \tag{4.6}$$

The average PD loss represents additional cavity loss caused by the PD. The average PD loss will be affected by the inversion level controlled by the cavity reflectivity.

Characteristic of the average PD loss vs. reflectivity is studied in Fig. 4.7. Here, the calculation results of 15 cm and 10 cm fiber of 0.1 dB/m fiber background loss are summarized.

Fig. 4.7 reveals that the total PD keeps decreasing with the growth of the reflectivity of the output coupler. The rate of the drop is very steep at the beginning, and it generally becomes flat with the reflectivity increasing. Hence, higher reflectivity helps suppress the additional cavity loss, but it will compromise extractable power.

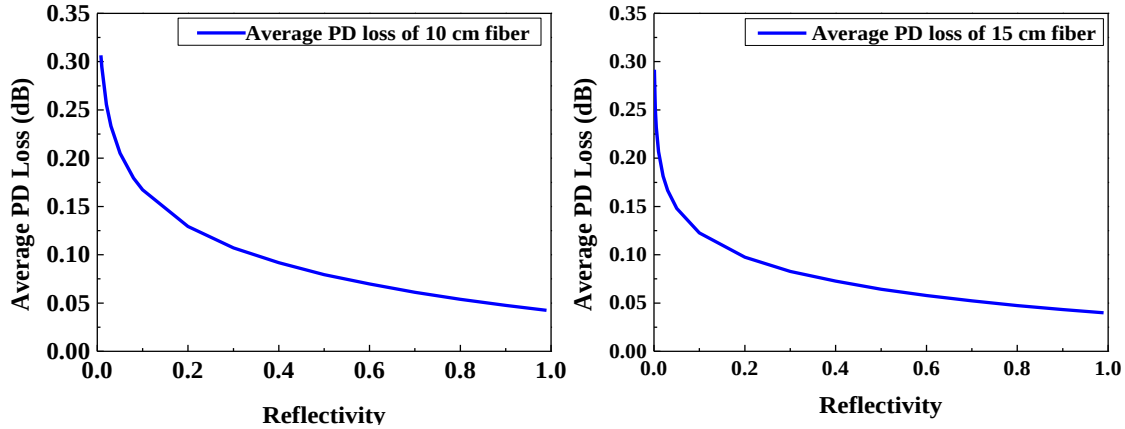

Fig. 4. 7. Variation of total PD loss with the reflectivity of output coupler Yb-doped fiber laser setup. (a): 10 cm Yb-doped fiber, (b): 15 cm Yb-doped fiber.

4.3 Optimal Reflectivity of Output Coupler in the presence of PD

According to the investigations in the last section, the PD induced loss is largely determined by the cavity design. In this section studies, the calculated PD loss is employed in rate equations for the laser operation calculation. Here, Yb-doped fiber with 0.1 dB/m background loss is investigated. For the 10 cm Yb-doped fiber, as shown in the Fig. 4.8 (a), without PD influence, the output lasing power reaches the maximum value of 511 mW when the reflectivity is around 10%. Once the PD factor is considered in the laser cavity, the optimal reflectivity for achieving the maximum output power shifts to 13% and the maximum power is affected by the PD loss and falls down to 482 mW. Regarding to the 15 cm Yb-doped fiber shown in Fig. 4.8 (b), the maximum lasing

power is 513 mW at reflectivity of 4% under the condition of no PD. However, the optimal reflectivity shifts to 5.8% with PD influence and the maximum output lasing power falls to 492 mW.

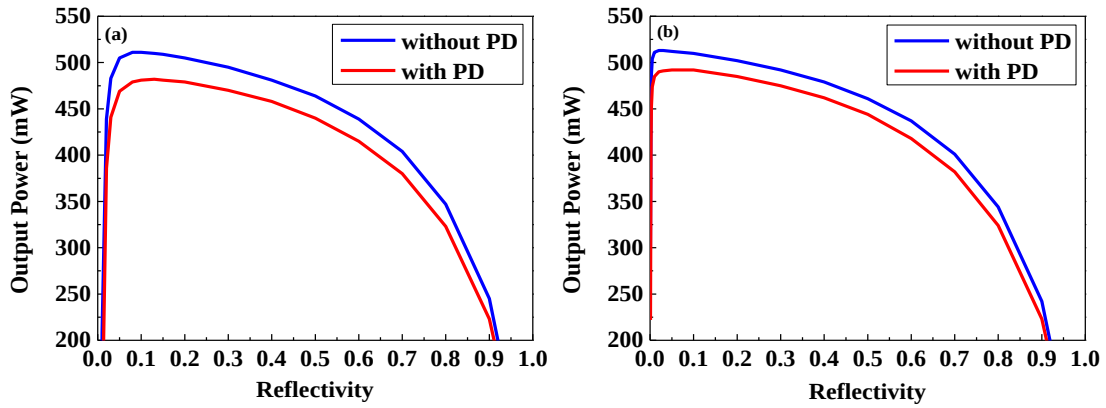

Fig. 4. 8. Variation of output lasing power with the reflectivity of output coupler. Blue curves show without PD and red curves represent with PD. (a): 10 cm length Yb-doped fiber, (b): 15 cm length Yb-doped fiber.

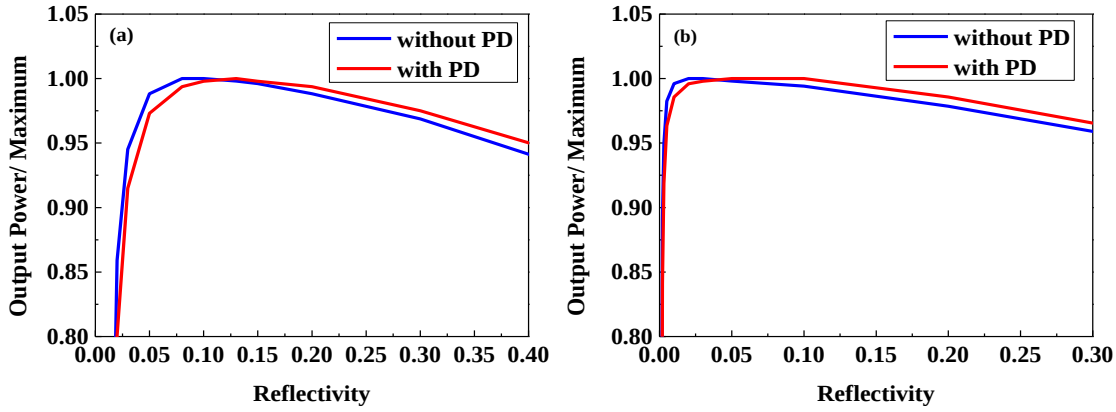

Fig. 4. 9. Variation of output lasing power ratio (peak value scaled to 1) with the reflectivity of output coupler. Blue curves show without PD and red curves represent with PD. (a): 10 cm length Yb-doped fiber, (b): 15 cm length Yb-doped fiber.

For observing the reflectivity shifting more clearly, the output lasing power at each reflectivity point is divided by the maximum power, thus the peak value for each curve is scaled to 1. The curves with new scaling are shown in Fig. 4.9. In this figure, it is clearer that the optimal reflectivity for output lasing power is right shift to the larger value. Both of the 10 cm Yb-doped fiber and 15 cm Yb-doped share the consistent

results. It can be clearly observed that, under 10 cm fiber length condition, the optimal reflectivity shifts from 10% to 13%, its increasing rate is 30% (calculation error 3.5%). Under 15 cm fiber length condition, as shown in Fig. 4.9 (b), the optimal reflectivity shifts from 4% to 5.8%, its increasing rate is 45% (calculation error 4.2 %). Therefore, it can be concluded that Yb-doped fiber laser with longer fiber length induces more significant change in the optimal reflectivity of the output coupler affected by PD loss.

Besides the different fiber length, Yb-doped fiber lasers with different cavity loss are discussed here. 15 cm Yb-doped fibers of 0.1 dB/m fiber background loss with 0.45 dB and 0.75 dB cavity loss are investigated. Here, the cavity loss is defined as the loss including fiber background loss and device loss. The average PD losses are calculated by the same procedures introduced in the previous section. The results are shown in the following Fig. 4.10. From Fig. 4.10, it can be observed that the average PD loss variation with reflectivity of 15 cm Yb-doped fibers with 0.45 dB and 0.75 dB cavity loss share similar trends as fibers of different fiber length discussed in the last section. From Fig. 4.10, it can be observed that 0.75 dB cavity loss leads to higher PD loss than 0.45 dB cavity loss. This is because larger cavity loss will enhance the general inversion level distribution along the fiber, thus, it will lead to higher PD loss.

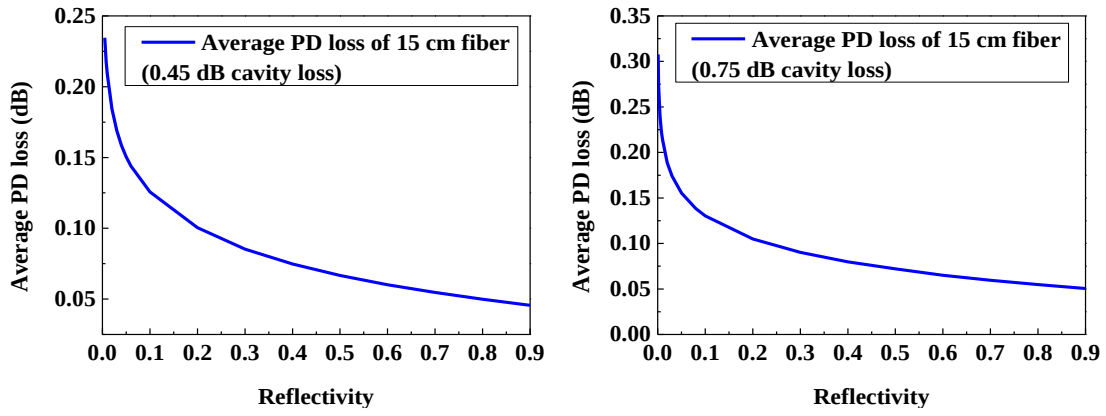

Fig. 4. 10. Variation of total PD loss with the reflectivity of output coupler of 15 cm length Yb-doped fiber. (a): 0.45 dB cavity loss, (b): 0.75 dB cavity loss.

Similar to the fibers with different fiber length discussed above, the calculated average PD losses are used in the laser operation calculation. The variations of output lasing power with reflectivity of 15 cm length Yb-doped fiber laser setup with 0.45 dB and 0.75 dB cavity loss are investigated, respectively, and the results are shown in the following Fig. 4.11(a) and Fig. 4.11(b).

For the Yb-doped fiber laser with 0.45 dB cavity loss, shown in Fig. 4.11(a), without PD influence, the output lasing power reaches the peak value of 487 mW when the reflectivity is near 4%. When the PD factor is considered in the laser cavity, the optimal reflectivity for achieving the maximum output lasing power shifts to 6% and the peak value of the output lasing power drops to 467 mW.

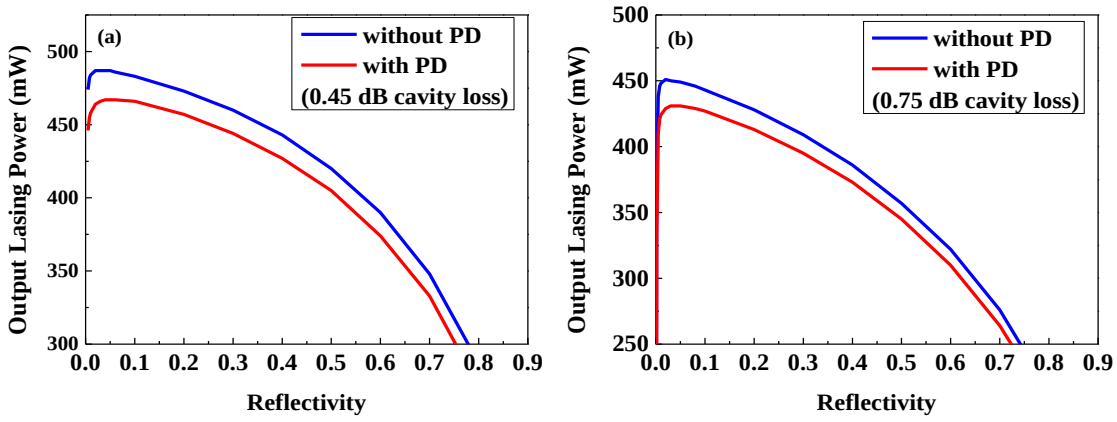

Fig. 4. 11. Variation of output lasing power with the reflectivity of output coupler for 15 cm Yb-doped fiber laser setup. Blue curves show without PD and red curves represent with PD. (a): 0.45 dB cavity loss, (b):0.75 dB cavity loss.

Regarding to the Yb-doped fiber laser with 0.75 dB cavity loss, as demonstrated in the Fig. 4.11 (b), without PD factor, when the reflectivity of the output coupler is approaching to 2%, the output lasing power can achieve its maximum power of 451 mW. Once the PD effects is considered in the laser cavity, the optimal reflectivity for achieving the maximum output lasing power moves to 5% and the maximum output lasing power falls down to 431 mW.

To observe the reflectivity shift more clearly, the same data manipulation to the fibers with different length has been done to Yb-doped fiber laser with different cavity loss. The output lasing power at each reflectivity point is divided by the maximum output lasing power and the peak value for each curve is scaled to 1. The curves with new scaling are shown in the following Fig. 4.12. It can be clearly observed that, under 0.45 dB cavity loss condition, the optimal reflectivity shifts from 4% to 6%, its increasing rate is 50% (calculation error 4.8%). Under 0.75 dB cavity loss condition, as shown in Fig. 4.12 (b), the optimal reflectivity shifts from 2% to 5%, its increasing rate is 150% (calculation error 7.3%). Therefore, it can be concluded that the higher cavity loss induces more significant change in the optimal reflectivity of the output coupler affected by PD loss.

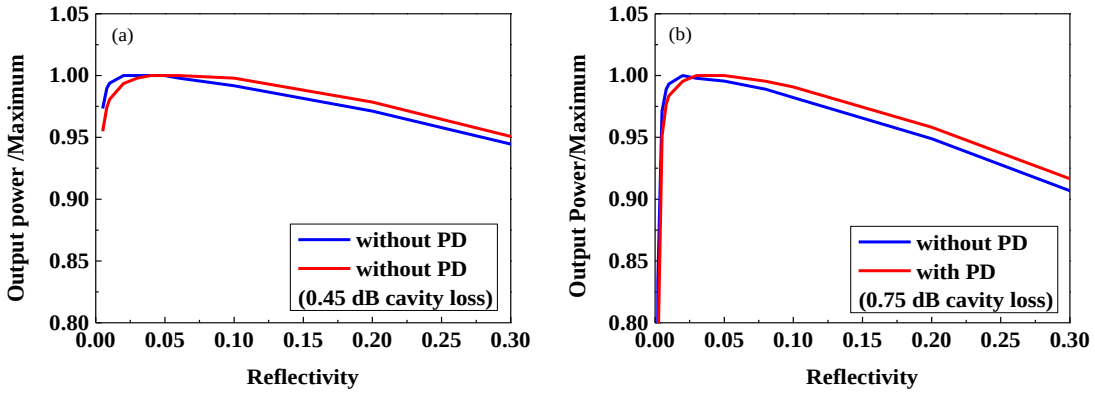

Fig. 4. 12. Variation of output lasing power ratio (peak value scaled to 1) to the reflectivity for 15 cm Yb-doped fiber laser setup. Blue curves show without PD and red curves represent with PD. (a): 0.45 dB cavity loss, (b): 0.75 dB cavity loss.

In terms of extractable power, for the 15 cm Yb-doped fiber laser with 0.45 dB cavity loss, the maximum output lasing power is 487 mW before PD at 4% reflectivity. After PD, the output lasing power drops to 464 mW, as shown in Fig. 4.11(a). Thus, the PD induces 4.7% of power degradation. By changing the reflectivity to 6%, the power drop is reduced to 467 mW. This corresponds to 0.65% of more extractible power by optimizing the cavity design. Similarly, for the 15 cm Yb-doped fiber laser with 0.75 dB cavity loss, the maximum output lasing power is 451 mW before PD at

2% reflectivity. After PD, the output lasing power drops to 427 mW, as shown in Fig. 4.11(b). Thus, the PD induces 5.3% of power degradation. By changing the reflectivity to 5%, the power drop is reduced to 431 mW. Thus, 0.93% of more extractable power is achievable by optimizing the cavity design. Therefore, in order to reach the maximum output power when considering PD, larger reflectivity is needed to compensate the excess loss in the cavity.

4.4 Conclusion

In this chapter, I discussed the output lasing power as a function of cavity reflectivity before and after considering PD effects. Without considering the PD factor, the results in this chapter are consistent with results shown in the references [105]. However, with the presence of the PD factor, it has been revealed that the extra cavity loss induced by PD is dependent on the selection of cavity reflectivity due to the variation of population inversion in the cavity. Conditions of different fiber lengths and laser cavity loss were discussed. It is concluded that, despite fiber length and cavity loss, the optimal reflectivity of the output coupler needs to be adjusted to larger value for achieving maximum output lasing power. Furthermore, the research results reveal that the longer the Yb-doped fiber or the larger the laser cavity loss is, the more significant shift of the reflectivity will take place. This finding firstly points out the PD influence on output coupler for fiber laser cavity improvement and possesses the significance of guiding more appropriate cavity parameters selection.

Chapter 5

Material Approach to Photodarkening Reduction

5.1 Background

The performance of Yb-doped fiber lasers has been greatly improved in recent years making them a good choice for a variety of industrial and medicinal applications. However, for applications requiring high peak powers and high pulse energies, such as in material processing, fiber lasers still lag behind solid-state lasers, mainly due to lower nonlinear threshold [88]. A shorter fiber with a large mode area is the design of choice for high energy pulsed laser applications. However, the short length requirements implies high Ytterbium (Yb) doping, which pushes up the core numerical aperture (NA) and increases the chances of clustering as well. It was discussed in Chapter 2 that the clustering causes the unwanted PD. Out of various approaches to mitigate the issues, codoping with Phosphorous (P) and Aluminum (Al) has been found to be a good method to satisfy the two contradicting requirements of low NA and high concentration [109]. When Al and P co-exist at an equivalent molar ratio, they form $AlPO_4$ that mimics the SiO_2 structure and possess a same refractive index of silica [110]. In addition, the presence of P greatly suppresses PD [110]. Consequently, a good deal of effort has been made towards achieving such Yb/Al/P co-doped core [20,88,111,112] , although previous reports seem to suggest that achieving highly Yb doped Al:P composition is very challenging in terms of index profile control and low background loss, in particular when Yb concentration is high (above 0.4 mol% Yb_2O_3), as shown in the following Fig. 5.1 [110]. From the Fig. 5.1, it is clearly observed that the index profile has a severe distortion and does not follow the dopants' concentration distribution along the diameter of the preform. This distorted index profile will squeeze

the mode field and make it becomes narrow. Therefore, it will impede the large mode area fiber fabrication.

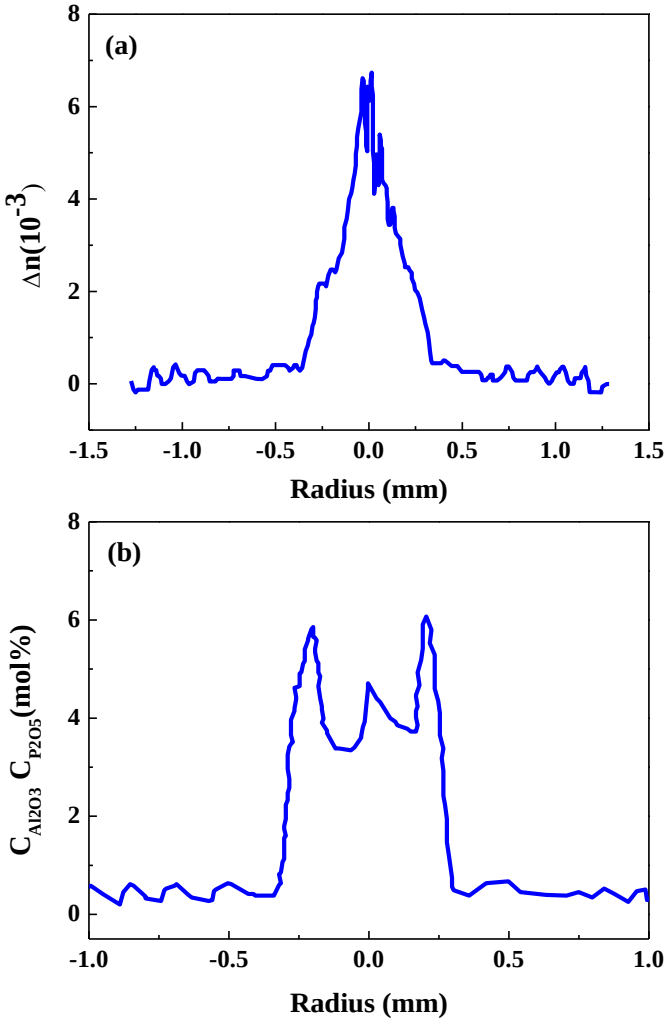

Fig. 5. 1. Radial profiles of refractive index (a) and dopant concentrations (b) of Yb-doped Al:P preform with equi-molar of Al:P

This severe distortion in the index profile is generally attributed to the evaporation of Yb or P [110,113], or non-uniform distribution of the dopants [109,110]. In addition, the background loss seems dependent on compositional ratios. It was reported that the loss is manageable in a ~10 dB/km level of a Yb-doped fiber with ~0.5 mol% Yb_2O_3 (but with a distorted index profile) when the equi-molar ratio is achieved [109,110]. The loss sharply increases when the host material becomes P dominated [110]. Hence, high Yb doping, refractive index profile control, and a low background loss in equi-

molar Al:P compositions have not been appropriately addressed as one package, either via solution doping [109–113] or chelate delivery method [113].

In this work, a step-index Al:P equi-molar fiber with 0.5 mol% Yb_2O_3 across the entire core, fabricated using MCVD and solution doping technique is reported. Despite the high Yb concentration, the core index contrast is as low as 0.0035 thanks to the equi-molar Al:P. The fiber shows a PD-suppressed characteristic and a low background loss of 10 dB/km. Laser output power of more than 100 W was achieved in the fiber (limited by pump power), with a slope efficiency of ~75%.

5.2 Fabrication of High Yb Doped Equi-molar Al:P Preform

Fabrication resorted on the MCVD technique together with solution doping to produce the highly Yb-doped Al:P fiber preform. The standard solution doping MCVD procedure is shown in the following Fig. 5.2. Fiber preform fabrication constituted of mainly three stages including Ge-doped cladding deposition, high Yb doped P: Al core deposition, and silica outer cladding removal and octagonal shaping. The raised cladding was realized by depositing multiple layers of GeO_2-SiO_2 by flowing in gas mixture of $SiCl_4$ and $GeCl_4$ into the silica substrate tube. Since the tube undergoes gradual collapsing over the depositions due to high temperature from a H_2/O_2 burner, a backward pressurizing system was employed to keep the tube open. During the deposition, the burner temperature and the gas flow rates were adjusted to compensate additional temperature gradient, thus maintaining same thermophoresis force over the depositions. With the developed recipe, I can routinely achieve raised Ge cladding of 6 - 9 mm thickness and a raised index contrast of 0.015 – 0.020 from silica. The doped Ge content is estimated in the range of ~12 mol% of GeO_2. Thus, the superior physical and chemical properties of silica are not compromised. I have not noticed abnormality while splicing and cleaving this fiber although more systematic study is required to confirm its characteristics. The Ge cladding deposition is followed by a core deposition of Yb:Al:P doped silica. I use phosphosilicate soot and a solution doping technique to

introduce Yb and Al. A uniform and stable P_2O_5–SiO_2 soot is deposited using the MCVD reagents of $SiCl_4$ and $POCl_3$. A pre-sintering pass was employed to stabilize the deposited P_2O_5–SiO_2 soot and control its porosity. Later Yb and Al were introduced via the solution doping technique. Subsequently, the conventional preform fabrication steps were carried out to sinter the soot, collapse the tube and seal it to a preform. I intentionally feed in extra $POCl_3$ flow during the high temperature collapse passes to compensate for the evaporation of P due to its high vapor pressure. The fabricated preform with triple layers of core, Ge cladding and silica cladding was later milled down to the Ge doped cladding layer, thus completely removing the outer silica layer from the preform rod. While removing the silica cladding, the preform was shaped to an octagonal cross-section under the milling to improve pump absorption. The milled preform was later polished and drawn in low index acrylic coating to form a double clad laser fiber.

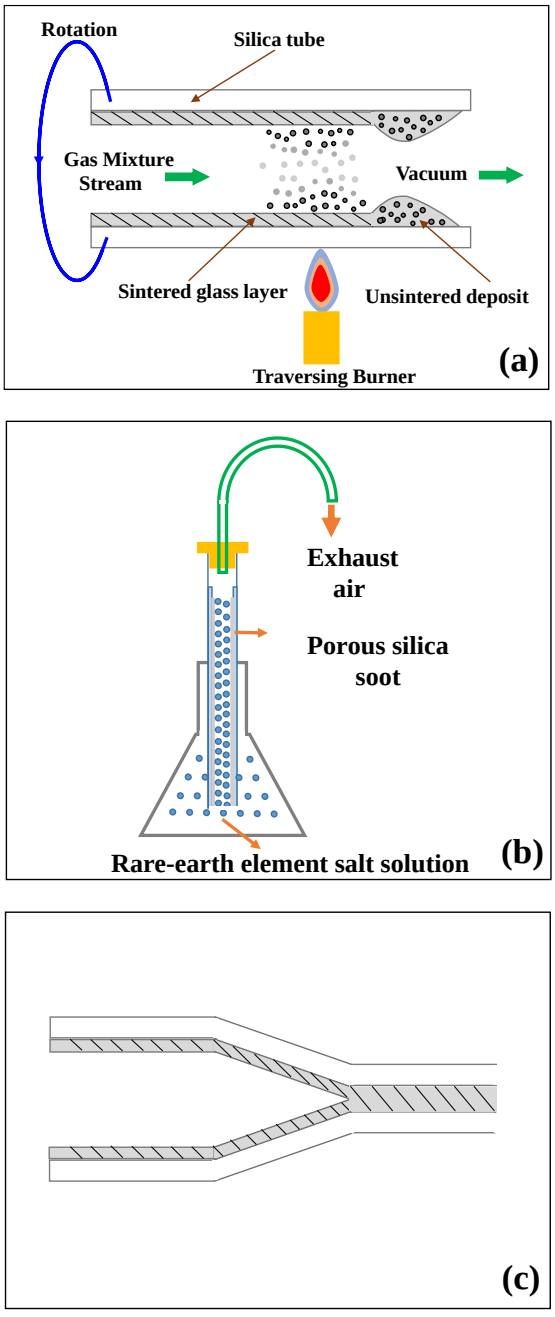

Fig. 5. 2. Fabrication procedure of preform by solution doping MCVD. (a) Silica soot fabrication (b) Solution absorbed by soot (c) Collapsing and sealing.

5.3 Characterization of Yb Doped Equi-molar Al:P Preform and Fibers.

After MCVD procedure, the preform is milled to an octagonal shape. Later, a standard fiber drawing tower is employed to draw the preform into an optical fiber. Fiber

drawing is initiated by heating one end of the preform above silica glass softening temperature and pulling a drop into a fiber. A fiber was drawn to 25 μm core, 250 μm flat-to-flat octagonal shaped cladding in a low index polymer coating. The characterization results of the preform and fiber are presented. The index profile of the fabricated preform is represented in Fig. 5.3. From 5.3, it is evident that we were able to achieve a good step index profile with Index difference of 0.0035±0.0006 despite the high Yb_2O_3 concentration of ~0.5 mol% as shown in Fig. 5.4. It is found that Al and P follow the same distribution profile, leading to the excellent index profile. Fig. 5.4 (a) represents a Scanning Electron Microscopy (SEM) image and concentration distributions of various oxides measured using *Energy Dispersive X-Ray* Analysis (EDX). The maximum Yb_2O_3, Al_2O_3 and P_2O_5 concentrations were found to be ~0.5 mol%, ~4.4 mol% and ~4.2 mol% respectively. A slightly higher P concentration compared to Al was intended to suppress PD [109]. And, the ratio between Al_2O_3/P_2O_5 and Yb_2O_3 was kept to ~9 so as to minimize background loss [111].

It should be noted that the overall index only increases by ~0.0035, despite the presence of high concentrations of the various oxides. A rare-earth oxide is known to contribute ~0.0067 index increase per mol% [8]. And the doped 0.5 mol% Yb_2O_3 is already sufficient to raise the index by ~0.00335. Hence, we can conclude that the measured refractive index contrast is almost fully contributed by the Yb_2O_3, and the incorporated Al_2O_3 and P_2O_5 are very well networked to form the desired $AlPO_4$. Background loss was measured using a cutback method and was found to be ~10 dB/km at 1200 nm, confirming the near uniform compositional distribution. Regarding the Yb absorption, measurements show that the fiber has an absorption value of 4.07 dB/m at 915 nm and 14.03 dB/m at 976 nm.

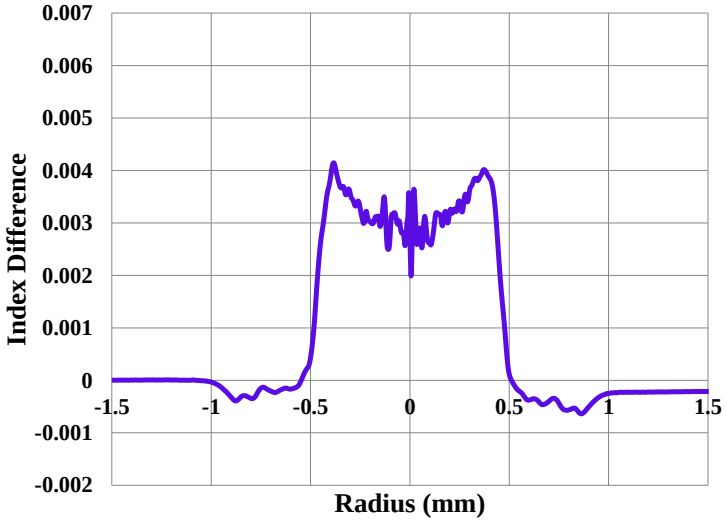

Fig. 5. 3. Refractive index profile of the fabricated Yb-Al-P doped fiber preform. Index difference in the core was found to be ~0.0035±0.0006

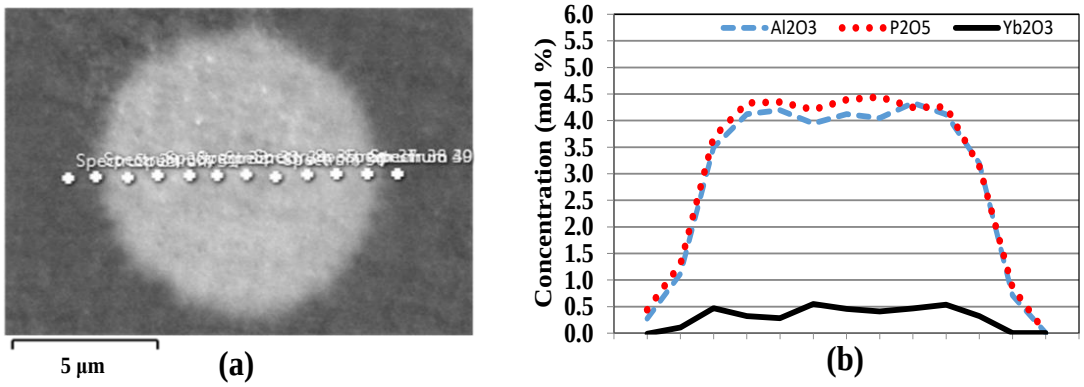

Fig . 5. 4. (a) SEM image of the fiber core & (b) Concentration of various oxides in the core in mol% measured using EDX. Oxides of Al and P can be seen to be almost perfectly matched in the core, which has led to index suppression.

5.4 Fiber Laser Performance and Photodarkening Measurement

A 4 meter length Yb-doped Al: P fiber is tested in a free running 4% - 4% linear cavity for laser efficiency. The fiber was pumped at 975 nm in the cladding pump configuration as shown in Fig. 5.5. In this fiber laser setup, L1 and L2 are employed to align the pump light and couple it into the Yb-doped Al: P fiber. L2 also shows aligning the backward output signal power for collection. Therefore, L1 and L2 are anti-

reflection coated both at pump wavelength and signal wavelength. L3 is utilized for aligning the forward output signal power and residual pump for collection. Thus, L3 is anti-reflection to pump wavelength and signal wavelength. Dichroic mirrors (DM) used in this fiber laser setup are for establishing beam paths. DM1, DM2 and DM3 in this setup are highly reflective at the pump wavelength and highly transmissive at a signal wavelength.

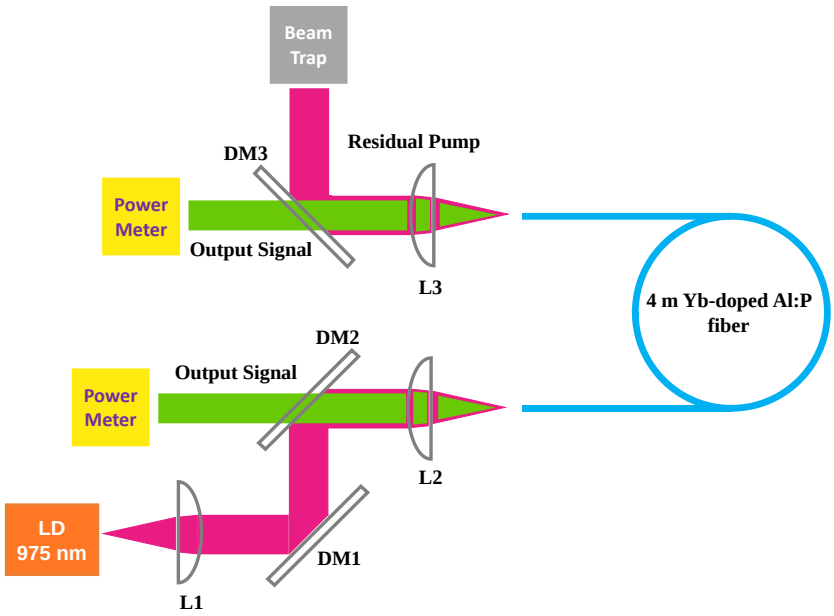

Fig. 5. 5. Yb-doped Al:P fiber laser setup

To investigate the laser performance, two sets of experiments are carried out here: the first using the wavelength unstabilized LD pumping a 2 m long fiber, and the second using a wavelength stabilized LD pumping a 0.5m long fiber. The 2m long fiber was cladding pumped by the unstabilized LD, and it generated 107 W of output power at 1050 nm. Its laser slope efficiency is measured as ~86%. The experiment was repeated using the wavelength stabilized LD. Thanks to the good overlap with the Yb peak absorption wavelength, the fiber length can be shortened to 0.5 m. A maximum output power of 58.6 W was observed at 71.5 W of launched pump power. The output power is only limited by the available pump power. Its laser slope efficiency is measured to be ~80%. The laser performance is shown in the following Fig. 5.6. The output lasing power is monitored for several hours, and no power decay is observed.

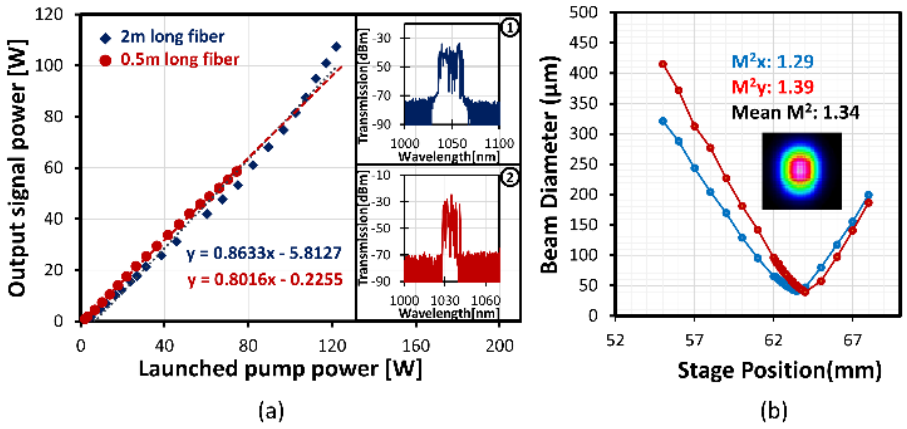

Fig. 5. 6. (a) Laser output power versus pump power in a 2m long fiber pumped using wavelength unlocked diode source and in a 0.5m long fiber pumped using 976nm wavelength locked diode source. The inset (1) shows the laser spectrum at full power in 2 m long fiber and inset (2) shows the laser spectrum at full power in 0.5 m long fiber; (b) measured beam quality factor at 107 W output power in a 2 m long fiber, with an inset showing beam profile.

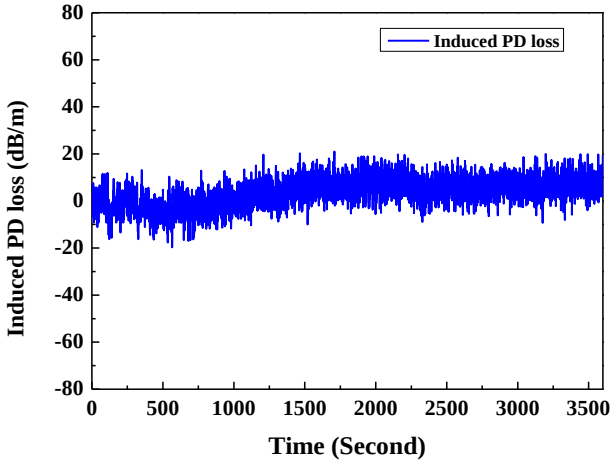

Fig. 5. 7. PD induced temporal excess loss for Yb-doped Al:P fiber at 634 nm under 120 mW 975 nm pumping.

To give a more thorough investigation on the PD effect of this Yb doped Al:P fiber, I used the typical experimental setup for Yb-doped fiber PD measurement mentioned in the Chapter 2 and the Chapter 3. The same experimental setup as illustrated in Fig. 3.7 was used for this fiber test. A 634 nm wavelength is selected as a probe since the PD induced loss can be easily detected and the wavelength is also located far from the Yb-band. A short fiber (~1.5 cm) is examined to suppress undesired amplified stimulated emission and maintain uniform inversion

level through the fiber. Following the calculation procedure described in Chapter 3, an inversion level is calculated at an available pump power level. In experiments, pump power at 975 nm is adjusted to 120 mW based on the calculation to obtain 42% inversion. The measurement is conducted continuously for around 1 hour. The measured temporal decay at 634 nm is shown in Fig. 5.7, which indicates that no PD decay is observed during the whole measurement. Therefore, it can be concluded here that this Yb-doped Al:P fiber exhibits negligible PD even at a high inversion level (~42%).

5.5 Conclusion

An equi-molar aluminium: phosphorus (Al:P) composition is known to suppress the PD in Yb-doped fiber significantly, but the realization of the equi-molar Al:P with very high Yb concentration has been hindered by complexity of the fabrication process. In this chapter, highly Yb-doped Al:P fiber with very good index profile using the conventional MCVD process is achieved by optimization of several aspects of the preform fabrication procedures from several aspects. PD suppression is realized in the fabricated fiber in conjunction with index suppression and low background loss. In addition, laser slope efficiency of ~75% is demonstrated with over 100W output power.

Chapter 6

Exploration of New Material as a Saturable Absorber for Pulsed Fiber Laser

6.1 Background

Short pulsed fiber laser, capable of achieving high output peak power and pulse energy with lower pump power demand, are anticipated to find wide applications in nonlinear optics, distributed sensing, optical signal processing, laser surgery, range finding and LIDAR systems. Fig. 6.1 presents the progress in pulse energy and average power generated by ultrafast pulsed fiber lasers achieved within the last decade [114]. It is shown that fiber laser has made great achievement in obtaining high average power and high pulse energy of ultrafast laser performance. High average powers of 800 W with moderate pulse energy (10 μJ) have been demonstrated [114]. On the other hand, appreciably high energy of 2 mJ with moderate average power of 10 W has been achieved. However, beyond 100 W in the high pulse energy regime (≥10 μJ) or 1 kW in the lower energy regime (≤ 10 μJ), delineated with the dashed line, the operation of pulsed fiber laser is severely limited by mode instabilities, resulting in significant output power fluctuation and beam pointing drift. However, there are several big breakthroughs of the short pulsed fiber lasers in the recent years. CPA (chirped-pulse-amplification) technique and large-mode-area fiber designs have been proposed and demonstrated to keep break the records in Fig. 6.1. In 2016, M. Kienel et al. present fs-pulses with 12 mJ pulse energy and 700 W average power by applying both temporal and spatial multiplexing in an FCPA (fiber-chirped-pulse-amplification) [115]. In 2017, extra-large mode area gain fibers together with pulse shaping capabilities of the seed laser were ultilized to suppress nonlinear effects and achieved 105 mJ pulse energy at more than 1 kW average output power [116].

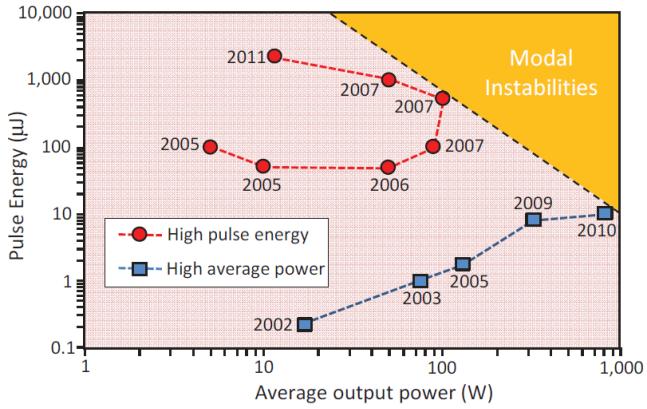

Fig. 6. 1. Ultrafast pulsed fiber laser parameter space [114]**.**

Passive mode-locked fiber lasers are one of the most common pulse-generation schemes available today because of their simplicity, flexibility and cost-effectiveness. One of the most efficient methods for realization passive Q-switching in fiber lasers is to employ the optical materials with saturable absorption feature (i.e. saturable absorbers, SAs) [117–119]. In the past decade, carbon based materials (single walled carbon nanotubes SWCNTs [120,121], graphene [122,123]), as shown in Fig. 6.2, have been consecutively discovered and have been demonstrated to be excellent SAs for Q-switched fiber lasers.

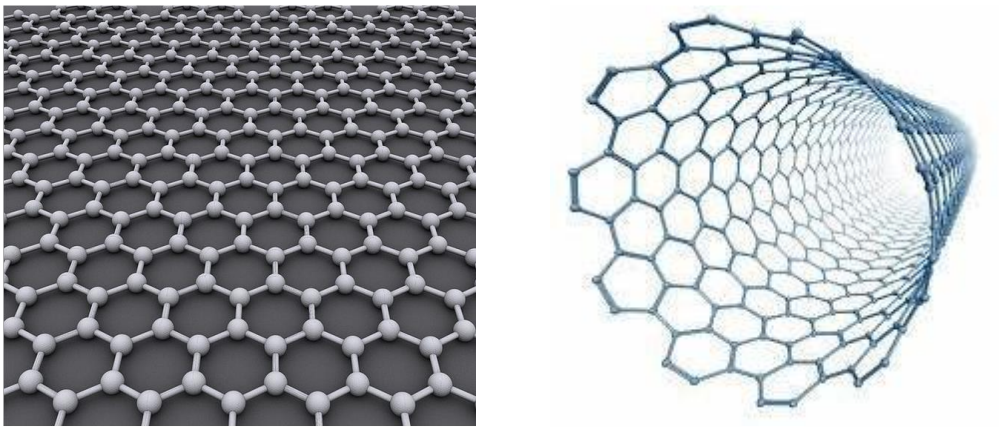

Fig. 6. 2. Schematic representation of graphene (left) and SWCNT (right).

Semiconductor SWCNTs possesses the semiconductor band-gap character. Once the excitation light intensity at sufficiently high level, the photon-generated-carriers fill the CNTs' conduction band, making the conduction band full but valence band empty,

which prevents further photon absorption. Therefore, optical absorption by SWCNTs decreases and tends to saturate with the increase of incident light intensity. When applied into a laser cavity, SWCNT-based SAs can facilitate laser system to achieve stable pulse formation. The SWCNTs have exhibited low saturable optical intensity and fast recovery time to serve as a good SA. However, SWCNTs have a constraint of spectral response bound to its diameter, thus restricting broadband tunability [124].

On the other hand, different from the conventional semiconductor saturable absorbers, the energy band diagram of graphene shows zero bandgap and a linear dispersion relation. These unique energy band features combined with the Pauli blocking principle enable graphene to possess a full band saturable absorber characteristic. Fig. 6.3 shows a schematic illustration of the energy band structure and different wavelength photon absorption of graphene [124].

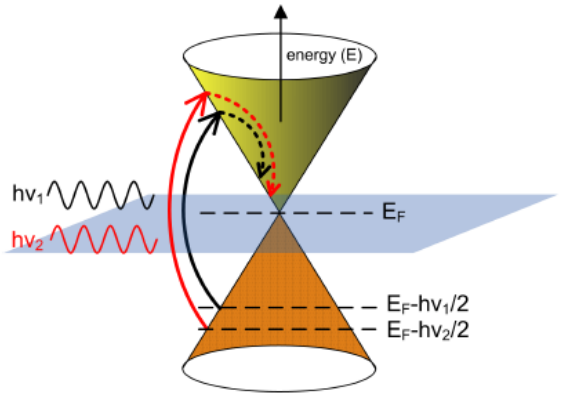

Fig. 6. 3. Schematic of graphene's energy band structure and photon absorption [124].

Even though graphene features wavelength-insensitive saturable absorption characteristic and wideband nonlinear optical response over visible to near-infrared because of its zero band gap property, it holds an intrinsic disadvantage of weak absorption efficiency due to a low modulation depth [122]. In addition, preparation of graphene-based SAs requires relatively complex and costly clean-room-based chemical vapor deposition (CVD) fabrication system [125].

Until now, researchers are still making great efforts to develop new SAs which are

expected to offer desirable characteristics including wavelength-independent saturable absorption, low saturable optical intensity, large modulation depth, simple preparation process and low fabrication cost.

6.2 Carbon Nanoparticles (CNPs) as a saturable absorber

Very recently, due to its unique photoluminescence properties among the carbon based materials (including SWCNTS and graphene), carbon nanoparticles (CNPs) have drawn great attention in the field of biomedical, life sciences and other different optoelectronic device applications [126–130]. Previously, semiconductor quantum dots such as CdSe were considered the best choice for optical imaging experiments in vitro and in vivo, according to their outstanding two-photon fluorescence characteristic [131,132]. However, serious concerns to the safety of those high performance semiconductor quantum dots has raised. Since the quantum dots are composed of heavy metals which is known for toxicity and potential environmental hazard. Therefore, carbon nanoparticles exhibiting bright photoluminescence in the visible are now considered as a good substitute for semiconductor quantum dots.

Once the CNPs' surface is passivated by attaching simple organic species to the acid-treated carbon particles, bright luminescence emissions can be observed as shown in Fig. 6.4. Organic molecules such as PEG1500N can serve the purpose of surface passivation [133]. Mechanistically, the carbon-based photoluminescence has been attributed to passivated defects on the carbon particle surface acting as excitation energy traps [129].

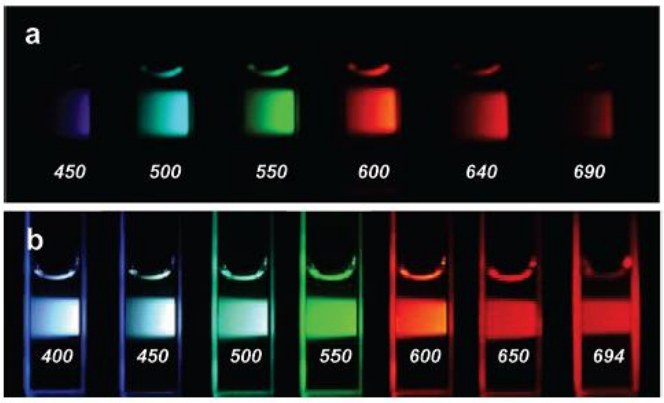

Fig. 6. 4. Aqueous solution of the PEG1500N-attached carbon dots (a) excited at 400 nm and photographed through band-pass filters of different wavelengths as indicated, and (b) excited at the indicated wavelengths and photographed directly [133]**.**

In terms of fabrication, the CNPs can be easily obtained via a simple and low- cost flame synthesis process [134] , thus not requiring large investment in equipment. More interestingly, producing CNPs does not require any starting material. They can be gathered via incomplete combustion of alcohol molecule in air. Thus, it is largely safe, abundant and cost-effective to prepare CNPs. As compared with other carbon-based materials, adoption of CNPs in a laser field has been slow. I investigated performance of the CNPs as a saturable absorber in a fiber laser ring cavity. The CNPs prepared in-house was inserted in a fiber ring cavity, and a successful pulse operation was demonstrated using the CNPs as a saturable absorber for the first time to my knowledge. Hence, this study adds another carbon based optical material which is abundantly obtainable and performs as a saturable absorber.

6.3 Fabrication and Characterization of CNPs

The CNPs used in the experiment are grown in the ceramic strips by a simple flame synthesis process [134]. In short, a ceramic strip is mounted at the ethanol flame top of a common alcohol burner for a several minutes. The experimental setting is shown in Fig. 6.5. When the color of the strip surface exposed to the flame turns from gray to black, the color change indicates growth of CNPs. The collected CNPs from the ceramic strip are then transferred to the annealing furnace and annealed at 500℃ for 1

hour to remove organic impurities generated during the flame synthesis. The dimension of the CNPs is characterized by Transmission Electron Microscope (TEM) images that are represented in Fig. 6.6. The low magnification TEM image shown in Fig. 6.6 (a) indicates that the CNPs have dendrite-like morphology and consist of nanoparticle network-like structures. A higher magnification image (Fig. 6.6 (b)) reveals that CNPs consist of many curved carbon lamellas with diameter of ~35 nm.

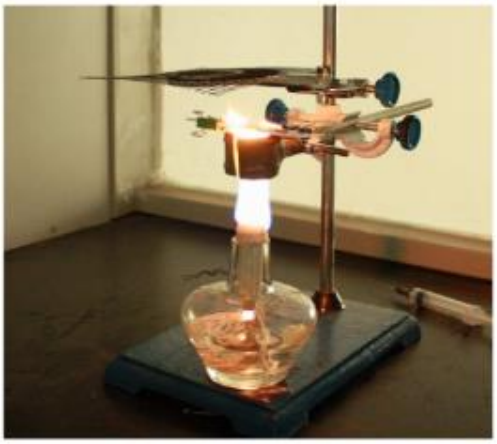

Fig. 6. 5. Experimental setup for the synthesis of CNPs [134]**.**

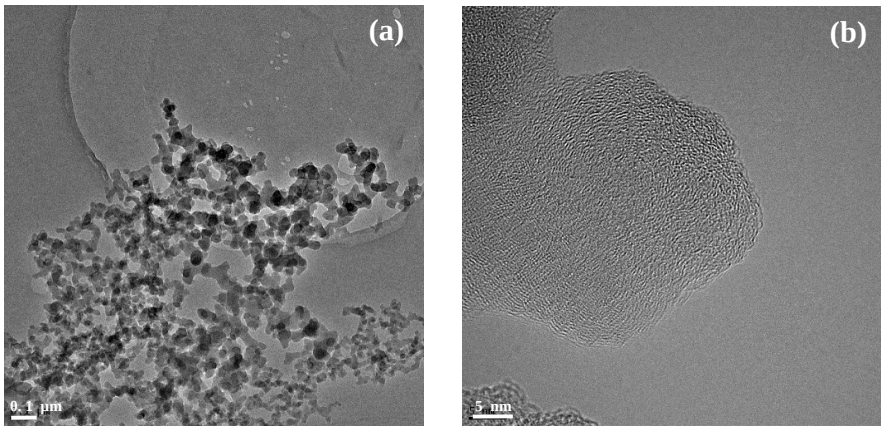

Fig. 6. 6. TEM images of in-house CNPs at (a) low magnification and (b) high resolution.

In order to measure optical properties of the prepared CNPs, 5 mg of the prepared CNPs flakes are added into 5 mL DI water. With being ultrasonicated for 30 minutes, the CNPs become well dispersed in the DI water (Step 1). Subsequently, 0.25 g of polyvinyl alcohol powder is added to the CNPs DI water suspension (Step 2). At the

same time, the same amount of polyvinyl alcohol powder is added to 5 mL pure DI water as the reference sample. In the following steps, the reference sample is proceeded by the same methods as the CNPs sample. The polyvinyl alcohol powders are well dissolved in the water after 1 hour stirring under 95℃(Step 3). This procedure is used to disperse CNPs into the colloidal solution, which is helpful to generate a polymerized film for measurement. The CNPs suspension is sprayed and deposited onto a glass substrate by spin-coating (Step 4). The deposited CNPs are dried on a heat plate at 120℃ for 35 minutes (Step 5). The schematic diagram of the process flow is shown in Fig. 6.7. The prepared CNP film and reference film are loaded in a visible-mid-IR spectrometer (Perkinelmer Lambda 7500) to measure their transmission. Fig. 6.8 presents the transmission spectrum of CNPs ranging from 500 nm to 2500 nm by subtracting the two transmissions using an optical spectrometer (Perkinelmer Lambda 7500). The transmission curve shows that the CNPs have a relatively flat transmission from visible to the mid-infrared wavelength band with 72% transmittance at 1035 nm, indicating their potential for broadband pulsed fiber lasers.

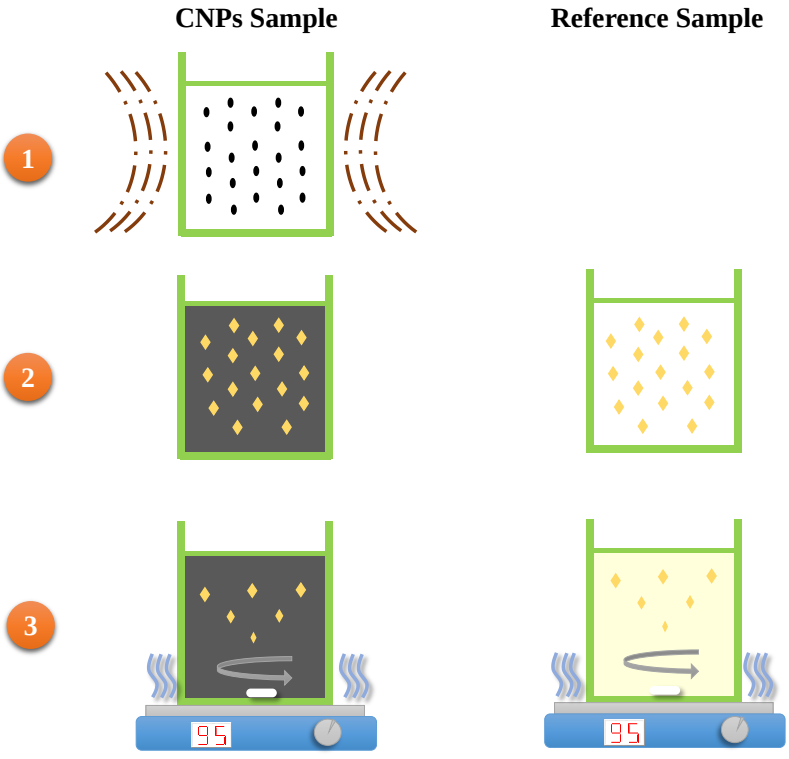

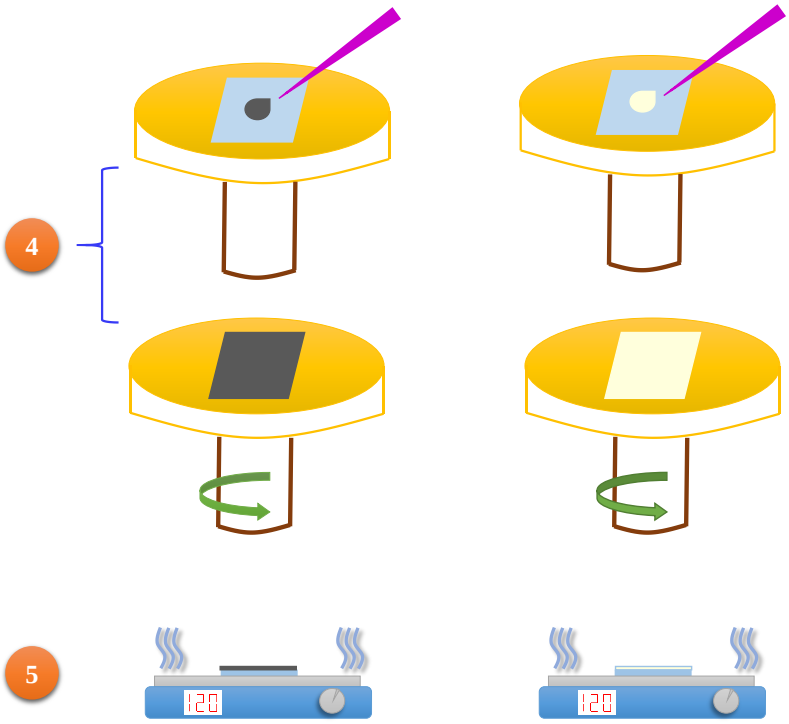

Fig. 6. 7. Schematic diagram of processing flow of CNPs sample and reference sample. The corresponding steps are described in the text.

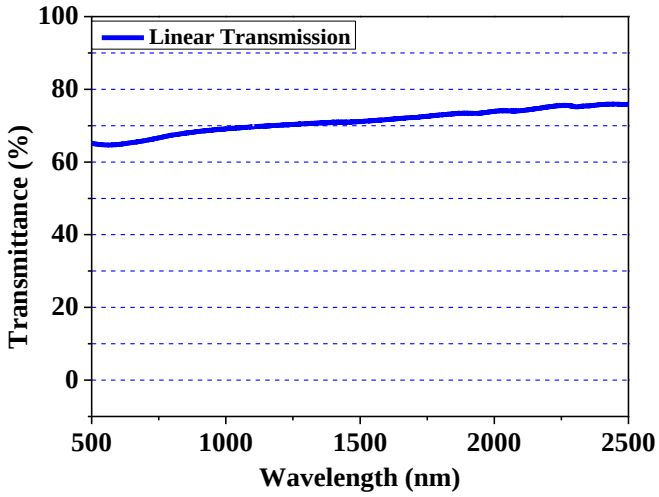

Fig. 6. 8. The linear transmission spectrum of the CNPs sample.

6.4 Carbon nanoparticles as saturable absorber

To integrate the CNPs into the laser with all-fiber structure, the CNPs saturable absorber is deposited onto a facet of a fiber ferrule. A well dispersed CNPs solution is prepared by adding 1 mg as-prepared CNPs into 5 ml ethanol and ultrasonicating for

30 minutes. To deposit the CNPs on the fiber core, optically driven deposition method is employed here [135]. In [135], the process for depositing the carbon nanotubes is presented in detail. The setup for depositing nanotubes on optical fiber end-facet is shown in Fig. 6.9. In the experiment, I employ

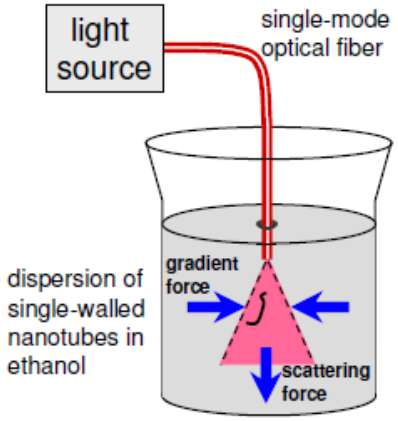

Fig. 6. 9. Setup for depositing carbon nanotubes on the ends of cleaved optical fibers using optical radiation. Forces due to optical radiation are also shown [135]**.**

the same setup to deposit the CNPs on fiber core. A 100 mW laser at 975 nm is coupled to a single mode fiber patch cord. The output end of the fiber is immersed in the prepared solution. The applied optical power is sufficient to generate thermophoretic force to move and deposit the CNPs on the fiber end-facet.

The CNPs-deposited fiber end facet is inserted in the laser cavity through a fiber mating sleeve as schematically shown in Fig. 6.10. A compact ring cavity consists of a 3.0 m long Yb-doped fiber with 10-15 dB/m core absorption at 975 nm. A pump laser at 975 nm is coupled to the cavity via a 980/1030 nm wavelength division multiplxer (WDM), and pumps the Yb-doped fiber. A polarization controller (PC) is inserted to adjust cavity birefringence and stabilize pulses. The CNP deposited facet is placed between the PC and a 90/10 coupler that induces 90% of signal output coupling. Since the Yb-doped fiber employed in this setup is a commercial PD-suppressed fiber, 90% output ratio can approach the maximum output lasing power according to the

discussion results in Chapter 4. A polarisation-independent isolator is also employed for ensuring unidirectional operation. Characteristics of the output laser are monitored by an optical spectrum analyzer (OSA, Advantest Q8384) and a high-speed photodetector together with a digital oscilloscope (Tektronix TDS2024).

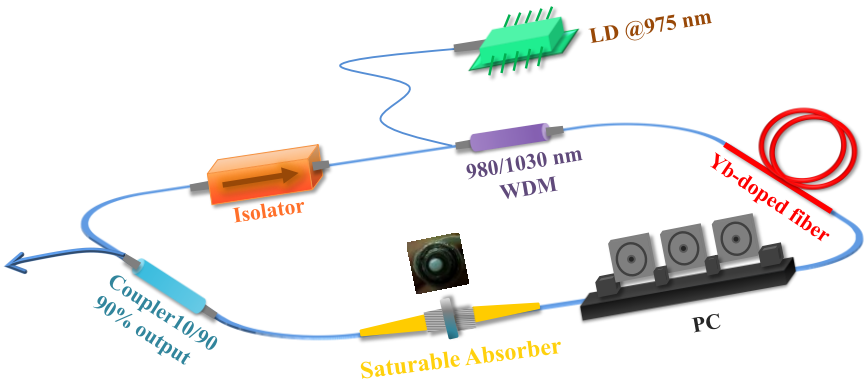

Fig. 6. 10. The schematic of the Q-switched laser setup based on CNPs.

In this experiment, the laser operates in a continuous-wave mode at low induced pump power. With pump power increasing, it transits to the Q-switching operation at 215 mW, demonstrating functionality of the CNPs as a modulator. With the pump power gradually increased from 215 mW to 325 mW, as shown in Fig. 6.11, the stable pulse trains with the higher repetition rates were observed, following typical feature of passive Q-switching. The center wavelength of the Q-switched pulses is at 1035 nm, measured under 215 mW pump power as shown in the inset of Fig. 6.11 (a). The average output power can reach the maximum value of 2.8 mW under 432 mW pump that is the largest incident pump power achieved in this experiment. The center wavelength is located at 1035 nm which is shown in the inset of Fig. 6.11(a). Its 3 dB bandwidth is 270 GHz (delta λ = 0.9 nm).

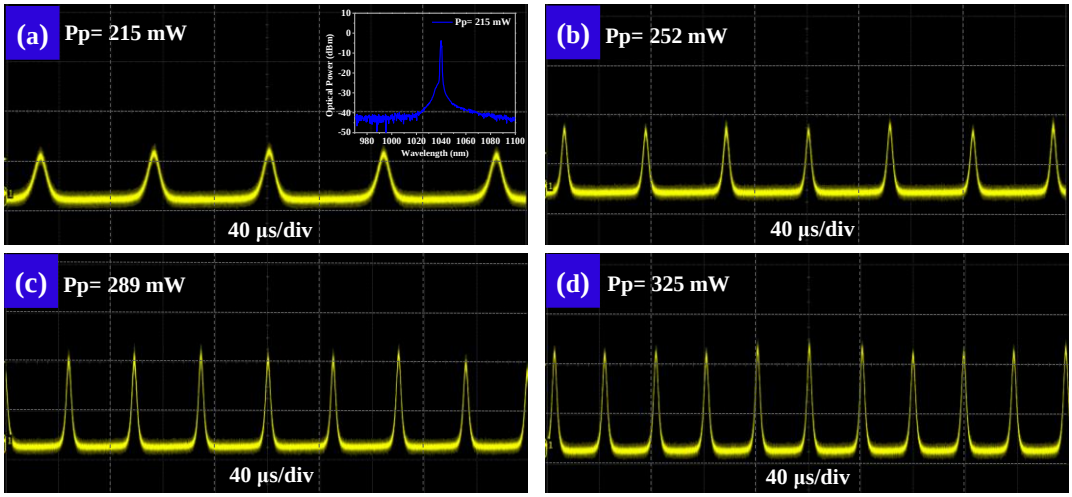

Fig. 6. 11. The Q-switched pulse trains under different pump powers Pp, (a) Pp =215 mW, repetition rate = 22.10 kHz, inset: lasing spectrum at 215 mW pump (b) Pp = 252 mW, repetition rate = 31.25 kHz (c) Pp = 289 mW, 40.00 kHz (d) Pp = 325 mW, 50.00 kHz.

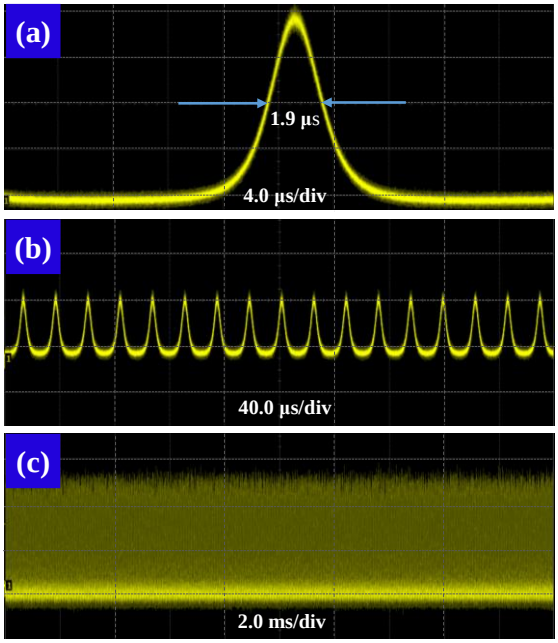

Fig. 6. 12. Typical Q-switched pulses at different time scale under the 432 mW pump power of the Q-switched laser.

Fig. 6.12 shows a typical Q switched pulse train measured with different time scales under 432 mW pump power. The shortest Q-switched pulse width was about 1.9 µs under 432 mW pump power as shown in Fig. 6.12(a). Fig. 6.12 reveals that very stable Q-switched pulses were achieved in this experiment.

The pulse repetition rate and the pulse duration vary as a function of the incident pump power, as shown in Fig. 6.13. As increasing the pump power from 215 mW to 432 mW, the pulse width significantly narrowed from 7.9 μs to 1.9 μs, and meanwhile the pulse repetition rate increase from 22.73 kHz to 86.96 kHz.

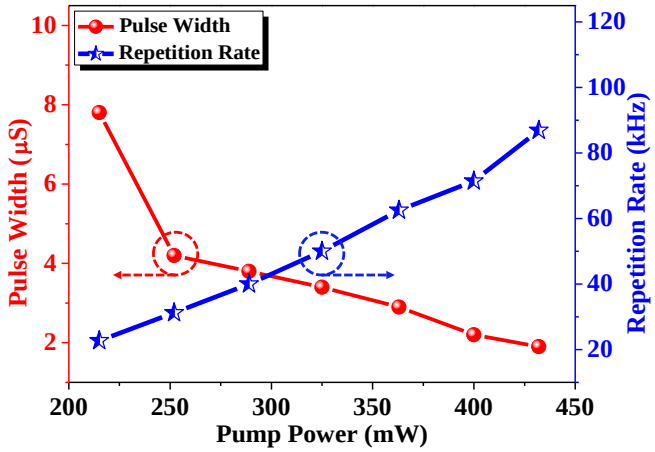

Fig. 6. 13. Pulse width and repetition rate versus the incident pump power.

To confirm the role of the CNP in the Q-switching experiments, I removed the CNP coated ferrule and introduced a new ferrule to maintain the same cavity configuration. Hence, the new setup provides the same cavity except absence of the CNPs. In the subsequent laser experiments, only CW operation was obtained even under the maximum pump power at 432 mW. This clearly confirms the CNPs role as a SA.

6.5 Conclusion

In conclusion, I present the first demonstration, to the best of my knowledge, of CNPs-based passive Q-switched fiber laser. In-house CNPs are successfully used in a diode-pumped Yb-doped fiber laser to generate stable 1.9 μs Q-switched short pulses with a pulse repetition of 86.96 kHz. This experimental result clearly shows that CNPs possesses the desired properties for optical modulation. Considering the broadband absorption band of the CNPs measured by transmission spectrophotometry, it is believed that CNPs could have a great potential as saturable absorbers to generate short or even ultrashort laser pulses in various wavelength regions.

In the aspect of fabrication, the CNPs can be easily obtained via a simple and low-cost flame synthesis process, thus do not requiring investment on heavy equipment. Fabricating CNPs does not require any starting material preparation either. They can be produced via incomplete combustion of alcohol molecules in ambient air. Thus, it is straightforward and cost-effective to produce the CNPs. In addition, considering the broadband absorption of CNPs, there is the possibility that CNPs could be a potential candidate to enable diverse applications including optical signal processing and ultrafast laser pulse generation at various wavelengths. At the present stage, this is the first experimental demonstration of CNPs as an optical modulator to generate Q-switched pulses in a fiber laser. The laser performance demonstrated in the thesis by employing CNPs is not that good as the mature pulsed laser employing CNT. Anyway, we will keep optimize the characters of CNPs saturable absorber in pulsed laser.

Chapter 7

Conclusion and Future Works

7.1 The Conclusion

In conclusion, this thesis presents investigations on PD reduction by improvement of lasing cavity design and material engineering. The relationship of pump wavelength and cavity reflectivity to PD significance are firstly disclosed in this thesis. A novel PD-free highly Yb-doped fiber with high lasing efficiency is achieved by improvement of preform fabrication. In addition, 1 μm pulsed fiber laser with new saturable absorber is investigated.

From the perspective of laser cavity design, strong dependence of the PD on the pump wavelengths of Yb-doped fibers is investigated. Experiment results reveal that the 976 nm pumping leads to more significant PD than 916 nm under the condition of same Yb inversion level. Investigations on fibers with different compositions including the widely used Yb:Al and Yb:P present persistent experimental results. Such dependence is persistent across various fibers with different compositions including the widely used Yb:Al and Yb:P. This research result has the guiding significance on pump wavelength selection in high power Yb-doped fiber lasers and optimizing long term performance of high-power laser devices.

Besides the improvement of pump wavelength selection, optimal reflectivity of the laser cavity needs to be adjusted with the presence of PD factor. It is revealed in this thesis that the extra cavity loss induced by PD is dependent on the selection of cavity reflectivity due to the variation of population inversion in cavity. The research results demonstrate that despite of the fiber length and cavity loss, the optimal reflectivity of the output coupler needs to be adjusted to larger value for achieving maximum

extractable output lasing power. This research result possesses the significance of guiding more appropriate cavity parameters selection.

From the perspective of material engineering, a PD free highly Yb-doped Al:P fiber with very good index profile using the conventional MCVD process is achieved by optimization several aspects of the preform fabrication procedure. Previous reports indicate that achieving highly Yb-doped Al:P composition is very challenging in terms of index profile control, and low background loss. With this preform fabrication method, the problem of severe distortion in the index profile of Yb-doped Al:P fibers is solved. High performance fiber laser with PD free feature has been realized with this fabricated Yb-doped Al:P fiber.

Finally, the study in this thesis provides exploration of new material as a saturable absorber for pulsed fiber laser. A novel carbon based material CNPs is applied in a passive Q-switched Yb-doped fiber laser as a modulator. Different from the majority of optical materials working as saturable absorber, CNPs can be efficiently prepared and obtained via a simple and low-cost flame synthesis process in-house, without the need of complicated equipment. The experimental result clearly illustrates that CNPs possesses the desired properties for optical modulation and it is believed that CNPs could have a great potential in various wavelength regions as saturable absorbers to generate short or even ultrashort laser pulses due to its broadband absorption band.

7.2 The Future Works

1. Pump wavelength dependence of PD in Yb-doped Fiber has been investigated in this thesis. From the temporal decay measurement, it is clearly observed that 976 nm pumping leads to more significant PD than 916 nm pumping. Besides the temporal decay measurement for probe light, it is also meaningful to check the fiber laser performance with different pump wavelengths. This is of great significance in practical application and should be carried out in the future.

2. The highly doped Yb-doped Al:P fiber has been verified to be PD free ~42 % inversion under 975 nm pumping. It is already around the maximum inversion value that can be realized by 975 nm pumping. In the future work, the PD loss should be measured under higher inversion level by 915 nm pumping. This will be very attractive to check the PD suppression performance of this Yb-doped Al:P fiber under higher inversion level (> 50%).

3. The new carbon based material, CNP, has been successfully used as the modulator into the passive Q-switched Yb-doped fiber laser. In the future work, CNPs could be used in 1.5 μm and 2 μm fiber lasers. Experiments should be carried out to verify the CNPs has a broadband saturable absorption character.

Publications

Journal Publications

1. **Huizi Li**, Liling Zhang, Raghuraman Sidharthan, Daryl Ho, Xuan Wu, Nalla Venkatram, Handong Sun, Tianye Huang, and Seongwoo Yoo*, “Pump Wavelength Dependence of Photodarkening in Yb-Doped Fibers,” J. Lightwave Technol. 35, 2535-2540 (2017).
2. **Huizi Li**, Jie Ma, Jun Wang, Dingyuan Tang and Seongwoo Yoo*, “Carbon Nanoparticles as a Novel Optical Modulator for Pulsed Fiber Laser,” (Submitted to Optics Express).
3. **Huizi Li**, Jie Ma, Jun Wang, Dingyuan Tang and Seongwoo Yoo*, “Photodarkening Impact on Laser Cavity Design with Output Coupler adjustment,” (In preparation).
4. Raghuraman Sidharthan, Junhua Ji, Kang Jie Lim, Serene Huiting Lim, **Huizi Li**, Jian Wei Lua, Yanyan Zhou, Chun Ho Tse, Daryl Ho, Yue Men Seng, Song Liang Chua, and Seongwoo Yoo, "Step-index high-absorption Yb-doped large-mode-area fiber with Ge-doped raised cladding," Opt. Lett. 43, 5897-5900 (2018).

Conference publications

1. **Huizi Li**, Liling Zhang, Raghuraman Sidharthan, Daryl Ho, Xuan Wu, Seongwoo Yoo* “Dependence of photodarkening under different wavelength pumping.” SPIE paper 9728-110, 2016
2. **Huizi Li**†, Jie Ma†, Mengying Zhang, Jun Wang, Dingyuan Tang, and Seongwoo Yoo* “Carbon Nanoparticles as an Optical Modulator for Passively Q-switched Fiber Laser.” in Conference on Lasers and Electro-Optics, OSA Technical Digest (online) (Optical Society of America, 2018), paper JTu2A.174.
3. R. Sidharthan, S. H. Lim, K. J. Lim, D. Ho, C. H. Tse, J. Ji, **H. Li**, Y. M. Seng, S.

L. Chua, and S. Yoo, "Fabrication of Low Loss Low-NA Highly Yb-doped Aluminophosphosilicate Fiber for High Power Fiber Lasers," in Conference on Lasers and Electro-Optics, OSA Terchnical Digest (online) (Optical Society of America, 2018), paper JTh2A.129.

4. R. Sidharthan, K. J. Lim, S. H. Lim, **H. Li**, Y. Zhou, J. Ji, Y. M. Seng, S. L. Chua, and S. Yoo, "High Absorption Low NA Step Index Large-Mode-Area Fiber for High Power Ultrafast Lasers," in Conference on Lasers and Electro-Optics, OSA Technical Digest (Optical Society of America, 2019), paper JW2A.89.

References

1. G. P. S. L. Griscom, *Defects in SiO2 and Related Dielectrcis*.
2. S. Basu, *CRYSTALLINE SILICON – Edited by Sukumar Basu*.
3. L. Skuja, “Optically active oxygen-deficiency-related centers in amorphous silicon dioxide,” J. Non. Cryst. Solids **239**(1–3), 16–48 (1998).
4. E. J. Friebele, D. L. Griscom, M. Stapelbroek, and R. A. Weeks, “Fundamental Defect Centers in Glass: The Peroxy Radical in Irradiated, High-Purity, Fused Silica,” Phys. Rev. Lett. **42**(20), 1346–1349 (1979).
5. H. Nakanishi, S. Endo, T. Irie, M. Tsukioka, E. Nagata, M. Baba, K. Shibata, F. Kherbouche, and B. Poumellec, “Related content Correlation between Ge E ′ Centers and Optical Absorption Bands in SiO 2 : GeO 2 Glasses” (1996).
6. K. O. Hill, Y. Fujii, D. C. Johnson, B. S. Kawasaki, K. O. Hill, Y. Fujii, D. C. Johnson, and B. S. Kawasaki, “Photosensitivity in optical fiber waveguides : Application to reflection filter fabrication Photosensitivity in optical fiber waveguides : Application to reflection filter fabrication,” 86–89 (2009).
7. R. Paschotta, J. Nilsson, P. R. Barber, J. E. Caplen, A. C. Tropper, and D. C. Hanna, “Lifetime quenching in Yb-doped fibres,” Opt. Commun. **136**(5–6), 375–378 (1997).
8. R. Paschotta, J. Nilsson, P. R. Barber, J. E. Caplen, A. C. Tropper, and D. C. Hanna, “Lifetime quenching in Yb-doped fibres,” Opt. Commun. **136**(5–6), 375–378 (1997).
9. J. J. Koponen, M. J. Söderlund, H. J. Hoffman, and S. K. T. Tammela, “Measuring photodarkening from single-mode ytterbium doped silica fibers,” Opt. Express **14**(24), 11539–11544 (2006).
10. J. J. Koponen, M. J. Söderlund, S. K. T. Tammela, H. Po, J. J. Koponen, M. J. Söderlund, S. K. T. Tammela, and H. Po, “Proceedings of spie” (2018).

11. S. Jetschke, S. Unger, U. Röpke, and J. Kirchhof, “Photodarkening in Yb doped fibers: experimental evidence of equilibrium states depending on the pump power,” Opt. Express **15**(22), 14838–14843 (2007).
12. J. Koponen, M. Laurila, and M. Hotoleanu, “Inversion behavior in core- and cladding-pumped Yb-doped fiber photodarkening measurements.,” Appl. Opt. **47**(25), 4522–4528 (2008).
13. S. Jetschke and U. Röpke, “Power-law dependence of the photodarkening rate constant on the inversion in Yb doped fibers.,” Opt. Lett. **34**(1), 109–111 (2009).
14. M. J. Söderlund, J. J. Montiel, and J. P. Koplow, “Heat-induced darkening and spectral broadening in photodarkened ytterbium-doped fiber under thermal cycling,” 3352–3354 (2009).
15. J. Jasapara, M. Andrejco, D. DiGiovanni, and R. Windeler, “Effect of heat and H2 gas on the photo-darkening of Yb +3 fibers,” in Conf. Lasers Electro-Optics 2006 Quantum Electron. Laser Sci. Conf. CLEO/QELS 2006, (2006).
16. J. Boullet, I. Manek-Hönninger, T. Cardinal, F. Guillen, M. Podgorski, S. Ermeneux, R. Bello Doua, and F. Salin, “Photodarkening and photobleaching of an ytterbium-doped silica double-clad LMA fiber,” Conf. Lasers Electro-Optics, 2007, CLEO 2007 **15**(4), 1606–1611 (2007).
17. S. Yoo, C. Basu, A. J. Boyland, C. Sones, J. Nilsson, J. K. Sahu, and D. Payne, “Photodarkening in Yb-doped aluminosilicate fibers induced by 488 nm irradiation,” Opt. Lett. **32**(12), 1626–1628 (2007).
18. M. Engholm and L. Norin, “Reduction of photodarkening in Yb/Al-doped fiber lasers,” 7 February 2008, 68731E.
19. S. Unger, A. Schwuchow, S. Jetschke, V. Reichel, A. Scheffel, and J. Kirchhof, “Optical properties of Yb-doped laser fibers in dependence on codopants and preparation conditions,” 689016 (2008).

20. S. Jetschke, S. Unger, A. Schwuchow, M. Leich, and J. Kirchhof, “Efficient Yb laser fibers with low photodarkening by optimization of the core composition,” Opt. Express **16**(20), 15540 (2008).
21. J. Allain, M. Monerie, and H. Poignant, “Tunable CW lasing around 610, 635, 695, 715, 885 and 910 nm in Praseodymium-doped fluorozirconate fibre,” Electron. Lett. **27**(2), 189–191 (1991).
22. D. S. Funk, J. G. Eden, and J. W. Carlson, “Ultraviolet (381 nm), room temperature laser in neodymium-doped fluorozirconate fibre,” Electron. Lett. **30**(22), 1859–1860 (1994).
23. R. G. Smart, D. C. Hanna, A. C. Tropper, S. T. Davey, S. F. Carter, and D. Szebesta, “Cw room temperature upconversion lasing at blue, green and red wavelengths in infrared-pumped Pr3+-doped fluoride fibre,” Electron. Lett. **27**(14), 1307 (1991).
24. H. M. Pask, R. J. Carman, D. C. Hanna, A. C. Tropper, C. J. Mackechnie, P. R. Barber, and J. M. Dawes, “Ytterbium-Doped Silica Fiber Lasers : Versatile Sources for the 1-1 . 2 pm Region,” Sel. Top. Quantum Electron. IEEE J. **I**(I), 2–13 (1995).
25. E. Shcherbakov, V. Fomin, A. Abramov, A. Ferin, D. Mochalov, and V. P. Gapontsev, “Industrial Grade 100 kW Power CW Fiber Laser,” in Adv. Solid-State Lasers Congr. **5**, (OSA, Washington, D.C., 2013).
26. A. Malinowski, P. Gorman, C. A. Codemard, F. Ghiringhelli, A. J. Boyland, A. Marshall, M. N. Zervas, and M. K. Durkin, “High-peak-power, high-energy, high-average-power pulsed fiber laser system with versatile pulse duration and shape,” Opt. Lett. **38**(22), 4686 (2013).
27. T. Eidam, S. Hanf, E. Seise, T. V Andersen, T. Gabler, C. Wirth, T. Schreiber, J. Limpert, and A. Tünnermann, “Femtosecond fiber CPA system emitting 830 W average output power.,” Opt. Lett. **35**(2), 94–96 (2010).

28. G. Krauss, S. Lohss, T. Hanke, A. Sell, S. Eggert, R. Huber, and A. Leitenstorfer, “Synthesis of a single cycle of light with compact erbium-doped fibre technology,” Nat. Photonics **4**(1), 33–36 (2010).
29. A. Sell, G. Krauss, R. Scheu, R. Huber, and A. Leitenstorfer, “8-fs pulses from a compact Er:fiber system: quantitative modeling and experimental implementation,” Opt. Express **17**(2), 1070 (2009).
30. W. Shi, Q. Fang, X. Zhu, R. A. Norwood, and N. Peyghambarian, “Fiber lasers and their applications [Invited],” Appl. Opt. **53**(28), 6554–6568 (2014).
31. J. P. A. Kaplan, “A Technical and Commercial Comparison of Fiber Laser and CO2 Laser Cutting,” <http://www.laserstoday.com/2013/09/a-technical-and-commercial-comparison-of-fiber-laser-and-co2-laser-cutting/>.
32. L. D. Scintilla, “Fusion cutting of aluminum, magnesium, and titanium alloys using high-power fiber laser,” Opt. Eng. **52**(7), 076115 (2013).
33. Industrial Laser Solutions Editors, “2 kW fiber laser for processing sheet metal.”
34. R. Paschotta, J. Nilsson, A. C. Tropper, and D. C. Hanna, “Ytterbium-doped fiber amplifiers,” IEEE J. Quantum Electron. **33**(7), 1049–1056 (1997).
35. C. Jauregui, H.-J. Otto, F. Stutzki, J. Limpert, and A. Tünnermann, “Simplified modelling the mode instability threshold of high power fiber amplifiers in the presence of photodarkening,” Opt. Express **23**(16), 20203 (2015).
36. H.-J. Otto, N. Modsching, C. Jauregui, J. Limpert, and A. Tünnermann, “Impact of photodarkening on the mode instability threshold,” Opt. Express **23**(12), 15265–15277 (2015).
37. L. Skuja, H. Hosono, and M. Hirano, “Laser-induced color centers in silica,” Proc. SPIE **4347**(April 2001), 155 (2001).
38. K. K. Bobkov, A. A. Rybaltovsky, V. V Vel’miskin, M. E. Likhachev, M. M. Bubnov, E. M. Dianov, A. A. Umnikov, A. N. Gur’yanov, N. N. Vechkanov, and I. A. Shestakova, “Charge-transfer state excitation as the main mechanism

of the photodarkening process in ytterbium-doped aluminosilicate fibres," Quantum Electron. **44**(12), 1129–1135 (2014).

39. M. Engholm and L. Norin, "Divalent ytterbium in ytterbium doped aluminosilicate glass - Aspects on photodarkening in fiber lasers," in Conf. Lasers Electro-Optics, 2007, CLEO 2007, (2007).
40. C. G. Carlson, K. E. Keister, P. D. Dragic, A. Croteau, and J. G. Eden, "Photoexcitation of Yb-doped aluminosilicate fibers at 250 nm: evidence for excitation transfer from oxygen deficiency centers to Yb^3+," J. Opt. Soc. Am. B **27**(10), 2087 (2010).
41. M. Engholm, L. Norin, and D. Aberg, "Strong UV absorption and visible luminescence in ytterbium-doped aluminosilicate glass under UV excitation.," Opt. Lett. **32**(22), 3352–3354 (2007).
42. Kenneth D. K, *Progress in Inorganic Chemistry* (2011).
43. A. J. Cohen and L. N. Makar, "Models for Color Centers in Smoky Quartz," Phys. status solidi **73**(2), 593–596 (1982).
44. R. Peretti, C. Gonnet, and A.-M. Jurdyc, "A new vision of photodarkening in Yb³⁺-doped fibers," 825705 (2012).
45. T. Ishii, "First-principles calculations for the cooperative transitions of Yb3+ dimer clusters in Y3Al5O12 and Y2O3 crystals," J. Chem. Phys. **122**(2), 024705 (2005).
46. M. Engholm and L. Norin, "Preventing photodarkening in ytterbium-doped high power fiber lasers; correlation to the UV-transparency of the core glass," Opt. Express **16**(2), 1260 (2008).
47. H. You and M. Nogami, "Three-photon-excited fluorescence of Al2O3-SiO 2 glass containing Eu3+ ions by femtosecond laser irradiation," Appl. Phys. Lett. **84**(12), 2076–2078 (2004).

48. H. You, T. Hayakawa, and M. Nogami, “Upconversion luminescence of Al2O3-SiO 2:Ce3+ glass by femtosecond laser irradiation,” Appl. Phys. Lett. **85**(16), 3432–3434 (2004).

49. L. J. Poyntz-Wright, M. E. Fermann, and P. S. J. Russell, “Nonlinear transmission and color-center dynamics in germanosilicate fibers at 420–540 nm,” Opt. Lett. **13**(11), 1023 (1988).

50. L. J. Poyntz-Wright and P. S. J. Russell, “Spontaneous relaxation processes in irradiated germanosilicate optical fibres,” Electron. Lett. **25**(7), 478 (1989).

51. S. M. Kaczmarek, T. Tsuboi, M. Ito, G. Boulon, and G. Leniec, “Optical study of Yb3+/Yb2+ conversion in CaF 2 crystals,” J. Phys. Condens. Matter **17**(25), 3771–3786 (2005).

52. and K. O. T. Kitabayashi, M. Ikeda, M. Nakai, T. Sakai, K. Himeno, “Population Inversion Factor Dependence of Photodarkening of Yb-Doped Fibers and Its Suppression by Highly Aluminum Doping,” in Popul. Invers. Factor Depend. Photodarkening Yb-Doped Fibers Its Suppr. by Highly Alum. Doping, (Optical Fiber Communication Conference and Exposition and The National Fiber Optic Engineers Conference, Technical Digest (CD), 2006).

53. H. Imai, K. Arai, J. Isoya, H. Hosono, Y. Abe, and H. Imagawa, “Generation of E’ centers and oxygen hole centers in synthetic silica glasses by γ irradiation,” Phys. Rev. B **48**(5), 3116–3123 (1993).

54. K. Arai, H. Imai, J. Isoya, H. Hosono, Y. Abe, and H. Imagawa, “Evidence for pair generation of an E ’ center and a nonbridging oxygen-hole center in γ-ray-irradiated fluorine-doped low-OH synthetic silica glasses,” Phys. Rev. B **45**(18), 10818–10821 (1992).

55. R. Peretti, A.-M. Jurdyc, B. Jacquier, C. Gonnet, A. Pastouret, E. Burov, and O. Cavani, “How do traces of thulium can explain photodarkening in Yb doped fibers?,” Opt. Express **18**(19), 20455 (2010).

56. J. . Bonar, M. V. . Vermelho, a. . McLaughlin, P. V. . Marques, J. . Aitchison, J. . Martins-Filho, a. . Bezerra, a. S. . Gomes, and C. . de Araujo, "Blue light emission in thulium doped silica-on-silicon waveguides," Opt. Commun. **141**(3–4), 137–140 (1997).

57. R. Piramidowicz, A. Bok, M. Klimczak, and M. Malinowski, "UV emission properties of thulium-doped fluorozirconate glasses," J. Lumin. **129**(12), 1874–1877 (2009).

58. P. Jenouvrier, G. Boccardi, J. Fick, a.-M. Jurdyc, and M. Langlet, "Up-conversion emission in rare earth-doped Y2Ti2O7 sol–gel thin films," J. Lumin. **113**(3–4), 291–300 (2005).

59. G. WANG, W. QIN, L. WANG, G. WEI, P. ZHU, D. ZHANG, and F. DING, "Enhanced ultraviolet upconversion in YF3:Yb3+/Tm3+nanocrystals," J. Rare Earths **27**(2), 330–333 (The Chinese Society of Rare Earths, 2009).

60. L. Dong, J. L. Archambault, L. Reekie, P. S. Russell, and D. N. Payne, "Photoinduced absorption change in germanosilicate preforms: evidence for the color-center model of photosensitivity.," Appl. Opt. **34**, 3436–3440 (1995).

61. S. Jetschke, M. Leich, S. Unger, A. Schwuchow, and J. Kirchhof, "Influence of Tm- or Er-codoping on the photodarkening kinetics in Yb fibers," Opt. Express **19**(15), 14473–14478 (2011).

62. S. Jetschke, U. Röpke, S. Unger, and J. Kirchhof, "Characterization of photodarkening processes in Yb doped fibers," 71952B (2009).

63. J. Koponen, M. Söderlund, H. J. Hoffman, D. a V Kliner, J. P. Koplow, and M. Hotoleanu, "Photodarkening rate in Yb-doped silica fibers," Appl. Opt. **47**(9), 1247–1256 (2008).

64. M. Leich, S. Jetschke, S. Unger, and V. Reichel, "Acceleration of photodarkening measurements in Yb-doped fibers by enhanced temperatures," in CLEO/Europe - EQEC 2009 - Eur. Conf. Lasers Electro-Optics Eur. Quantum Electron. Conf. **4528**(2008), (IEEE, 2009).

65. M. Leich, S. Jetschke, S. Unger, and J. Kirchhof, “Temperature influence on the photodarkening kinetics in Yb-doped silica fibers,” J. Opt. Soc. Am. B **28**(1), 65 (2011).

66. M. Engholm and L. Norin, “Reduction of photodarkening in Yb/Al-doped fiber lasers,” Proceeding Spie **6873**, 68731E–68731E–8 (2008).

67. and R. W. Jayesh Jasapara, Matthew Andrejco, David DiGiovanni, “Effet of heat and H2 gas on the photo-darkening of Yb3+ fibers,” in Conf. Lasers Electro-Optics/Quantum Electron. Laser Sci. Conf. Photonic Appl. Syst. Technol., (2006).

68. K. Arai, H. Namikawa, K. Kumata, T. Honda, Y. Ishii, and T. Handa, “Aluminum or phosphorus co-doping effects on the fluorescence and structural properties of neodymium-doped silica glass,” J. Appl. Phys. **59**(10), 3430–3436 (1986).

69. A. V. Shubin, M. V. Yashkov, M. A. Melkumov, S. A. Smirnov, I. A. Bufetov, and E. M. Dianov, “Photodarkening of alumosilicate and phosphosilicate Yb-doped fibers,” in Conf. Lasers Electro-Optics Eur. - Tech. Dig., (2007).

70. M. a Mel’kumov, I. a Bufetov, K. S. Kravtsov, A. V Shubin, and E. M. Dianov, “Lasing parameters of ytterbium-doped fibres doped with P_2O_5 and Al_2O_3,” Quantum Electron. **34**(9), 843–848 (2004).

71. S. Unger, A. Schwuchow, J. Dellith, and J. Kirchhof, “Codoped materials for high power fiber lasers - diffusion behaviour and optical properties,” proceeding spie **6469**, 646913-646913–12 (2007).

72. S. Jetschke, S. Unger, M. Leich, and J. Kirchhof, “Photodarkening kinetics as a function of Yb concentration and the role of Al codoping.,” Appl. Opt. **51**, 7758–7764 (2012).

73. S. Taccheo, H. Gebavi, A. Monteville, O. Le Goffic, D. Landais, D. Mechin, D. Tregoat, B. Cadier, T. Robin, D. Milanese, and T. Durrant, “Concentration

dependence and self-similarity of photodarkening losses induced in Yb-doped fibers by comparable excitation," Opt. Express **19**(20), 19340 (2011).

74. S. Jetschke, S. Unger, A. Schwuchow, M. Leich, J. Fiebrandt, M. Jäger, and J. Kirchhof, "Evidence of Tm impact in low-photodarkening Yb-doped fibers," Opt. Express **21**(6), 7590–7598 (2013).
75. C. Barnard, P. Myslinski, J. Chrostowski, and M. Kavehrad, "Analytical model for rare-earth-doped fiber amplifiers and lasers," IEEE J. Quantum Electron. **30**(8), 1817–1830 (1994).
76. C. R. Giles and E. Desurvire, "Modeling erbium-doped fiber amplifiers," J. Light. Technol. **9**(2), 271–283 (1991).
77. B. Pedersen, A. Bjarklev, J. H. Povlsen, K. Dybdal, and C. C. Larsen, "The design of erbium-doped fiber amplifiers," J. Light. Technol. **9**(9), 1105–1112 (1991).
78. M. N. Zervas and C. A. Codemard, "High Power Fiber Lasers: A Review," IEEE J. Sel. Top. Quantum Electron. **20**(5), 219–241 (2014).
79. P. Barua, E. H. Sekiya, K. Saito, and A. J. Ikushima, "Influences of Yb3+ ion concentration on the spectroscopic properties of silica glass," J. Non. Cryst. Solids **354**(42–44), 4760–4764 (Elsevier B.V., 2008).
80. D. E. McCumber, "Einstein relations connecting broadband emission and absorption spectra," Phys. Rev. **136**(4A), 16–19 (1964).
81. F. Auzel and P. Goldner, "Towards rare-earth clustering control in doped glasses," Opt. Mater. (Amst). **16**(1–2), 93–103 (2001).
82. A. S. Kurkov, A. Y. Laptev, E. M. Dianov, A. N. Guryanov, V. I. Karpov, V. M. Paramonov, O. I. Medvedkov, A. A. Umnikov, V. N. Protopopov, N. N. Vechkanov, S. A. Vasiliev, and E. V. Pershina, "Yb $^{3+}$ -doped double-clad fibers and lasers," 118 (2000).

83. M. Weber, J. Lynch, D. Blackburn, and D. Cronin, “Dependence of the stimulated emission cross section of Yb< sup> 3+</sup> on host glass composition,” Quantum Electron. IEEE J. **19**(10), 1600–1608 (1983).
84. T. Murata, H. Takebe, and K. Morinaga, “Compositional dependence of infrared-to-visible upconversion in Yb3+- and Er3+-codoped germanate, gallate, and tellurite glasses.,” J. Am. Ceram. Soc. **81**(1), 249–251 (1998).
85. X. Zou and H. Toratani, “Evaluation of spectroscopic properties of Yb 3 + -doped glasses,” Phys. Rev. B **52**(22), 15889–15897 (1995).
86. K. Lu and N. K. Dutta, “Spectroscopic properties of Yb-doped silica glass,” J. Appl. Phys. **91**(2), 576–581 (2002).
87. A. V. Shubin, M. V. Yashkov, M. A. Melkumov, S. A. Smirnov, I. A. Bufetov, and E. M. Dianov, “Photodarkening of alumosilicate and phosphosilicate Yb-doped fibers,” in 2007 Eur. Conf. Lasers Electro-Optics Int. Quantum Electron. Conf., (IEEE, 2007).
88. S. Suzuki, H. A. McKay, X. Peng, L. Fu, and L. Dong, “Highly ytterbium-doped silica fibers with low photo-darkening,” Opt. Express **17**(12), 9924 (2009).
89. S. Taccheo, H. Gebavi, A. Monteville, O. Le Goffic, D. Landais, D. Mechin, D. Tregoat, B. Cadier, T. Robin, D. Milanese, and T. Durrant, “Concentration dependence and self-similarity of photodarkening losses induced in Yb-doped fibers by comparable excitation,” Opt. Express **19**(20), 19340 (2011).
90. S. Jetschke, S. Unger, M. Leich, and J. Kirchhof, “Photodarkening kinetics as a function of Yb concentration and the role of Al codoping,” Appl. Opt. **51**(32), 7758 (2012).
91. S. Yoo, A. J. Boyland, R. J. Standish, and J. K. Sahu, “Measurement of photodarkening in Yb-doped aluminosilicate fibres at elevated temperature,” Electron. Lett. **46**(3), 233–234 (2010).
92. R. P. Fiber and V. Power, “RP Fiber Power V5.0” (2013).

93. T. Kilabayashi, M. Ikeda, M. Nakai, T. Sakai, K. Himeno, and K. Ohashi, "Population inversion factor dependence of photodarkening of Yb-doped fibers and its suppression by highly aluminum doping," in 2006 Opt. Fiber Commun. Conf. Natl. Fiber Opt. Eng. Conf., (IEEE, 2006).

94. T. Arai, K. Ichii, S. Tanigawa, and M. Fujimaki, "Gamma-radiation-induced photodarkening in ytterbium-doped silica glasses," 79140K (2011).

95. T. Deschamps, N. Ollier, H. Vezin, and C. Gonnet, "Clusters dissolution of Yb^{3+} in codoped SiO_2-Al_2O_3-P_2O_5 glass fiber and its relevance to photodarkening," J. Chem. Phys. **136**(1), 014503 (2012).

96. M. Engholm, P. Jelger, F. Laurell, and L. Norin, "Improved photodarkening resistivity in ytterbium-doped fiber lasers by cerium codoping," Opt. Lett. **34**(8), 1285 (2009).

97. M. Engholm, L. Norin, and D. Åberg, "Strong UV absorption and visible luminescence in ytterbium-doped aluminosilicate glass under UV excitation," Opt. Lett. **32**(22), 3352 (2007).

98. P. D. Dragic, Y.-S. Liu, T. C. Galvin, and J. G. Eden, "Ultraviolet absorption and excitation spectroscopy of rare-earth-doped glass fibers derived from glassy and crystalline preforms," 82370T (2012).

99. T. E. Tsai, J. M. Jewell, and J. S. Sanghera, "Dynamics of the 5 eV optical absorption in SiO2glass," Appl. Phys. Lett. **62**(26), 3396–3398 (1993).

100. S. Rydberg and M. Engholm, "Experimental evidence for the formation of divalent ytterbium in the photodarkening process of Yb-doped fiber lasers," Opt. Express **21**(6), 6681 (2013).

101. Y.-S. Liu, T. C. Galvin, T. Hawkins, J. Ballato, L. Dong, P. R. Foy, P. D. Dragic, and J. G. Eden, "Linkage of oxygen deficiency defects and rare earth concentrations in silica glass optical fiber probed by ultraviolet absorption and laser excitation spectroscopy," Opt. Express **20**(13), 14494 (2012).

102. A. V. Amossov and A. O. Rybaltovsky, “Oxygen-deficient centers in silica glasses: a review of their properties and structure,” J. Non. Cryst. Solids **179**, 75–83 (1994).
103. L. Skuja, “Optically active oxygen-deficiency-related centers in amorphous silicon dioxide,” J. Non. Cryst. Solids **239**(1–3), 16–48 (1998).
104. C. V. Poulsen and M. Sejka, “Highly optimized tunable Er/sup 3+/-doped single longitudinal mode fiber ring laser, experiment and model,” IEEE Photonics Technol. Lett. **5**(6), 646–648 (1993).
105. T. Pfeiffer, H. Schmuck, and H. Bulow, “Output power characteristics of erbium-doped fiber ring lasers,” IEEE Photonics Technol. Lett. **4**(8), 847–849 (1992).
106. T. Pfeiffer and H. BüLow, “Analytical Gain Equation For Erbium-Doped Fiber Amplifiers Including Mode Field Profiles And Dopant Distribution,” IEEE Photonics Technol. Lett. **4**(5), 449–451 (1992).
107. C. Jauregui, H.-J. Otto, F. Stutzki, J. Limpert, and A. Tünnermann, “Simplified modelling the mode instability threshold of high power fiber amplifiers in the presence of photodarkening,” Opt. Express **23**(16), 20203 (2015).
108. H. Gebavi, S. Taccheo, L. Lablonde, B. Cadier, T. Robin, D. Méchin, and D. Tregoat, “Mitigation of photodarkening phenomenon in fiber lasers by 633 nm light exposure.,” Opt. Lett. **38**(2), 196–198 (2013).
109. S. Jetschke, S. Unger, A. Schwuchow, M. Leich, and J. Kirchhof, “Efficient Yb laser fibers with low photodarkening by optimization of the core composition,” Opt. Express **16**(20), 15540 (2008).
110. S. Unger, A. Schwuchow, S. Jetschke, V. Reichel, M. Leich, A. Scheffel, and J. Kirchhof, “Influence of aluminum-phosphorus codoping on optical properties of ytterbium-doped laser fibers,” 12 February 2009, 72121B.

111. Kentaro, Ichii, Sakura, (JP);, Shoji, Tanigawa, Sakura, (JP);, Tomofumi, Arai, Sakura, and (JP), “Ytterbium-doped optical fiber,” in U.S.Patent USOO8774590B2, (July 8, 2014). (2014).
112. C. Hupel, S. Kuhn, S. Hein, N. Haarlammert, J. Nold, F. Beier, B. Sattler, T. Schreiber, R. Eberhardt, and A. Tünnermann, “MCVD Based Fabrication of Low-NA Fibers for High Power Fiber Laser Application,” 5–7 (2015).
113. A. Lin, X. Tang, H. Zhan, Q. Li, Y. Wang, K. Peng, L. Ni, X. Wang, C. Gao, Y. You, Z. Jia, Y. Li, A. You, H. Lin, J. Wang, and F. Jing, “6 kW Yb-doped aluminophosphosilicate laser fiber,” Qiangjiguang Yu Lizishu/High Power Laser Part. Beams **28**(12), 5170–5174 (2016).
114. C. Jauregui, J. Limpert, and A. Tünnermann, “High-power fibre lasers,” Nat. Photonics **7**(11), 861–867 (Nature Publishing Group, 2013).
115. M. A. K. Ienel, M. I. M. Üller, A. R. N. O. K. Lenke, J. E. N. S. L. Impert, and A. N. T. Ünnermann, “12 mJ kW-class ultrafast fiber laser system using multidimensional coherent pulse addition,” 3343–3346 (2016).
116. R. Dinger, F. Grundmann, C. Hapke, P. Kallage, R. Dinger, F. Grundmann, C. Hapke, P. Kallage, W. Rath, and S. Ruppik, “Short-pulse MOPA fiber laser with kilowatt average power and multimegawatt peak power, applying advanced XLMA fiber amplifiers,” in Proc. SPIE 10083, Fiber Lasers XIV Technol. Syst.(March 2017), (2017).
117. T. Hakulinen and O. G. Okhotnikov, “8 ns fiber laser Q switched by the resonant saturable absorber mirror,” Opt. Lett. **32**(18), 2677 (2007).
118. U. Keller, K. J. Weingarten, F. X. Kärtner, D. Kopf, B. Braun, I. D. Jung, R. Fluck, C. Hönninger, N. Matuschek, and J. Aus Der Au, “Semiconductor saturable absorber mirrors (SESAM’s) for femtosecond to nanosecond pulse generation in solid-state lasers,” IEEE J. Sel. Top. Quantum Electron. **2**(3), 435–451 (1996).

119. J. Li, D. D. Hudson, Y. Liu, and S. D. Jackson, “Efficient 2.87 μm fiber laser passively switched using a semiconductor saturable absorber mirror,” Opt. Lett. **37**(18), 3747–3749 (2012).

120. W. B. Cho, A. Schmidt, J. H. Yim, S. Y. Choi, S. Lee, F. Rotermund, U. Griebner, G. Steinmeyer, V. Petrov, X. Mateos, M. C. Pujol, J. J. Carvajal, M. Aguiló, and F. Díaz, “Passive mode-locking of a Tm-doped bulk laser near 2 μm using a carbon nanotube saturable absorber,” Opt. Express **17**(13), 11007 (2009).

121. S. Y. Set, H. Yaguchi, Y. Tanaka, and M. Jablonski, “Ultrafast fiber pulsed lasers incorporating carbon nanotubes,” IEEE J. Sel. Top. Quantum Electron. **10**(1), 137–146 (2004).

122. Q. Bao, H. Zhang, Y. Wang, Z. Ni, Y. Yan, Z. X. Shen, K. P. Loh, and D. Y. Tang, “Atomic-layer craphene as a saturable absorber for ultrafast pulsed lasers,” Adv. Funct. Mater. **19**(19), 3077–3083 (2009).

123. Z. Luo, M. Zhou, J. Weng, G. Huang, H. Xu, C. Ye, and Z. Cai, “Graphene-based passively Q -switched dual-wavelength erbium-doped fiber laser,” Opt. Lett. **35**(21), 3709–3711 (2010).

124. H. Zhang, D. Tang, R. J. Knize, L. Zhao, Q. Bao, and K. P. Loh, “Graphene mode locked, wavelength-tunable, dissipative soliton fiber laser,” Appl. Phys. Lett. **96**(11), 1–5 (2010).

125. X. Li, W. Cai, L. Colombo, and R. Ruoff, “Evolution of graphene growth on Ni and Cu by carbon isotope labeling,” Nano Lett. **12**(Cvd), 1–15 (2009).

126. Y. Laurent Gautron, Joseph M. Rutkowski, Michael D. Burton, Wei Wei and and J. K. E. Wan, “Bandgap-Like Strong Fluorescence in Functionalized Carbon Nanoparticles,” J Comp Neurol. 2013 Novemb. ; 521(16) 3741–3767. doi10.1002/cne.23376 **521**(Serres 1985), 759–785 (2014).

127. H. Li, X. He, Y. Liu, H. Huang, S. Lian, S. T. Lee, and Z. Kang, “One-step ultrasonic synthesis of water-soluble carbon nanoparticles with excellent

photoluminescent properties," Carbon N. Y. **49**(2), 605–609 (Elsevier Ltd, 2011).

128. H. Liu, T. Ye, and C. Mao, "Fluorescent carbon nanoparticles derived from candle soot," Angew. Chemie - Int. Ed. **46**(34), 6473–6475 (2007).
129. Y. P. Sun, B. Zhou, Y. Lin, W. Wang, K. A. S. Fernando, P. Pathak, M. J. Meziani, B. A. Harruff, X. Wang, H. Wang, P. G. Luo, H. Yang, M. E. Kose, B. Chen, L. M. Veca, and S. Y. Xie, "Quantum-sized carbon dots for bright and colorful photoluminescence," J. Am. Chem. Soc. **128**(24), 7756–7757 (2006).
130. S. C. Ray, "Fluorescent Carbon Nanoparticle : Synthesis , Characterization and Bio-imaging Application," 1–27.
131. L. Cao, X. Wang, M. J. Meziani, F. Lu, H. Wang, P. G. Luo, Y. Lin, B. A. Harruff, L. M. Veca, D. Murray, S. Y. Xie, and Y. P. Sun, "Carbon dots for multiphoton bioimaging," J. Am. Chem. Soc. **129**(37), 11318–11319 (2007).
132. D. R. Larson, "Water-Soluble Quantum Dots for Multiphoton Fluorescence Imaging in Vivo," Science (80-.). **300**(5624), 1434–1436 (2003).
133. I. L. Medintz, H. T. Uyeda, E. R. Goldman, and H. Mattoussi, "Quantum dot bioconjugates for imaging, labelling and sensing," Nat. Mater. **4**(6), 435–446 (2005).
134. L. Yuan, J. Dai, X. Fan, T. Song, Y. T. Tao, K. Wang, Z. Xu, J. Zhang, X. Bai, P. Lu, J. Chen, J. Zhou, and Z. L. Wang, "Self-cleaning flexible infrared nanosensor based on carbon nanoparticles," ACS Nano **5**(5), 4007–4013 (2011).
135. J. W. Nicholson, R. S. Windeler, and D. J. Digiovanni, "Optically driven deposition of single-walled carbon-nanotube saturable absorbers on optical fiber end-faces.," Opt. Express **15**(15), 9176–9183 (2007).